THE HONG KONG
POLYTECHNIC UNIVERSITY
香港理工大學
Pao Yue-kong Library
包玉剛圖書館

Copyright Undertaking

This thesis is protected by copyright, with all rights reserved.

By reading and using the thesis, the reader understands and agrees to the following terms:

1. The reader will abide by the rules and legal ordinances governing copyright regarding the use of the thesis.

2. The reader will use the thesis for the purpose of research or private study only and not for distribution or further reproduction or any other purpose.

3. The reader agrees to indemnify and hold the University harmless from and against any loss, damage, cost, liability or expenses arising from copyright infringement or unauthorized usage.

Pao Yue-kong Library, The Hong Kong Polytechnic University, Hung Hom, Kowloon, Hong Kong

http://www.lib.polyu.edu.hk

INHIBITING BREAST CANCER PROGRESSION BY TARGETING SND1 USING A NOVEL PEPTIDE IDENTIFIED FROM PHAGE DISPLAY

LI PENG

PhD

The Hong Kong Polytechnic University

2019

The Hong Kong Polytechnic University

Department of Applied Biology and Chemical Technology

INHIBITING BREAST CANCER PROGRESSION BY TARGETING SND1 USING A NOVEL PEPTIDE IDENTIFIED FROM PHAGE DISPLAY

LI Peng

A thesis submitted in partial fulfillment of the requirements for the degree of Doctor of Philosophy

Jan 2019

CERTIFICATE OF ORIGINALITY

I hereby declare that this thesis is my own work and that, to the best of my knowledge and belief, it reproduces no material previously published or written nor material which has been accepted for the award of any other degree or diploma, except where due acknowledgement has been made in the text.

LI Peng

Signature:

Abstract

Breast cancer is the most common cancer in women, causing 626,679 deaths worldwide in 2018. SND1 is a multifunctional oncoprotein overexpressed in almost all cancers, especially in advanced and metastatic cases. SND1-MTDH interaction contributes to the initiation and progression of breast cancer, making it a promising target for breast cancer treatment.

In this study, recombinant SN1/2 domain of SND1 was expressed in *E.coli* and purified with HisTrap affinity column. SN1/2 was used as bait in a phage display screening. After 4 rounds of screening, 20 phages were randomly picked and sequenced. Amino acids W and Y were found to be highly enriched in these phages. The most repeated peptide 4-2 was demonstrated to have high binding affinity towards SN1/2. Peptide 4-2 could disrupt 22-mer MTDH peptide from interacting with SN1/2 in ELISA assay and could also disrupt SND1-MTDH full-length protein interaction in co-immunoprecipitation assay.

An RR-TAT cell penetrating peptide was attached to the N-terminus of peptide 4-2 to generate CPP-4-2 peptide. CPP-4-2 peptide could penetrate and preferentially kill breast cancer cells by inducing apoptosis compared to other cancer types or normal cells. Mechanistic investigation suggested that peptide 4-2 could interact with SND1 and disrupt SND1-MTDH interaction, which probably lead to the degradation

of SND1. Overexpression of SND1 could reduce the cytotoxicity of peptide 4-2 to breast cancer cells, indicating that the disruption of SND1-MTDH interaction and subsequent degradation of SND1 by peptide 4-2 was the possible reason for breast cancer cell death.

It was found that peptide 4-2 could regulate Akt pathway by upregulating p-Akt S473 and degrading Akt. The degradation of Akt by peptide 4-2 was proteasome-dependent and was partially dependent on the phosphorylation of Akt at S473. On the other hand, peptide 4-2 could also regulate another SND1 downstream target NF-κB2 by enhancing the transcription of pro-apoptotic NF-κB2. The degradation of Akt and the enhanced transcription of NF-κB2 induced by peptide 4-2 might be the reasons for breast cancer cell death.

Mutational analysis suggested that W10 but not Y4 or Y11 was essential in the activities of peptide 4-2, including cytotoxicity, SND1-interaction, SND1 downregulation, Akt degradation and NF-κB2 activation.

In summary, peptide 4-2 selectively killed breast cancer cells by inducing apoptosis possibly through interacting with SND1, disrupting SND1-MTDH interaction and inducing SND1 degradation. Peptide 4-2 could also affect SND1 downstream targets, Akt and NF-κB2 by degrading Akt and enhancing the transcription of pro-apoptotic NF-κB2, which possibly lead to breast cancer cell death. W10 rather than Y4 or Y11 was the essential amino acid in the activities of peptide 4-2.

Acknowledgement

student from Prof. Abgyan' lab to thank for his very selfless help in teaching and helping me to accomplish the molecular docking experiment.

Great thanks are also given to Ms. Josephine Leung who very nicely helps me to correct my PhD thesis.

Again, thank you all for the unforgettable help during my PhD study!

Table of contents

List of figures

List of tables

List of Abbreviations

BCRP   Breast cancer resistant protein

BRCA1   Breast cancer susceptibility gene 1

CHIP   Chromatin immunoprecipitation

CPP   Cell-penetrating peptides

CSC   Cancer stem cells

CTC   Circulating tumor cells

DCIS   Ductal carcinoma *in situ*

dsRNA   Double-stranded RNA

dTp   Deoxythymidine 3', 5'-bisphosphate

EBNA2   Epstein-Barr virus nuclear antigen 2

E.coli   *Escherichia coli*

ELISA   Enzyme-linked immunosorbent assay

EMT   Epithelial-mesenchymal transition

FoxO   Forkhead Box O

FPLC   Fast Protein Liquid Chromatography

GPCR   G-protein-coupled receptors

GSK3   Glycogen synthase kinase 3

GST   Glutathione S-transferase

HCC   Hepatocellular carcinoma

HRV   Human rhinovirus

ICM   Internal Coordinate Mechanics

IDC	Invasive ductal carcinoma
IPA	Ingenuity Pathway Analysis
ITGB4	Integrin, beta 4
MALS	Multi-angle light scattering
MET	Mesenchymal-epithelial transition
MGLL	Monoglyceride Lipase
MTDH	Metastasis adhesion protein, Metadherin
mTOR	Mechanistic target of rapamycin
NF-κB	Nuclear factor-kappaB
NLS	Nuclear localization signals
NSCLC	Non-small cell lung cancer
NTA	Nitrilotriacetic acid
OD	Optical density
PDK1	Phosphoinositide-dependent protein kinase 1
EP400	E1A-binding protein p400
pI	Isoelectric point
PI3K	Phosphoinositide-3-kinase
PIP3	Phosphatidylinositol 3-phosphate
PIWIL1	Piwi-like protein 1
PKB	Protein kinase B
PMS	Phenazine methyl sulfate
RISC	RNA-induced silencing complex

RNAi	RNA interference
RTK	Receptor Tyrosine kinase
siRNA	Small interfering RNA
SEC	Size exclusion chromatography
SG	Stress granule
SN	Staphylococcal nuclease
SND1	Staphylococcal nuclease domain-containing protein 1
snRNP	Small nuclear ribonucleoprotien
STAT	Signal transducer and activator of transcription
TGFβ	Transforming growth factor β
TMD	Transmembrane domain
TNM	Tumor Node Metastasis
TTC3	Tetratricopeptide repeat domain 3
ZEB1	Zinc finger E-box binding homeobox 1

Chapter 1 Introduction

1.1 Background

1.1.1 Breast cancer

1.1.1.1 Pathology of breast cancer

Breast cancer was the second most common cancer in the world and the most common cancer among women, with an estimation of 2.09 million new cases worldwide in 2018. The incidence rate varied by almost three folds across different parts of the world, ranging from <24.8 cases per 100,000 in the South-Central Africa to 72.9 cases per 100,000 in Australia/New Zealand, Europe and Northern America (Figure 1.1.a and b) (WHO, 2018). Mortality rate of breast cancer was ranked number 5, with an annual death rate of 626,679 in the world in 2018. The regional difference in mortality rate was relatively small compared to the incidence rate, possibly due to the high survival rate of breast cancer patients in the developed world (Figure 1.2.a and b) (WHO, 2018).
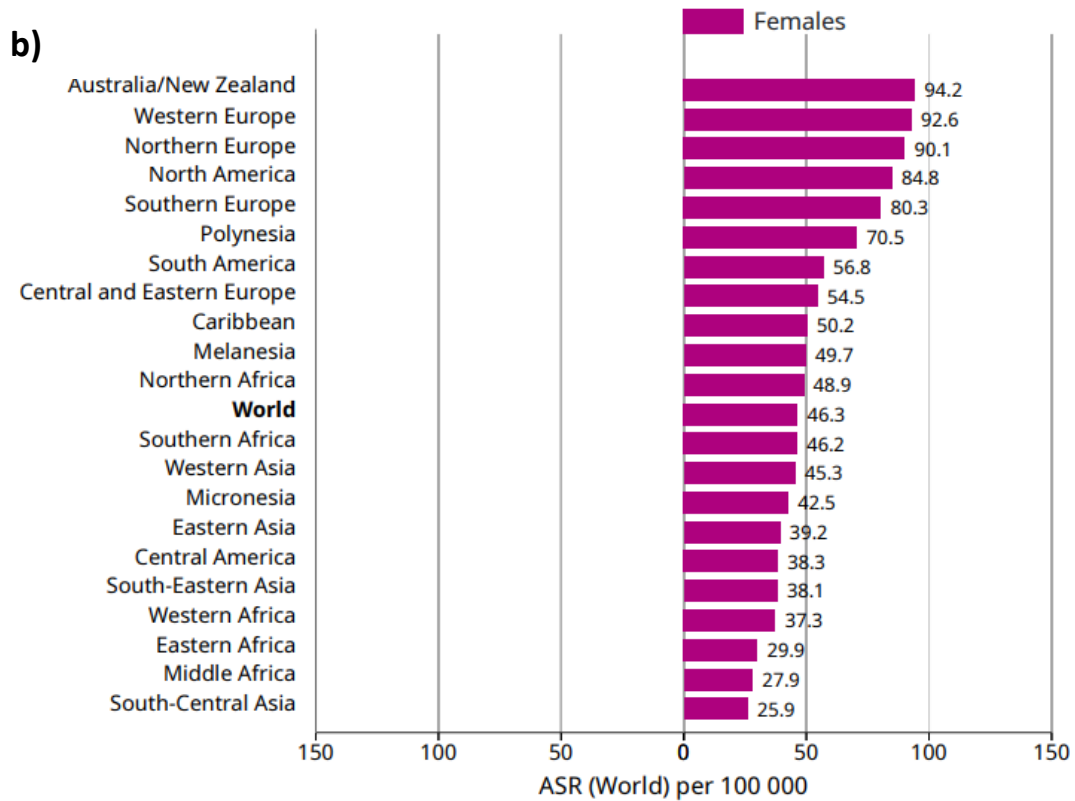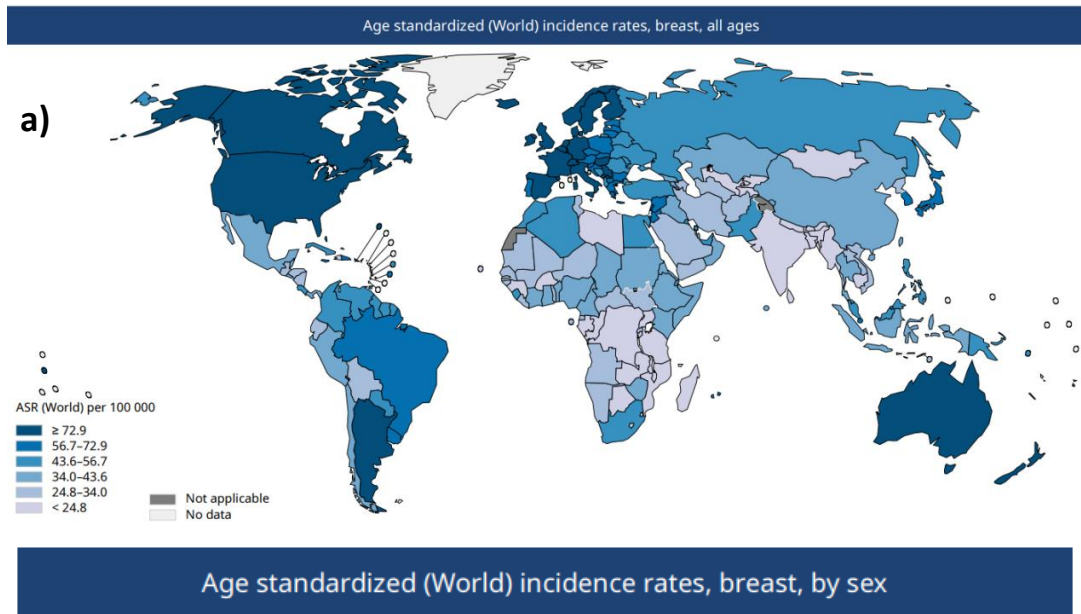
Figure 1.1 Age standardized rate of breast cancer incidence worldwide in 2018 (WHO, 2018)

ASR: Age standardized rate; Highest ASR (~90 per 100,000) of breast cancer incidence happened in Australia/New Zealand, Europe and Northern America; Lowest SAR (25.9 per 100,000) of breast cancer incidence happened in South-Central Africa.
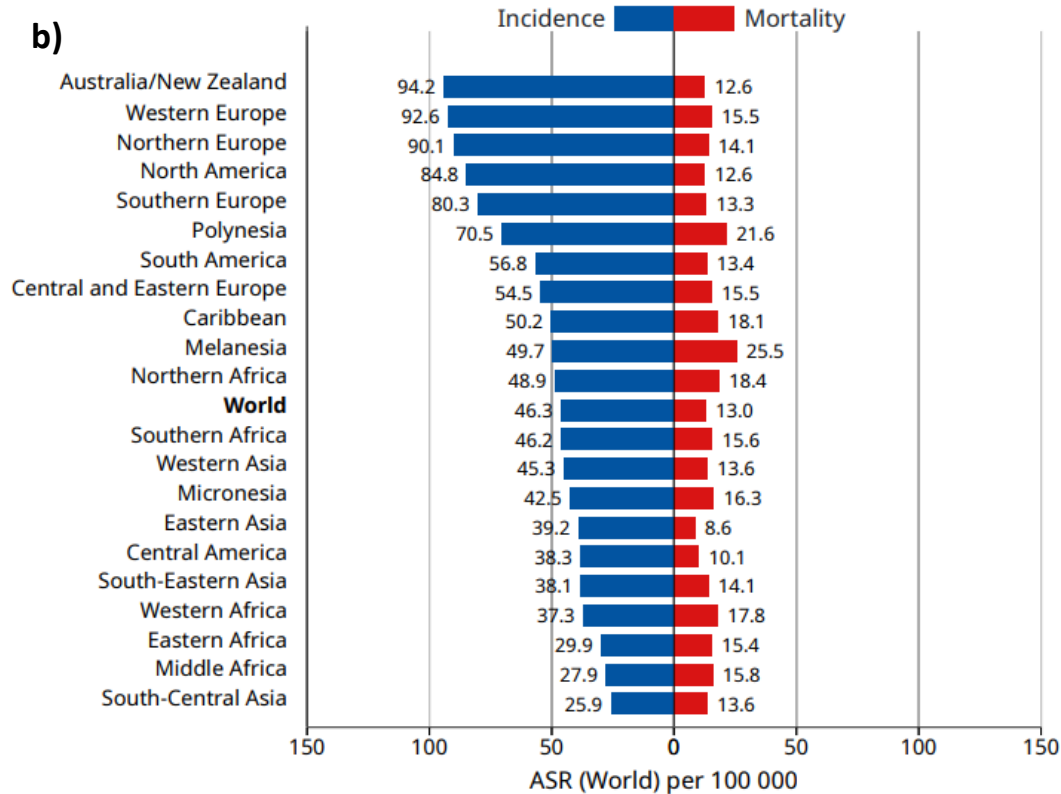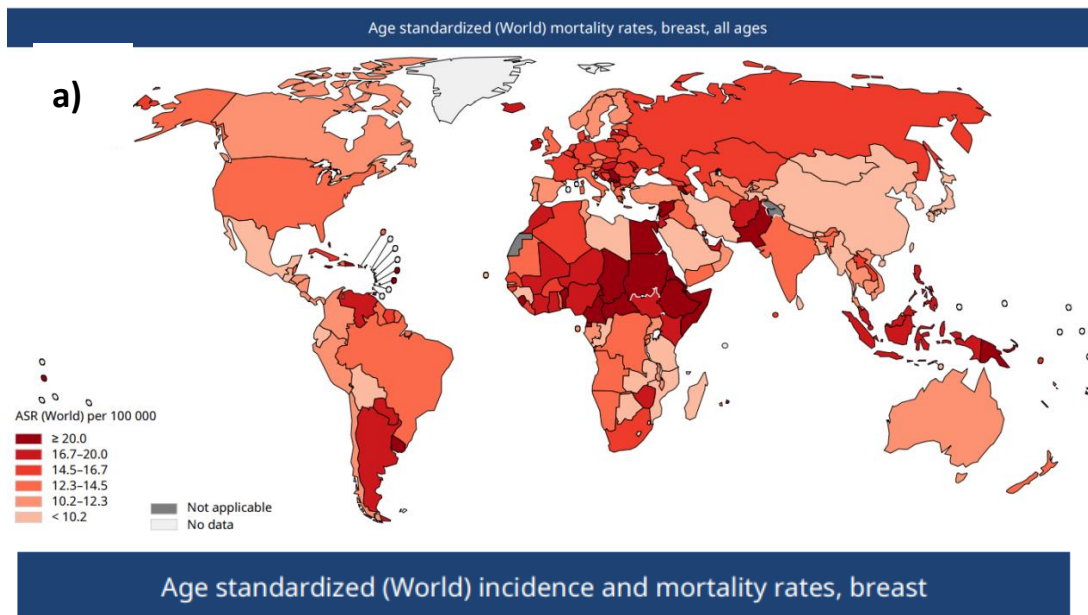
Figure 1.2 Age standardized rate of breast cancer mortality worldwide in 2018 (WHO, 2018)

ASR: Age standardized rate; ASR of breast cancer mortality did not vary a lot across the world (8.6-25.5 cases per 100,000), though ASR of breast cancer incidence varied significantly (25.9-94.2 cases per 100,000).

1.1.1.2 Cell origin of Breast cancer

Breast cancer was a very heterogeneous disease, involving many different types of cells with different biological properties (Al-Hajj et al., 2003). There were two generally-accepted hypotheses on the cellular origin of breast cancer.

In one theory, cancer was believed to originate from genetic mutations. An accumulation of a large number of mutations resulted in an alteration of complex internal signaling in cells. The accumulation of these genetic abnormalities resulted in the development of a colony of cells which are pathologically abnormal or malignant (Wren, 2007).

BRCA1 or *BRCA2* gene, two predisposing genes for breast cancer development, was found to be mutated in 5-10% of all newly diagnosed breast cancers in the western world (Peshkin et al., 2010). Women with an inherited *BRCA1* mutation would have a lifetime risk of 65-80% of developing breast cancer, and those with an inherited *BRCA2* mutation would have 45-85% risk of developing breast malignancy (Balmana et al., 2009). Besides the *BRCA* genes, other genes such as *TP53*, *PTEN*, *CDH11* and *STK11* were also found to be associated with breast cancer as well (Peng et al., 2016).

The second theory postulated that tumor was consisted of heterogeneous cancer cells that had different functions during tumorigenesis. The development of cancer was driven by a specialized

subset of cells with self-renewal and tumor-initiating properties. Most likely they were generated from normal stem cells or progenitor cells within tissues after oncogenic hit (Figure 1.3) (Papaccio et al., 2017b). Although there were different opinions on how breast cancer initiated, more and more recent research findings supported the theory that cancer was caused by a small population of cancer cells called cancer stem cells (CSCs), which accounted for only 1-5% of tumor cells (Al-Hajj et al., 2003).
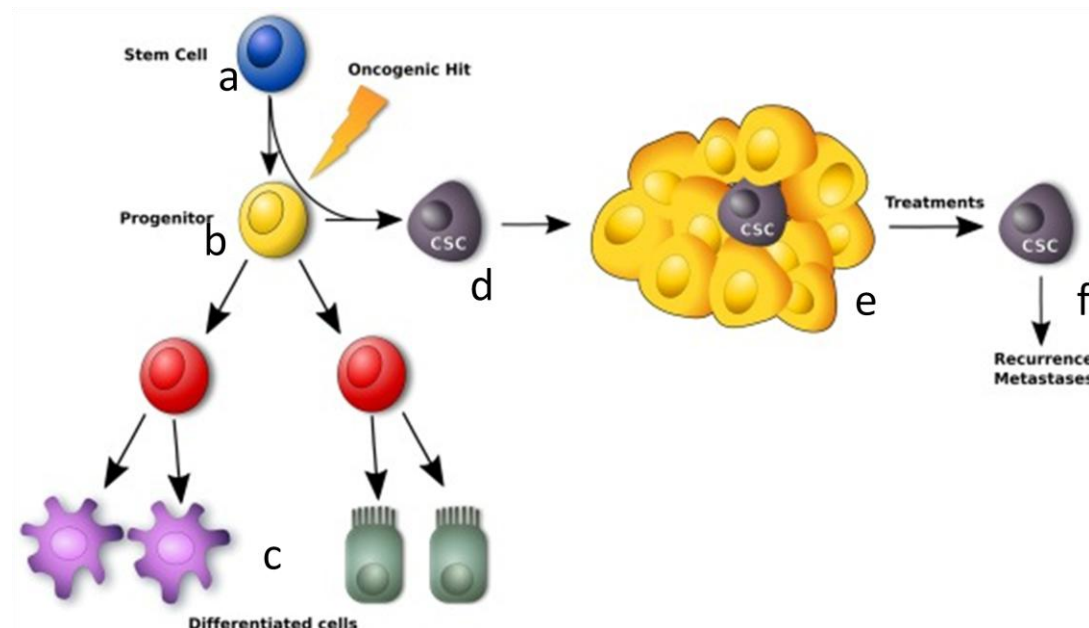
Figure 1.3 Cell origins of cancer from CSCs

In normal state, progenitor cells as immediate descendants of stem cells would differentiate into well-differentiated cells (a→b→c). CSCs originated from stem cells or progenitor cells after oncogenic hit and subsequently developed into tumors (a→d→e). Traditional therapy of cancer such as chemotherapy killed differentiated cancer cells instead of CSCs. The remaining CSCs would lead to metastasis or recurrence (f). This figure was adapted from (Papaccio et al., 2017a).

CSCs had the ability to initiate tumors from a limited number of cells after being injected into immunocompromised mice (Economopoulou et al., 2012). According to CSC theory, tumors were derived from mutated tissue stem cells which had an infinite capability of self-renewal. After generating daughter cells from asymmetrical division, one daughter cell kept the intrinsic ability of initiating tumors while the other would differentiate and proliferate into tumors. As a result, in tumor, there were a small population of CSCs remaining with stem cell like properties and a large number of cancer cells undergoing rapid proliferation (Wicha et al., 2006).

This small population of CSCs showed very high invasive property, clonal evolution, and dormancy. They were also demonstrated to be capable of promoting blood vessel formation. Besides the capability of triggering tumorigenesis, CSCs could also contribute to cancer progression, metastasis and recurrence (Economopoulou et al., 2012). Surface markers like $CD44^{+}/CD24^{-/low}$ and aldehyde dehydrogenase 1 high ($ALDH^{hi}$) were employed as surface markers of breast CSCs (Al-Hajj et al., 2003; Ginestier et al., 2007). The proposal of CSC theory provided novel insights on how cancer initiated, and more importantly, how cancer could be treated and eventually eradicated in the future.

1.1.1.3 Breast cancer metastasis

Approximately 90% of cancer-related deaths were caused by cancer metastases (Spano et al., 2012). Metastasis was a complicated multistep biological event that involved a number of signaling pathways. Patients with metastatic disease had poor prognosis of only 25% 5-year overall survival rate (Rabbani and Mazar, 2007). Cancer metastasis required cancer cells from primary tumor to spread to distant organs where they could attach and proliferate into neoplastic foci (Steeg, 2006). The traditional "seed and soil" theory of cancer metastasis was first proposed in 1889 by Stephen Paget (Paget, 1989). The cascade of metastasis events happened through the following steps as shown in Figure 1.4, mainly through two opposite processes: epithelial-mesenchymal transition (EMT) and mesenchymal-epithelial transition (MET).
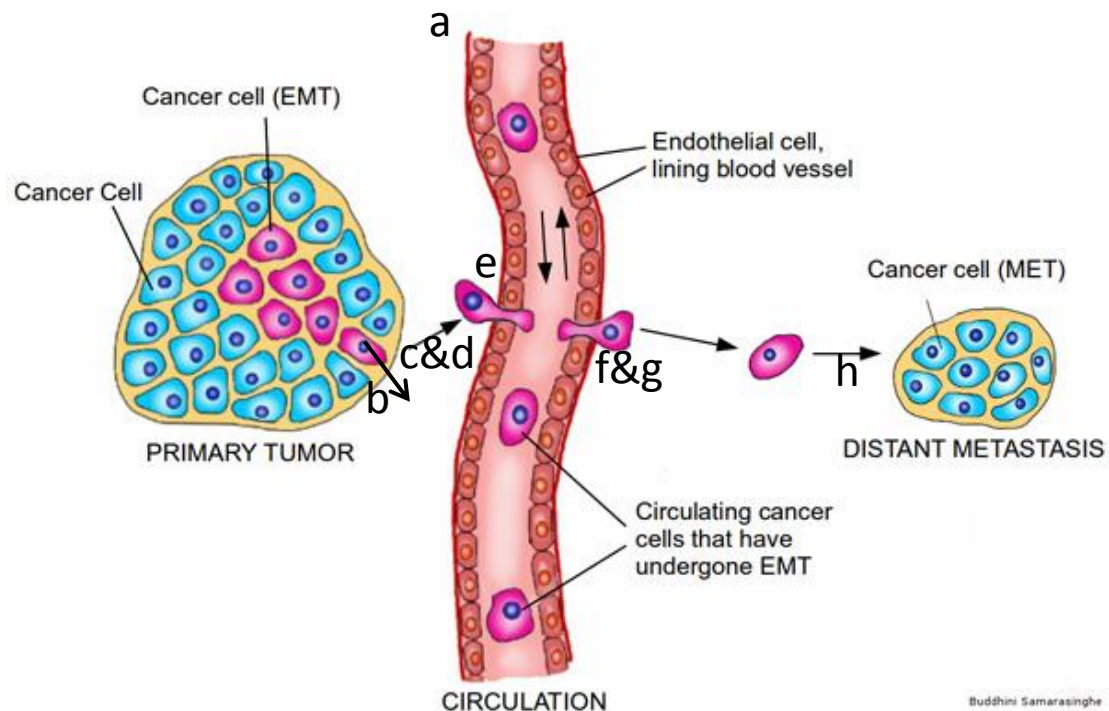
Figure 1.4 EMT and MET processes of cancer metastasis

Cancer cells from the primary tumor migrated to the distant metastatic site through the following processes (Kozlowski et al., 2015): a) angiogenesis, b) escape of tumor cells from the primary tumor, c) migration through the basement membrane and the extracellular matrix around the tumor, d) invasion through the basement membrane of local blood vessels or lymphatics, e) intravasation of the tumor cells into blood or lymphatic vessels, f) homing of circulating tumor cells onto the endothelium of capillaries of distant organs, g) extravasation of tumor cells through endothelial cells, basement membrane and tissue of target organs, h) colonization of tumor cells at the secondary neoplastic foci. This figure was adapted from (Samarasinghe, 2013).

Recent evidence strongly suggested that CSCs played an important role in metastasis. Only a small population of circulating tumor cells (CTCs) were sufficient to initiate metastasis, but the identification of this subpopulation of cells remained elusive (Weiss, 1990).

Since CSCs had the ability to initiate tumor (Economopoulou et al., 2012),

it was reasonable to hypothesize that CSCs were actually the very small subpopulation of CTCs, with increasing evidence supporting this hypothesis.

Firstly, data of 226 blood samples from cancer patients indicated the majority of the CTCs exhibited EMT and CSC properties (Aktas et al., 2009). Additional study of 1439 CTCs identified from 20 out of 30 patients suggested that 35.2% of the CTCs exhibited a $CD44^+/CD24^{-/low}$ breast CSC phenotype (Theodoropoulos et al., 2010) and these $CD44^+/CD24^{-/low}$ CSCs favored distant metastasis especially bone metastasis (Abraham et al., 2005). Moreover, $CD44^+/CD24^{-/low}$ breast CSCs were found to be prevalent in metastatic pleural effusions from patients with late-stage or recurrent breast cancer (Yu et al., 2007). Lastly, in an immunohistochemistry study of 50 bone marrow specimens from breast cancer patients, the percentage of $CD44^+/CD24^{-/low}$ CSCs was significantly increased from <10% in primary tumor to 72% in bone marrow (Balic et al., 2006).

1.1.1.4 Classification of breast cancer

1.1.1.4.1 Histopathological classification of breast cancer

WHO recommended breast tumor to be classified from a histopathological point of view. In the latest 4th edition of *WHO Classification of Tumor of the Breast*, breast tumor was mainly divided

into the following categories: epithelial tumors, mesenchymal tumors, fibroepithelial tumors, metastatic tumors and etc.

The largest category, epithelial tumor, could be further divided into several subcategories: invasive breast carcinoma, epithelial-myoepithelial tumors, precursor lesions, intraductal proliferative lesions, papillary lesions, and benign epithelial proliferations. WHO classification of breast tumor was very thorough and detailed; while some of the subtypes of breast tumors were not very common. The most common breast carcinomas were described in the following parts.

Invasive ductal carcinoma (IDC), the most common subtype of invasive breast carcinoma, accounted for 40-75% of breast cancer upon diagnosis (Sunil R. Lakhani, 2012). Ductal carcinoma *in situ* (DCIS) was another major subgroup of breast carcinoma which falled into the category of precursor lesions. It was a noninvasive, potentially malignant, intraductal proliferation of epithelial cells confined to the ducts and lobules. Death caused by DCIS was extremely rare, usually due to the undetected invasive component or recurrence (Makki, 2015; Sunil R. Lakhani, 2012).

1.1.1.4.2 Molecular classification of breast cancer

Heterogeneity in breast cancer was very common and it can potentially affect the effectiveness of breast cancer therapy. Intra- and inter-tumor

heterogeneity were frequently seen in breast cancer as a result of genetic or non-genetic alterations which potentially enhanced the malignancy of cancer cells (Koren and Bentires-Alj, 2015). There were many factors that might contribute to the heterogeneity of breast cancer, such as differentiation state of cell-of-origin, cell plasticity and tumor cell hierarchy and genetic evolution (Koren and Bentires-Alj, 2015).

A distinctive "molecular portrait" of breast cancer was discovered after analyzing 456 cDNA clones of different breast cancer subtypes (Table 1.1) (Dai et al., 2015).

Table 1.1 A summary of breast cancer molecular subtypes

Intrinsic subtype	IHC status	Grade	Outcome	Prevalence
Luminal A	ER+/PR+, HER2-, Ki67-	1/2	Good	23.7%
Luminal B	ER+/PR+, HER2-, Ki67+	2/3	Intermediate	38.8%
	ER+/PR+, HER2+, Ki67+		Poor	14%
HER2 overexpression	ER-/PR-, HER2+	2/3	Poor	11.2%
Basal	ER-/PR-, HER2-, basal marker+	3	Poor	12.3%
Normal-like	ER+/PR+, HER2-, Ki67-	1/2/3	Intermediate	7.8%

IHC: immunohistochemistry; ER: estrogen receptor; PR: progesterone receptor; HER2: human epidermal growth factor receptor 2; Ki67: cellular marker for proliferation. This table was adapted from (Dai et al., 2015).

Luminal subtype of breast cancer

ER expression played a major role in determining the potential response to hormone therapy of breast cancer. Hormone-dependent and ER-positive luminal subtype of breast cancer accounted for

approximately 70% of all breast cancer cases (Lumachi et al., 2013). They could be treated relatively easily with endocrine therapy and usually with better outcomes. With the development of microarray technology, breast cancer could be classified according to gene expression profiling, which was especially useful for identifying markers associated with good prognosis (Dai et al., 2015).

Sørlie et al reported the data reanalysis of the molecular portraits of 456 cDNA clones of breast cancer (Sorlie et al., 2001). A total of 23.7% of the patient cohort of the luminal A subtype of breast cancer expressed higher level of ER-related genes and a lower level of proliferative genes compared with patients of the luminal B subtype of breast cancer. The luminal A subtype breast cancer correlated with a lower grade exhibited the best outcome among all the subtypes of breast cancer. Luminal B (38.8%) and Luminal B-like (14%) cancers with Ki67-positive expression showed intermediate to poor outcome involving higher grades (Table 1.1) (Dai et al., 2015).

HER2-positive breast cancer

The HER2-positive subtype of breast cancer was ER- and PR- negative with an incidence rate of 11.2% of all breast cancer cases (Table 1.1). It was more likely to be Grade 3 breast cancer with poor prognosis. Fortunately, this subtype of tumor was sensitive to chemotherapy with a much higher response rate compared to luminal breast cancer (Brenton

et al., 2005). There were more treatment options for HER2 positive cases than triple negative breast cancer such as trastuzumab, an antibody against HER2, which was effective against HER2-positve breast cancer (Dai et al., 2015).

Triple negative or basal-like breast cancer

Triple negative breast cancer (ER⁻, PR- and HER2⁻) accounted for 10-17% of all breast cancer cases (Badve et al., 2011). Missing these receptors made this type of cancer the most difficult to treat. This type of cancer was more frequently found among younger patients (<50 years old) and was much more aggressive and has poorer prognosis than any other types of breast tumors (Badve et al., 2011).

The exact definition of basal-like breast cancer was controversial since some groups define it using the microarray-based expression profiling while others use immunohistochemical markers as surrogate markers. From an immunohistochemical point of view, basal-like breast cancer should be missing ER, PR or HER2 and has a high level of basal-like markers such as CK5/6 and epidermal growth factor receptor (Badve et al., 2011). Approximately 71% of triple-negative breast cancer was of basal subtype according to gene expression profiling and 77% of the basal subtype of breast cancer was determined as triple-negative (Bertucci et al., 2008). Triple-negative breast cancer and basal-like breast cancer were often used as synonymous since they shared numerous

similarities (Badve et al., 2011).

1.1.1.4.3 TNM classification of breast cancer

Since the introduction of the Tumor Node Metastasis (TNM) system by Pierre Denoix in the 1940s, TNM has been providing an invaluable means to describe the anatomic extent of cancer and to determine its stages (Cserni et al., 2018). Unlike the anatomical classification based on histology or molecular gene expression profiling, TNM classified tumors by clinical presentation such as primary tumor, feature of regional lymph nodes and distant metastasis of tumors (Sunil R. Lakhani, 2012). The 4th edition of WHO Classification of Tumor of the Breast was shown in Figure 1.5 (Sunil R. Lakhani, 2012).

T – Primary tumour

TX   Primary tumour cannot be assessed
T0   No evidence of primary tumour
Tis   Carcinoma in situ
Tis (DCIS)   Ductal carcinoma in situ
Tis (LCIS)   Lobular carcinoma in situ
Tis (Paget)   Paget disease of the nipple not associated with invasive carcinoma and/or carcinoma in situ (DCIS and/or LCIS) in the underlying breast parenchyma.

Note: Carcinomas in the breast parenchyma associated with Paget disease are categorized based on the size and characteristics of the parenchymal disease, although the presence of Paget disease should still be noted.

T1   Tumour 2 cm or less in greatest dimension
T1mi   Microinvasion 0.1 cm or less in greatest dimension*

Note: *Microinvasion is the extension of cancer cells beyond the basement membrane into the adjacent tissues with no focus more than 0.1 cm in greatest dimension. When there are multiple foci of microinvasion, the size of only the largest focus is used to classify the microinvasion. (Do not use the sum of all individual foci.) The presence of multiple foci of microinvasion should be noted, as it is with multiple larger invasive carcinomas.

T1a   More than 0.1 cm but not more than 0.5 cm in greatest dimension
T1b   More than 0.5 cm but not more than 1 cm in greatest dimension
T1c   More than 1 cm but not more than 2 cm in greatest dimension
T2   Tumour more than 2 cm but not more than 5 cm in greatest dimension
T3   Tumour more than 5 cm in greatest dimension
T4   Tumour of any size with direct extension to chest wall and/or to skin (ulceration or skin nodules)

Note: Invasion of the dermis alone does not qualify as T4. Chest wall includes ribs, intercostal muscles, and serratus anterior muscle but not pectoral muscle.

T4a   Extension to chest wall (does not include pectoralis muscle invasion only)
T4b   Ulceration, ipsilateral satellite skin nodules, or skin oedema (including peau d'orange)
T4c   Both 4a and 4b, above
T4d   Inflammatory carcinoma

Note: Inflammatory carcinoma of the breast is characterized by diffuse, brawny induration of the skin with an erysipeloid edge, usually with no underlying mass. If the skin biopsy is negative and there is no localized measurable primary cancer, the T category is pTX when pathologically staging a clinical inflammatory carcinoma (T4d). Dimpling of the skin, nipple retraction, or other skin changes, except those in T4b and T4d, may occur in T1, T2, or T3 without affecting the classification.

N – Regional lymph nodes

NX   Regional lymph nodes cannot be assessed (e.g. previously removed)
N0   No regional lymph-node metastasis
N1   Metastasis in movable ipsilateral level I, II axillary lymph node(s)
N2   Metastasis in ipsilateral level I, II axillary lymph node(s) that are clinically fixed or matted; or in clinically detected* ipsilateral internal mammary lymph node(s) in the absence of clinically evident axillary lymph-node metastasis
N2a   Metastasis in axillary lymph node(s) fixed to one another (matted) or to other structures
N2b   Metastasis only in clinically detected* internal mammary lymph node(s) and in the absence of clinically detected axillary lymph-node metastasis
N3   Metastasis in ipsilateral infraclavicular (level III axillary) lymph node(s) with or without level I, II axillary lymph-node involvement; or in clinically detected* ipsilateral internal mammary lymph node(s) with clinically evident level I, II axillary lymph-node metastasis; or metastasis in ipsilateral supraclavicular lymph node(s) with or without axillary or internal mammary lymph node involvement
N3a   Metastasis in infraclavicular lymph node(s)
N3b   Metastasis in internal mammary and axillary lymph nodes
N3c   Metastasis in supraclavicular lymph node(s)

Note: * "Clinically detected" is defined as detected by clinical examination or by imaging studies (excluding lymphoscintigraphy) and having characteristics highly suspicious for malignancy or a presumed pathological macrometastasis based on fine-needle aspiration biopsy with cytological examination. Confirmation of clinically detected metastatic disease by fine-needle aspiration without excision biopsy is designated with an (f) suffix, e.g., cN3a(f).
Excisional biopsy of a lymph node or biopsy of a sentinel node, in the absence of assignment of a pT, is classified as a clinical N, e.g., cN1. Pathological classification (pN) is used for excision or sentinel lymph node biopsy only in conjunction with a pathological T assignment.

M – Distant metastasis

M0   No distant metastasis
M1   Distant metastasis

Figure 1.5 TNM classification of tumors of the breast

TNM classified tumors by primary tumor size, feature of regional lymph nodes, and distant metastasis of tumors. This figure was adapted from (Sunil R. Lakhani, 2012).

1.1.1.5 Treatment of breast cancer

1.1.1.5.1 General treatment of breast cancer

General treatment of breast cancer included local treatment such as surgery and radiation, systematic treatment such as chemotherapy, hormone therapy and molecular targeted therapy. The choice of treatment of breast cancer depended on the stage, molecular portrait and aggressiveness of the disease.

Newly-diagnosed non-metastatic breast cancer cases could be divided into two categories: early stage (I, IIA, T2N1) and locally advanced stage (T3N0, IIIA to IIIC) (Alphonse Taghian, 2017). Early-stage cases should undergo primary surgery followed by an optional radiation therapy. Adjuvant systemic therapy might be offered depending on primary tumor characteristics. Patients who were diagnosed with locally advanced breast cancer would receive neoadjuvant systemic therapy to induce tumor response before surgery. After the primary surgery, the choice of adjuvant therapy (chemotherapy and/or endocrine therapy) was guided by the clinical status and the characteristics of the tumor.

Approximately 5% of breast cancer patients were diagnosed with metastasis at the initial presentation. Metastatic breast cancer was very difficult to treat so the main goal of treatment was to prolong survival, alleviate symptoms and improve the quality of life. Treatment of

metastatic breast cancer was a far more complicated task compared to non-metastatic ones.

Daniel F Hayes has provided a thorough review of the treatments of metastatic breast cancer (Hayes, 2018). In this review, disease assessment of breast cancer was a very important procedure that would guide the whole process of treatment. Biological markers such as ER, PR and HER2 overexpression should be evaluated before treatment. There might be discordance of these markers between the primary tumor and the metastatic one, which would lead to dramatic changes in therapy option. Treatment selection could be made after disease assessment.

1.1.1.5.2 Endocrine therapy of breast cancer

Endocrine therapy was the best choice for hormone receptor-positive cases because of the fewer side effects compared to chemotherapy. Tamoxifen, a nonsteriodal estrogen agonist was approved by US Food and Drug Administration to treat metastatic breast cancer in postmenopausal females in the 1970s (Robert, 1997). Extensive research suggested that 5-year tamoxifen treatment was the backbone of adjuvant hormonal therapy, especially for premenopausal cases (Jankowitz and Davidson, 2013).

In postomenopausal females, estrogen was predominantly synthesized from nonglandular sources through aromatase. As a result, aromatase

inhibitors were especially important for postomenopausal cases. Treatment with Letrozole, a nonsteriodal aromatase inhibitor had a better 5-year overall survival rate compared to tamoxifen treatment (Tremont et al., 2017). Endocrine therapy has been considered as a standard choice for ER-positive patients or older patients unfit for aggressive chemotherapy regimens (Lumachi et al., 2011).

1.1.1.5.3 HER2-targeted therapy of breast cancer

HER2-targeted therapy was an important targeted therapy for first-line treatment to improve survival of HER2-positive patients. Tyrosine kinase inhibitor such as lapatinib bound to the intracellular ATP-binding pocket of the protein kinase domain of HER2. Lapatinib regulated tumor cell growth by inhibiting the phosphorylation of the cytoplasmic domain of HER2 (Schramm et al., 2015). Another HER2-targeting drug was monoclonal antibody such as trastuzumab that interacted with the extracellular subdomain IV of HER2. Trastuzumab inhibited tumor cell proliferation and angiogenesis by blocking the ligand-independent HER2 signaling pathway (Schramm et al., 2015).

1.1.1.5.4 Chemotherapy of breast cancer

To patients who were hormone receptor negative or those who were hormone receptor positive but did not respond to endocrine therapy,

chemotherapy was the only remaining choice. Hormone receptor positive cases could occasionally progress rapidly with metastases. Since chemotherapy would induce higher response rates than endocrine therapy, first-line chemotherapy would still be a better choice for stabilizing this kind of cases before switching to other maintenance therapy.

Doxorubicin, one of the clinically used anthracyclines, was one of the most active cytotoxic agents in treating metastatic breast cancer but inevitably causing cardiotoxicity (Tan et al., 1973).

Paclitaxel was another effective drug for treating breast cancer. It suppressed breast tumor growth by binding to microtubules and subsequently stabilizing them by inhibiting depolymerization, which lead to a mitotic arrest (Schiff et al., 1979). It was approved by the US Food and Drug Administration for the treatment of metastatic cases which did not respond to anthracycline-based combination chemotherapy or relapse in less than six months after adjuvant therapy (Rowinsky and Donehower, 1995).

The widespread uses of adjuvant systemic therapy such as endocrine therapy, HER2-targeted therapy and chemotherapy has contributed to a dramatic reduction in overall mortality rate of breast cancer.

1.1.1.6 Breast cancer recurrence

1.1.1.6.1 CSC and breast cancer recurrence

Breast cancer recurrence was a serious problem and was responsible for the majority of cancer-related deaths (Moody et al., 2005). Recurrence occurred 5 to 20 years after endocrine treatment. The rate of distant recurrence was strongly correlated with the TN status when the disease was first diagnosed (Pan et al., 2017). The mechanism behind breast cancer recurrence and the possible strategies to stop it remained elusive. There was a strong correlation between CSC and chemoresistance, radioresistance and relapse. CSCs were intrinsically resistant to chemotherapy (Li et al., 2008c). After a 12-week chemotherapy, there was a great increase in CSC markers (CD44^{+}/CD24$^{-/low}$) in breast tumor core biopsies (Chang et al., 2005). Ionizing radiation could also induce breast CSC properties such as increased mammosphere formation, tumorigenicity and elevated expression of CSC markers (Lagadec et al., 2012).

In summary, both chemotherapy and radiotherapy selectively enriched CSCs, resulting in chemoresistance, radioresistance and metastasis (Figure 1.6). Targeting CSCs could be a possible way to reduce metastasis and relapse.
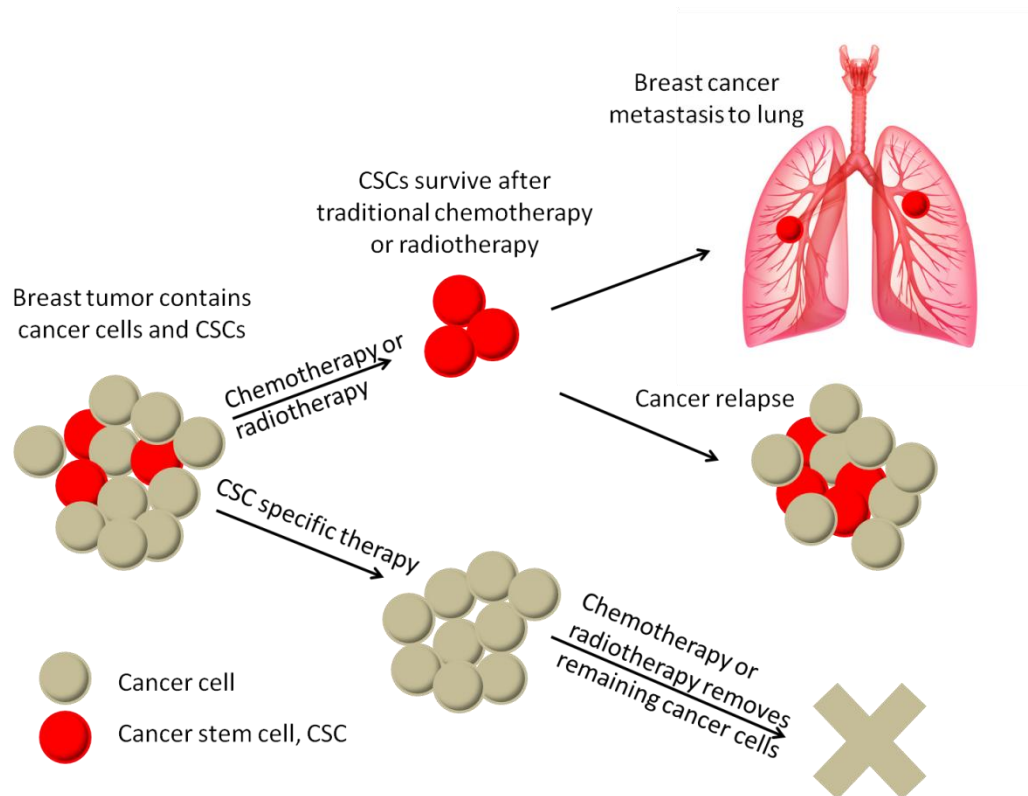
Figure 1.6 CSCs lead to breast cancer recurrence

Targeting CSCs together with traditional chemotherapy might reduce metastasis and relapse. Traditional cytotoxic chemotherapy or radiotherapy could not remove CSCs, which would lead to cancer relapse or metastasis to distant organs. CSC specific therapy combined with traditional chemotherapy or radiotherapy might eradicate cancer. Red cells: CSCs; Grey cells: differentiated cancer cells.

1.1.1.6.2 EMT lead to breast cancer recurrence

Breast cancer recurrence could also be explained by epithelial mesenchymal transition. The EMT process (Figure 1.4) has been demonstrated to be involved in antagonizing chemotherapy in breast cancer.

Slug, as a transcription factor of E-cadherin, also served as a

mesenchymal marker of EMT and was found to be transcriptionally activated in paclitaxel-, docetaxel- and doxorubicin-resistant breast cancer sublines (Iseri et al., 2011). Immunohistochemistry staining of breast cancer tissues showed that Snail was highly correlated with breast cancer resistant protein (BCRP).

Moreover, overexpression of E-cadherin in MCF7 cell line induced BCRP (Chen et al., 2010). The EMT-inducing transcription factor, zinc finger E-box binding homeobox 1 (ZEB1) was demonstrated to be a regulator of radiosensitivity. Radio-resistant breast cancer cells showed upregulation of ZEB1, which by itself can promote tumor cell radio-resistance both *in vitro* and *in vivo* (Zhang et al., 2014). All these findings indicated that EMT process was closely associated with chemoresistance and radioresistance.

There was a direct link between EMT and CSCs. Induction of EMT in immortalized human mammary epithelial cells would not only lead to the acquisition of mesenchymal traits but also an increase in CSC markers and an increase in mammosphere formation. On the other hand, stem-like cells isolated from breast carcinomas expressed high level of mesenchymal markers (Mani et al., 2008).

1.1.2 SND1

SND1 (Staphylococcal nuclease domain-containing protein 1) is a

multifunctional protein with diverse functions. It regulates gene expression at both transcriptional and post-transcriptional levels (Jariwala et al., 2015a). It is a multifunctional protein with numerous binding partners. In addition, it is a key component of RNA-induced silencing complex (RISC) with nuclease activity (Gutierrez-Beltran et al., 2016).

SND1 is found to be overexpressed in breast, prostate, lung, colorectal and hepatocellular carcinomas and malignant glioma (Jariwala et al., 2015a; Xing et al., 2018). Apart from its multifunctional role in normal cells, SND1 also plays different roles in carcinogenesis, making it a very attractive target for cancer treatment.

1.1.2.1 Identification of SND1

SND1 was initially identified in 1995 as a transcription co-activator by interacting with transcription activator Epstein-Barr virus nuclear antigen 2 (EBNA2) which was involved in B-lymphocyte transformation. SND1 was found to bind with the acidic domain of EBNA2 (Tong et al., 1995).

1.1.2.2 Structure of SND1

1.1.2.2.1 Secondary structure of SND1

SND1 was evolutionarily conserved. Human SND1 gene was found at chromosome 7q31.3 (Jariwala et al., 2015b). SND1 sequence contained

four similar domains with a 20-33% sequence identity to staphylococcal nuclease (SN) (Figure 1.7) (Callebaut and Mornon, 1997; Chesneau and Elsolh, 1994). The fifth domain of SND1 was named as "tudor domain", a highly modified nuclease domain originally found in the tudor protein, which was required during oogenesis for the establishment of a functional posterior organizing center in *Drosophila melanogaster* (Figure 1.7) (Callebaut and Mornon, 1997). Different parts of SND1 had different functions by interacting with diverse binding partners.
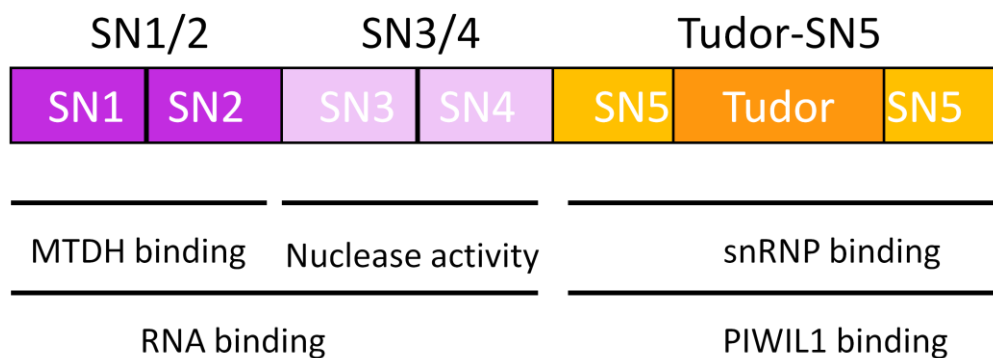
Figure 1.7 Schematic representation of the secondary structure of SND1

SND1 was composed of 5 domains, including 4 tandem repeats of SN domains and a Tudor-SN5 domain. Different parts of SND1 were identified with different functions. SN1/2 domain interacted with Metadherin (MTDH). SN3/4 domain showed nuclease activity. SN1-4 domain had RNA binding activity. Tudor-SN5 domain interacted with snRNP and Piwi-like protein 1 (PIWIL1).

1.1.2.2.2 Crystal structure of SND1 and its associated-functions

SND1 was an important component of RISC complex (Caudy et al., 2003b; Yoo et al., 2011c) and its nuclease activity was similar to that of other

staphylococcal nuclease because it recognized nucleic acid through the conserved oligosaccharide-binding-fold domain in its structure (Theobald et al., 2003).

Tudor-SN5 domain of SND1 interacted with small nuclear ribonucleoprotien (snRNP), suggesting that SND1 was involved in the processing of precursor mRNA.

SND1 interacted with PIWIL1 in an arginine methylation-dependent manner, especially with a preference for symmetrically dimethylated arginine. The co-crystal structure of tudor-SN5 domain and PIWIL1 peptides (PDB code: 3OMC) revealed an extended Tudor domain of SND1 accommodating the distinct symmetrically dimethylated arginine of PIWIL1 through an aromatic cage (Liu et al., 2010).

Besides, the four N-terminal tandem repeats of SND1, especially SN3/4 domain, were required for RNA binding and cleavage. A crystal structure (PDB code: 3BDL) of SN3, SN4 and Tudor domain of SND1 was solved revealing a concave basic surface formed by SN3/4 domain, likely to be involved in RNA binding (Figure 1.8) (Li et al., 2008a).
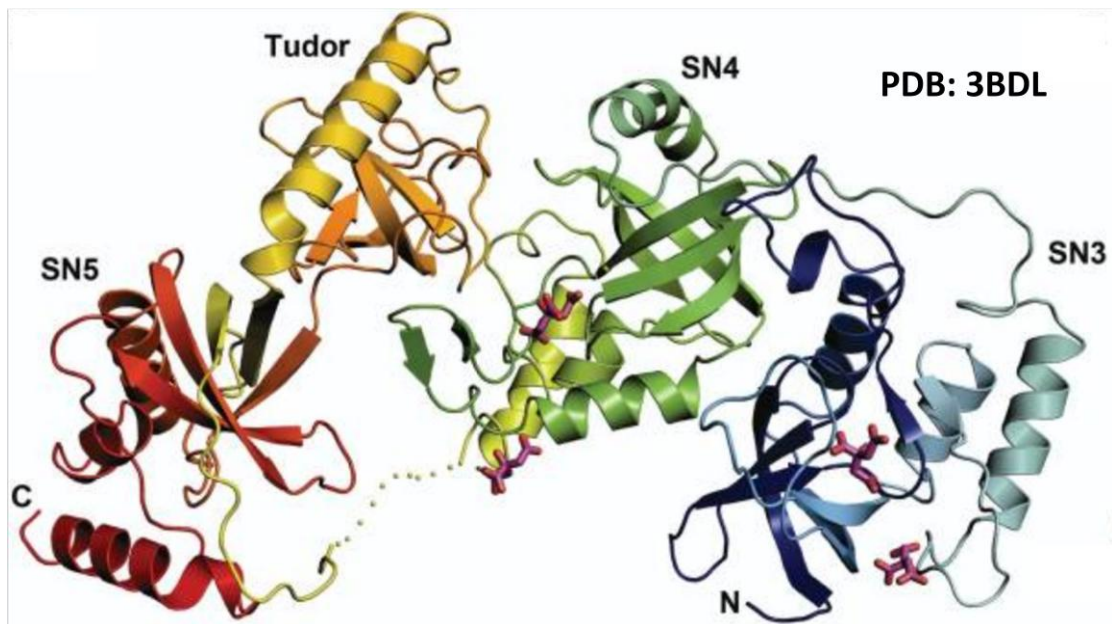
Figure 1.8 Ribbon model of the crystal structure of SN3/4-Tudor-SN5 domains of SND1 (PDB: 3BDL)

The Tudor domain (yellow) was inserted in SN5 (red) and packed between SN4 (green) and SN5 (red). This figure was adapted from (Li et al., 2008a)

SND1 interacted with MTDH, an important protein involved in many oncogenic processes (Lee et al., 2013). A co-crystal structure of the SN1/2 domain of SND1 and an 11-residue MTDH peptide (PDB: 4QMG) revealed that MTDH peptide occupied an extended groove between SN1 and SN2 domains of SND1 with two tryptophans (W394 and W401) nestled into two well-defined hydrophobic binding pockets (Figure 1.9). These two important tryptophans played major roles in MTDH-SND1 interaction and cancer cell survival. In addition, the long protruding arms and deep surface valleys at the back side of binding interface on SND1, might be involved in the interactions with other binding partners (Guo et al., 2014; Wan et al., 2014).
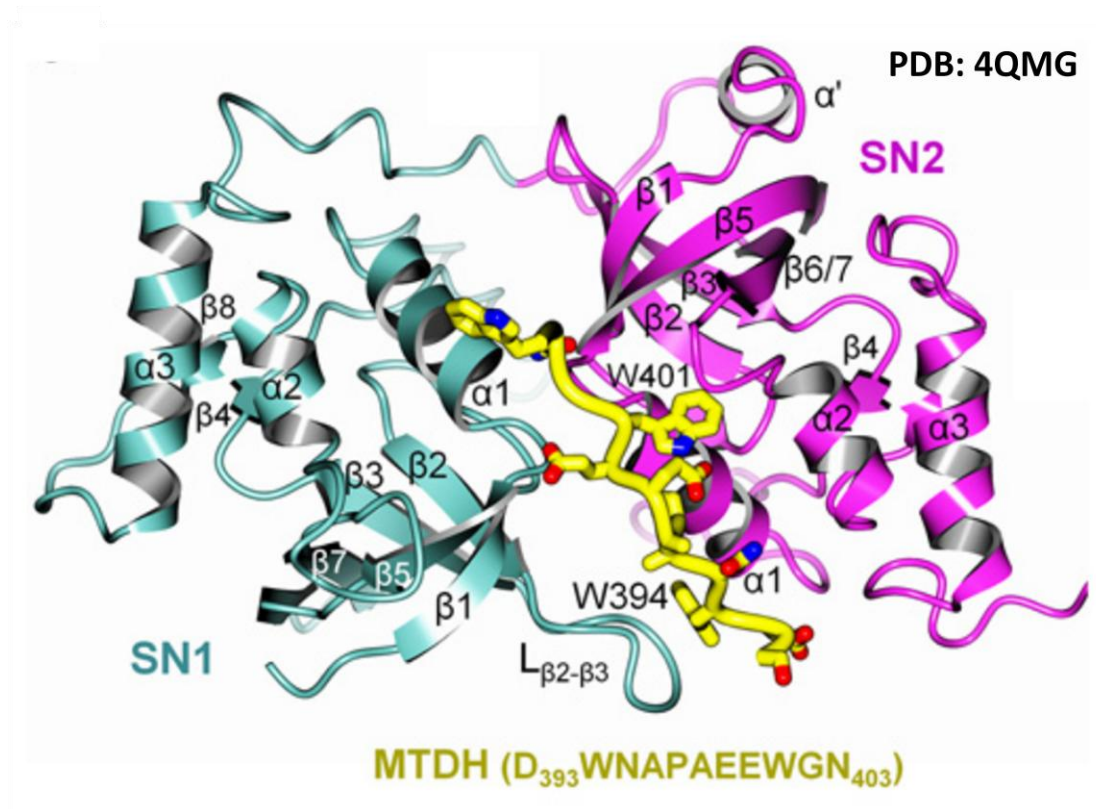
Figure 1.9 Co-crystal structure of SN1/2 domain of SND1 with an 11-residue MTDH peptide (PDB: 4QMG)

Green structure represented SN1 domain of SND1; Purple structure represented SN2 domain of SND1; Yellow linear structure represented MTDH 11-residue peptide (sequence: DWNAPAEEWGN). W394 and W401 in MTDH sequence were very important amino acids in MTDH binding to SND1. Lβ2-β3 was an essential loop in MTDH-SND1 binding. This loop was the major difference between SN1/2 domain and SN3/4 domain, which explained why MTDH interacted with SN1/2 rather than SN3/4 domain of SND1. This figure was adapted from (Guo et al., 2014)

1.1.2.3 Multifunctional roles of SND1

1.1.2.3.1 SND1-mediated regulation of transcription

SND1 as a transcriptional coactivator of EBNA2

SND1 was first identified to be p100, a coactivator specifically binding to the acidic domain of EBNA2. EBNA2 was critical for Epstein-Barr virus in transforming B-lymphocyte. Overexpression of SND1 in B-lymphocytes specifically augmented EBNA2 acidic domain-mediated activation. The co-activating effect was probably mediated by p100 interacting with TFIIE. (Tong et al., 1995).

SND1 as a transcriptional coactivator of c-Myb

C-Myb was a transcriptional activator involved in the regulation of cell proliferation, differentiation, and apoptosis. c-Myb was also a regulatory protein in various types of proliferating cells such as immature hematopoietic cells (Ness, 1996). c-Myb could interact with SND1, which could enhance the transcriptional activation of the c-Myb downstream genes like Pim-1 (Dash et al., 1996). Pim-1 was a serine/threonine protein kinase and its interaction with SND1 was identified through yeast two-hybrid screen. SND1-Pim complex functioned as a downstream of Ras to stimulate c-Myb transcriptional activity in a SND1-dependent manner (Leverson et al., 1998).

SND1 as a transcriptional coactivator of STAT family

SND1, as a transcriptional coactivator, was also found to interact with a class of transcription factors: the signal transducer and activator of transcription (STATs) family (Jariwala et al., 2015a). SND1 could interact with STAT6, an important mediator of IL-4-regulatory pathway.

SND1-STAT6 interaction was mediated by the TAD domain of STAT6 and the SN-like domain of SND1. SND1 enhanced STAT6-mediated transcriptional activation and the IL-4-induced Ig epsilon gene transcription in human B-cell line. In addition, SND1 was found to be associated with the large subunit of RNA polymerase II and could mediate the interaction between STAT6 and RNA polymerase II (Yang et al., 2002).

SND1 could mediate the interaction between STAT6 and CBP, a co-activator for STAT-mediated gene activation. Chromatin immunoprecipitation (CHIP) study revealed that SND1 could enhance the STAT6-SND1-CBP ternary complex formation in the human Ig epsilon promoter. SND1 was also demonstrated to increase acetylated histone H4 at the Ig epsilon promoter region (Valineva et al., 2005). Physical interaction was identified between SND1 and another member of STAT family STAT5 and their interaction was mediated through both the SN and the tudor domain of SND1. SND1 also functioned as a transcriptional coactivator of STAT5 dependent gene regulation (Paukku et al., 2003).

SND1 as a transcriptional coactivator of Smads

Transforming growth factor β (TGFβ) signaling activation was a hallmark event in the process of cancer metastasis, which regulated the expression of series of genes involved in tumor invasion and migration. The TGFβ pathway was mediated by different R-Smads (Smad1, Smad2,

Smad3 and Smad5) and Co-Smad (Smad4) transcription factors (Yu et al., 2017). It was recently demonstrated that SND1 physically interacted with histone acetylase and recruited it to the promoter regions of Smad2/3/4, thereby enhancing the gene transcriptional activation of Smad2/3/4. Smad2/3/4 were critical downstream regulators in the TGFβ1 pathway, which promoted metastasis of breast cancer (Yu et al., 2017).

1.1.2.3.2 SND1-mediated regulation of post-transcriptional modification

RNA interference (RNAi) was a process that regulated gene expression and the final protein synthesis. RISC was the major machinery that exerted all these functions (Agrawal et al., 2003). SND1 was the first identified RISC subunit that contained a recognizable nuclease domain, which contributed to the RNA degradation observed in RNAi in *Caenorhabditis elegans*, *Drosophila* and mammals (Caudy et al., 2003b). Diverse RISC complexes existed ubiquitously in living organisms but the central components were similar. A member of the Argonaute proteins bound to a small interfering RNA (siRNA) and siRNA guided RISC to its target mRNAs (Figure 1.10) (Pratt and MacRae, 2009).
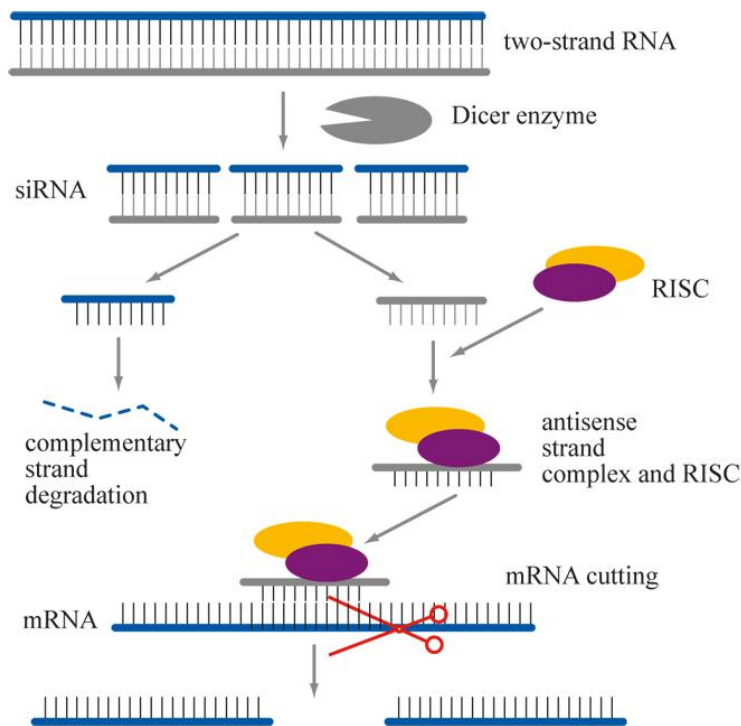
Figure 1.10 The process of RNA interference

Two-stranded RNA was cut by Dicer enzyme, producing siRNAs. Single-stranded siRNA after its complementary strand degradation would combine with RISC to specifically decompose mRNA and prevent translation. This figure was adapted from (Vladimir, 2018).

MTDH, an oncogenic protein found to be overexpressed in different types of cancers (Shi and Wang, 2015), was also demonstrated to be a component of RISC. Both MTDH and SND1 were necessary for the optimal activity of RISC in facilitating siRNA or miRNA-mediated silencing of genes. MTDH and SND1 overexpression induced RISC activation, which might contribute to hepatocarcinogenesis (Yoo et al., 2011c).

1.1.2.3.3 SND1 regulated RNA editing

SND1 was a central component of RISC, but it also played an important

role in an antagonistic pathway, the degradation of I-dsRNAs and pre-I-miRNAs in RNA editing process. Long perfect double-stranded RNA (dsRNA) molecules were important in various cellular pathways. dsRNAs were extensively modified (hyper-editing) by adenosine deaminases that acted on RNA, leading to a conversion of 50% adenosine residues to inosine (I). *X. laevis* SND1 specifically associated with and promoted cleavage of model hyper-edited dsRNA substrates, which contained multiple I·U and U·I pairs (Scadden, 2005). In mammalian cells, SND1 could also degrade pri-miRNA-142 which was edited by ADAR1 and ADAR2 (Yang et al., 2006).

1.1.2.3.4 SND1 regulated mRNA splicing

Spliceosome, a machinery assembled by small nuclear riboncleoproteins (snRNP) and associated protein factors, functioned to splice the precursor mRNA in order to remove introns to produce a mature and functional mRNA (Will and Luhrmann, 2001). The Tudor domain of SND1 has been shown to interact with snRNPs and Sm proteins, thereby facilitating spliceosome complex formation and enhancing splicing rate *in vitro* (Gutierrez-Beltran et al., 2016; Yang et al., 2007). SND1 might be involved in alternative splicing in oncogenic processes (David and Manley, 2010).

1.1.2.3.5 SND1 as a component of stress granule and its stabilizing effect of mRNAs

Stress granules (SGs) were composed of non-translating mRNAs, translation initiation components and many additional proteins affecting mRNA function. It might affect mRNA translation and stability and might be linked to nuclear processes and apoptosis (Buchan and Parker, 2009). SGs also interacted with processing bodies, another cytoplasmic ribonucleoprotein granule to metabolize cytoplasmic mRNA (Decker and Parker, 2012).

The interaction of SND1 with core proteins of SGs, such as Pabp1, eIF4E, eIF5A, TIAR and TIA1 in different organisms, suggested that SND1 was an essential component of these cytoplasmic foci (Gutierrez-Beltran et al., 2016). Besides, SND1 might participate in stress-induction by regulating the aggregation dynamics of poly(A) mRNA-containing SGs selectively facilitating the stabilization of SG-associated mRNAs during cellular stress in mammalian cells (Gao et al., 2015). The SND1-dependent stabilization of specific mRNA might be important for stress adaptation.

1.1.2.4 Role of SND1 in different cancer types

Overexpression of SND1 has been detected in different types of cancers including liver cancer (Yoo et al., 2011c), breast cancer (Yu et al., 2015a), colon cancer (Tsuchiya et al., 2007), prostate cancer (Kuruma et al., 2009),

lung cancer (Xing et al., 2018) and brain tumor (Tong et al., 2016). Overexpression and knockdown of SND1 revealed that SND1 participated in different important process of cancer, such as proliferation, EMT, angiogenesis, and metastasis.

1.1.2.4.1 Roles of SND1 in breast cancer

SND1 overexpression in breast cancer, especially in metastatic regions

Data from 4 cohorts of breast cancers (containing 818-1105 patient samples) from *The Cancer Genome Atlas* (TCGA) indicated that gene amplification of SND1 was not very significant (0.6-1.5%) in breast cancer. Mutation and deletion also existed in breast cancer patient samples (Figure 1.11) (Cerami et al., 2012; Gao et al., 2013). But subsequent studies revealed a much higher percentage of SND1 overexpression in protein level in breast cancer (Blanco et al., 2011; Ho et al., 2009a; Yu et al., 2017; Yu et al., 2015b).
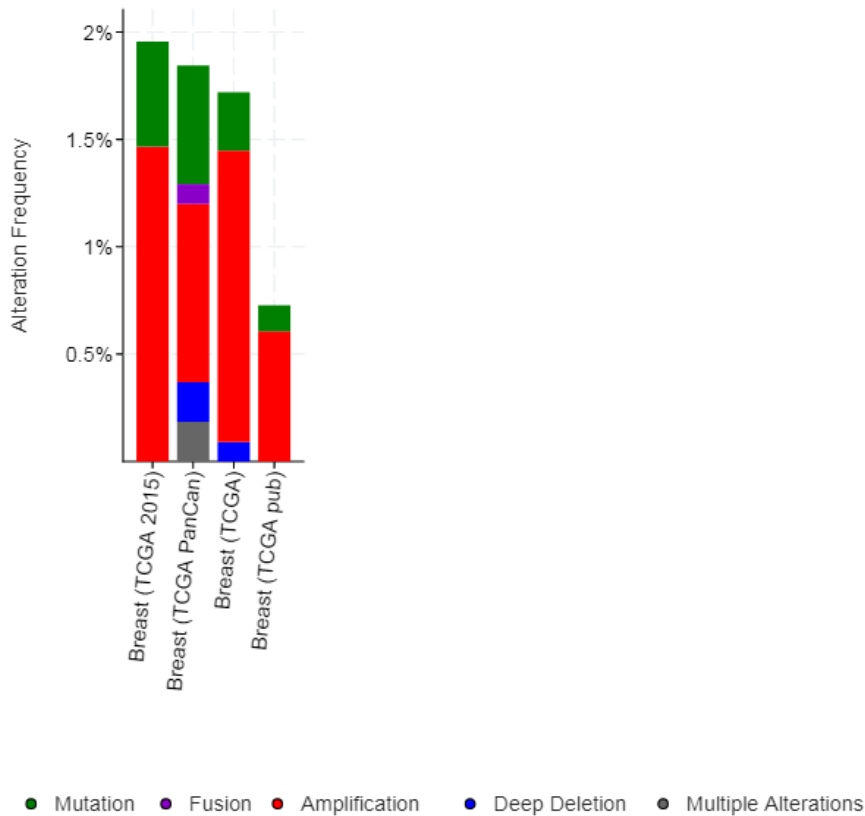
Figure 1.11 Breast cancer genomics data of SND1 (TCGA)

Cancer genomics data from cBioportal analyzing data from 4 separate research of the genomics data of SND1 in invasive breast carcinoma containing 818 (TCGA, Cell 2015), 825 (TCGA, Nature 2012), 1084 (TCGA, PanCancer Atlas) and 1105 (TCGA, Provisional) patient samples (Cerami et al., 2012; Gao et al., 2013).

SND1 was found to be upregulated in breast cancer tissues, particularly in primary invasive ductal carcinomas (Yu et al., 2015b). In order to investigate the relevance of SND1 expression to the invasiveness of breast cancer, immunohistochemical analysis was performed to detect SND1 in primary IDC (Invasive ductal carcinoma) and DC (ductal carcinoma) *in situ* breast tumor compared with normal tissues. The expression of SND1 in the IDC samples was significantly higher than that

in DC *in situ* samples. In IDC samples, SND1 expression was positive in all the 23 studied cases: 78% highly positive and 22% weakly positive (Yu et al., 2015b).

SND1 overexpression was detected in primary breast cancer. However, much higher expression of SND1 was detected in long distant metastatic regions (Yu et al., 2017), which might be the reason of cancer recurrence. By analyzing tissue microarray data derived from 50 matched cases of invasive and metastatic lesions, the expression profiles of SND1 were found to be up-regulated during clinical progression from carcinoma *in situ* to invasive and metastatic carcinomas (Ho et al., 2009b).

In another study investigating the relevance of SND1 expression to breast cancer metastasis, SND1 expression level was detected in primary breast cancer tissue. SND1-positive breast cancer cells (~80%) in lymph-node-positive cases were found to be much more than those in lymph-node-negative cases (~30%) (Yu et al., 2017).

In addition, data reanalysis was conducted on a MSK-82 data set, and the mean expression of SND1 was found to be significantly higher ($p<0.01$, Student's *t* test) in patients who developed lung metastases (Figure 1.12) (Blanco et al., 2011).
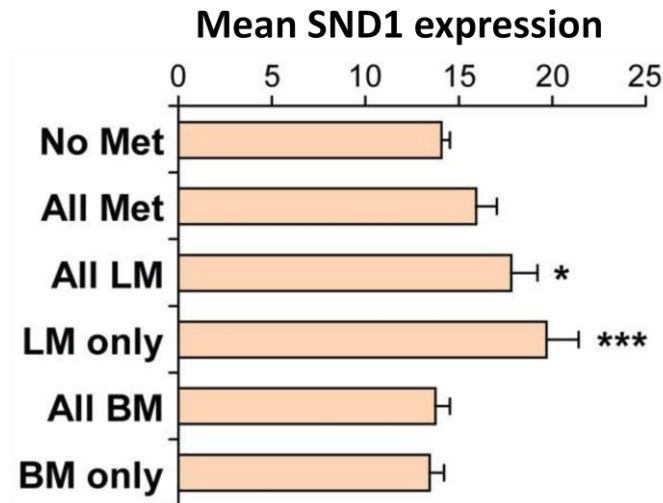
Figure 1.12 High SND1 expression correlated with increased risk of lung metastasis of breast cancer

SND1 expression in the primary breast tumor in MSK-82 data set was shown. No Met: no metastasis; All Met: metastasis to any organ; All LM: lung non-exclusively; LM only: lung exclusively; All BM: bone non-exclusively; BM only: bone exclusively. This figure was adapted from (Blanco et al., 2011).

Poor outcomes of breast cancer patients with SND1 overexpression

Survival time was analyzed using clinical data from 23 breast cancer patients with invasive ductal carcinoma. As shown in Figure 1.13, the median survival time of patients with high SND1 expression (n=18) was found to be significantly shorter (57 months) than those with low SND1 expression (n=5, >107 months, p=0.00306) (Yu et al., 2015b).
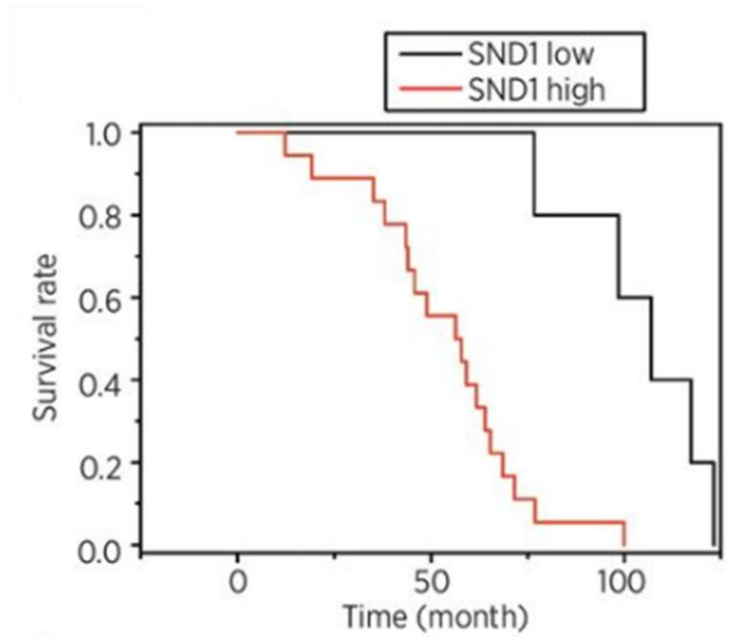
Figure 1.13 Kaplan-Meier survival curves based on SND1 expression in IDC patients

Median survival time was >107 months (n=5) for SND1 low expression patients and 57 months (n=18) for SND1 high expression patients (P=0.00306). This figure was adapted from (Yu et al., 2015b).

After analyzing the data from 1133 breast cancer cases (lymph node positive) with Kaplan-Meier Plotter, patients with high SND1 expression showed significant reduction in the probability of survival (HR=1.26, logrank P=0.021) (Figure 1.14).
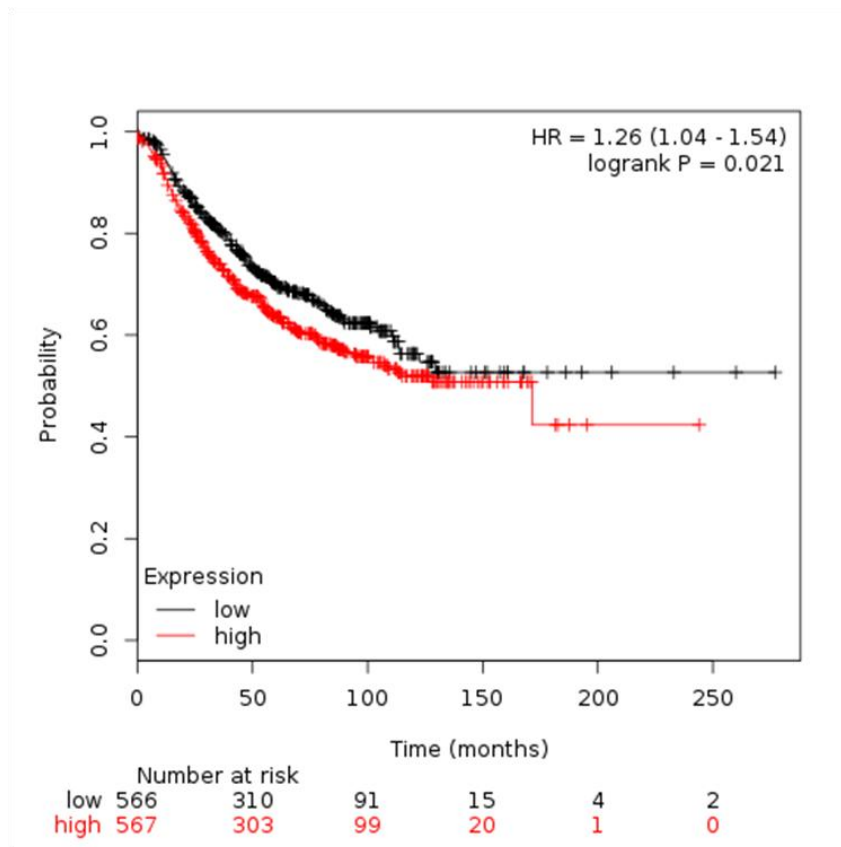
Figure 1.14 Kaplan-Meier survival curves based on SND1 expression in lymph-node-positive breast cancer patients

A total of 1133 lymph-node-positive breast cancer cases were analyzed with Kaplan-Meier Plotter. Probability represented the possibility of survival in a given length of time. SND1 overexpression significantly reduced survival probability of lymph-node-positive breast cancer patients (Gyorffy et al., 2010).

SND1 promoted metastasis in breast cancer

Breast cancer xenograft mouse model showed that knockdown of SND1 slowed down tumor growth *in situ* compared with the scrambled control, indicating SND1 could promote breast cancer tumorigenesis *in vivo* (Yu et al., 2015a).

Several Smad-specific recognition domains which were recognized and

bound by the Smad complex were identified on the promoter region of SND1. Under the control of TGFβ1/Smad pathway, SND1 could promote the expression of E3 ubiquitin ligase Smurf1, leading to RhoA ubiquitination and degradation. The loss of RhoA subsequently disrupted F-actin cytoskeletal organization, reduced cell adhesion and promoted cell migration, invasion and metastasis (Yu et al., 2015b).

The essential role of SND1-MTDH interaction in initiating breast tumor in transgenic mouse models

The importance of SND1-MTDH interaction was studied by knockout and add-back experiments (Wan et al., 2014). When SND1-MTDH interaction was disrupted through mutagenesis of important residues in MTDH, mammosphere formation *in vitro*, tumor initiation and tumor growth *in vivo* was suppressed (Wan et al., 2014). Under stress conditions, SND1 degradation could be rescued by MTDH-mediated stabilization of SND1 (Wan et al., 2014).

1.1.2.4.2 Roles of SND1 in hepatocellular carcinoma (HCC)

Hepatocellular carcinoma was the most common primary liver malignancy (Balogh et al., 2016). Liver cancer was the third most common cause of death from cancer all over the world (WHO, 2018). SND1 as a multifunctional protein, especially as a metastasis-associated protein, was found to be overexpressed in ~74% HCC cases compared

with normal tissue (Yoo et al., 2011c).

SND1 promoted tumor growth in HCC

Knockdown of SND1 in HCC cell line SMMC-7721 resulted in reduced cell proliferation, clonal formation and tumor formation in nude mice. SND1 could downregulate IGFBP3, which would explain why SND1 affected HCC cell proliferation (Yin et al., 2013). In addition, both SND1 and its binding partner MTDH were upregulated in human HCC cells, which could be another mechanism explaining hepatocarcinogenesis (Yoo et al., 2011c).

Moreover, in a very recent study, hepatocyte-specific SND1 transgenic mice (Alb/SND1 mice) were established and data suggested that these mice would develop HCC spontaneously with partial penetrance and exhibit more highly aggressive HCC when chemical carcinogenesis was included. A relative increase in inflammatory markers and spheroid-generating tumor-initiating cells (TIC) were observed in the livers of Alb/SND1 mice, possibly through the Akt and NF-κB signaling pathways to promote TIC formation in Alb/SND1 mice (Jariwala et al., 2017).

SND1 promoted angiogenesis in HCC

SND1 also played a role in promoting angiogenesis in liver cancer. SND1 knockdown in liver cancer resulted in a reduction of angiogesis in both chicken chorioallantoic membrane assay and human umbilical vein

endothelial cell differentiation assay. The mechanism was revealed to be the SND1-induced activation of NF-κB, resulting in the induction of miR-221 and subsequent induction of angiogenic factors Angiogenin and CXCL16 (Santhekadur et al., 2012).

SND1 regulated EMT in HCC

Another important event regulated by SND1 in HCC was the EMT process. By increasing AT1R mRNA stability, SND1 increased angiotensin II type 1 receptor (AT1R) levels, which resulted in an activation of ERK, Smad2 and the TGFβ signaling pathway. SND1 promoted EMT, migration and invasion in human HCC cells through this pathway (Santhekadur et al., 2014).

SND1 regulated cholesterol homeostasis in HCC

SND1 was also found to regulate cholesterol homeostasis in HCC. An increased cholesterol synthesis was observed in SND1-overexpressing HCC cells (Navarro-Imaz et al., 2016). Two regulators, SREBP-2 (sterol regulatory element binding proteins) and SREBP-1 bound to specific sites in SND1 promoter and regulated SND1 transcription oppositely. SND1 promoter was induced by SREBP-2 activating conditions and repressed by SREBP-1 overexpression. As a result, a potential contribution of SREBPs/SND1 pathway to lipid metabolism reprogramming in human hepatoma cells was proposed (Armengol et al., 2017).

Apart from this, SND1 was also reported to be involved in other lipid

metabolism pathways. The interaction between SND1 and a novel binding partner monoglyceride lipase (MGLL) was recently identified. SND1 and MGLL interaction resulted in ubiquitination and proteosomal degradation of MGLL. Overexpression of MGLL in human HCC cells resulted in a remarkable inhibition of cell proliferation with a significant delay in cell cycle progression and a remarkable decrease in tumor growth in nude mice xenograft models, which could be explained by an inhibition of Akt signaling pathway (Rajasekaran et al., 2016a).

1.1.2.4.3 Roles of SND1 in lung cancer

Lung cancer was the most common cancer for decades and the most lethal cancer wordwide, causing 1.76 million tumor-related deaths in 2018 (WHO, 2018). Non-small cell lung cancer (NSCLC) was the most common subtype of lung cancer, accounting for approximately 85% of lung cancers (Reck and Rabe, 2017).

SND1 induced chemoresistance in lung cancer

SND1, which was overexpressed in NSCLC clinical samples and cell lines, was found to be very important in maintaining chemoresistance in NSCLC (Zagryazhskaya et al., 2015). Knockdown of SND1 led to the increase in the sensitivity of NSCLC to cisplatin, oxaliplatin and 5-fluorouracil, possibly by downregulating S100A11 (S100 calcium-binding protein A11). This would further deregulate the

expression of phospholipase A2 in lung cancer (Zagryazhskaya et al., 2015).

SND1 promoted tumor initiation and progression in lung cancer

A BRAF-SND1 fusion transcript was newly identified in 2015, which played a potential role in lung cancer development. In an oncogene fusion transcript screening of 89 lung adenocarcinomas from non-smokers, a SND1-BRAF fusion transcript formed between exons 1-9 of *SND1* and exons 2 to 3' end of *BRAF* was detected. After ectopic expression of SND1-BRAF in H1299 cells, increased levels of MEK/ERK phosphorylation, cell proliferation, and spheroid formation were observed (Jang et al., 2015).

SND1 promoted cell migration in lung cancer

A very recent study revealed the role of SND1 in regulating cell migration in lung cancer. Knockdown of SND1 significantly inhibited lung cancer cell migration *in vitro* via miR-320a. Besides, an inverse expression pattern of SND1 and miR-320a was found in lung cancer tissue and cell lines (Xing et al., 2018).

1.1.2.5 Current inhibitors of SND1

Deoxythymidine 3', 5'-bisphosphate (pdTp) was a strong competitive inhibitor of staphylococcal nuclease (SN) identified after screening a series of synthetic substrates (Cuatrecasas et al., 1969). Enzymatic

reaction between SN and its substrate 4'-*p*-aminophenylphosphate 5'-phosphate could be inhibited by the competitive inhibitor pdTp (Cuatrecasas, 1970).

Crystal structure of staphylococcal nuclease-pdTp-Ca^{2+} complex was solved to illustrate how this interaction contributed to the inhibition of the enzymatic activity of SN. Arg-35 and Arg-87 at the active site might be the dual binding and catalytic residues of this nuclease (Cotton et al., 1979). Among the four tandem SN domains and the Tudor-SN5 domain, pdTp showed a highly selective inhibition of SND1 nuclease activity and the inhibiting concentration is 100μM (Caudy et al., 2003a).

pdTp could inhibit both the proliferation of human liver cancer cell line *in vitro* (Yoo et al., 2011c) and tumor growth in human liver cancer xenografted mice models *in vivo* (Jariwala et al., 2017). Immunohistochemical analysis of the tumor sections from the *in vivo* mouse model showed a dose-dependent decrease in proliferating cell nuclear antigen (PCNA), CD133, CD44 and p-p65 staining and an increase in apoptosis (Jariwala et al., 2017).

1.1.3 MTDH

Metadherin (metastasis adhesion protein or MTDH, also known as lysine-rich CEACAM1 co-isolated protein (LYRIC) or astrocyte elevated gene-1 protein (AEG-1)) was an oncogene overexpressed in 44% of

breast cancer patients (Li et al., 2008b). It was first identified as an 8q22 genomic gain in breast cancer (Yoo et al., 2011a).

1.1.3.1 MTDH and poor clinical outcomes

Statistical analysis of 225 breast cancer cases revealed a significant correlation of MTDH status with clinical staging (p=0.001), tumor classification (p=0.004), node classification (p=0.026), metastasis classification (p=0.001) and overall survival (Li et al., 2008b). A more recent meta-analysis comprising 8 studies and covering a total of 1167 breast carcinoma cases, revealed that elevated MTDH would predict distant and lymph node metastasis in breast cancer (Hou et al., 2016).

1.1.3.2 MTDH structure

Using mouse model injected with cDNAs from lung metastatic breast carcinoma, Ruoslahti E. and his colleagues successfully identified a lung-homing domain of MTDH (Figure 1.15) (Brown and Ruoslahti, 2004).

MTDH was highly conserved, encoding for a protein of 582 amino acids (64kD) in human. MTDH had no conserved functional domains (Britt et al., 2004; Sutherland et al., 2004). It was a lysine (12.3%) and serine (11.6%) rich protein with three nuclear localization signals (NLS) and a single predicted transmembrane domain (TMD) at the N-terminus of the

protein, which contained putative dileucine repeats involved in protein trafficking (Figure 1.15) (Sutherland et al., 2004). Besides, MTDH protein also contained a C-terminal "GALPTGKS" sequence, which was postulated to be an ATP/GTP binding site (Thirkettle et al., 2009).
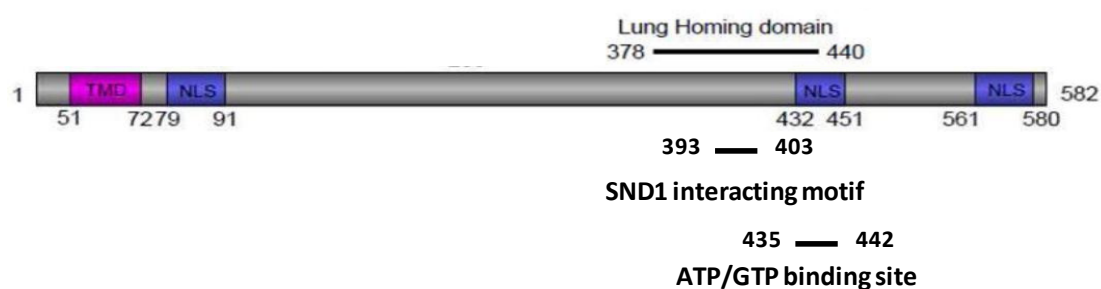
Figure 1.15 A schematic diagram of MTDH protein and its postulated functional domains

MTDH (378-440) was identified as the lung-homing domain of MTDH in an in vivo phage display study in mice (Brown and Ruoslahti, 2004). MTDH (393-403) interacted with SND1. MTDH (435-442) was postulated to be the ATP/GTP binding site. TMD: transmembrane domain; NLS: nulear localization signal. This figure was adapted from (Yoo et al., 2011b).

1.1.3.3 MTDH promoted cell proliferation and metastasis of breast cancer

Biological function of MTDH in breast cancer was investigated extensively. Ectopic expression or silencing of MTDH in breast cancer cell line MCF7 and MDA-MB-435 significantly enhanced or inhibited cell proliferation and tumorigenicity, respectively. The proliferation-stimulating effect was

strongly associated with the down-regulation of the two important cell-cycle inhibitors p27^{Kip1} and p21^{Cip1}. Besides, it was demonstrated that the promotion of proliferation by MTDH was mediated by the regulation of Akt/FOXO1 signaling pathway (Li et al., 2009).

Knockdown of MTDH in breast cancer cell line LM2, a subline with high lung metastasis propensity, significantly reduced lung metastasis and extended mice survival (Hu et al., 2009). Overexpression of MTDH in breast cancer led to the upregulation of mesenchymal markers and the downregulation of epithelial markers, resulting in an enhanced invasion and migration of breast cancer cells (Li et al., 2011).

1.1.3.4 MTDH promoted angiogenesis of breast cancer

Overexpression of MTDH in rat embryo fibroblasts could increase microvessel formation (Emdad et al., 2009). MTDH overexpression also increased angiogenesis markers such as angiopointin-1 and tube formation in matrigel and invasion of human umbilical vein endothelial cells by upregulating PI3K/Akt signaling pathway (Emdad et al., 2009).

1.1.3.5 MTDH promoted tumor initiation and metastasis in transgenic mouse model

Functions of MTDH were studied in a MTDH knockout mouse model. knockout of MTDH significantly inhibited tumor initiation and lung

metastasis of mammary tumors in mice (Wan et al., 2014). Pro-tumorigenic role of MTDH required its binding partner SND1. Interaction between MTDH and SND1 was required for tumor initiation and metastasis of mammary tumor in mice. MTDH stabilized SND1, conferring a survival advantage of mammary cells under stress conditions. This might explain the crucial role of SND1-MTDH interaction in mammary tumor formation of mice (Wan et al., 2014).

1.2 Objectives

The main purpose of this project was to inhibit breast cancer by targeting SND1, which was divided into 5 objectives, a) to identify SND1-interacting peptides through phage display screening; b) to test if the SND1-interacting peptides could disrupt MTDH-SND1 interaction; c) to investigate how the disruption of SND1-MTDH interaction resulted in cytotoxicity in breast cancer; d) to investigate the effect of the disruption of SND1-MTDH interaction on cell signaling and e) to identify the critical amino acids in SND1-interacting peptides in cytotoxicity and cell signaling.

Chapter 2 Screening of SND1-interacting peptides using phage display

2.1 Abstract

SN1/2 domain of SND1 protein was expressed in *E.coli* and purified with HisTrap affinity column. Recombinant SN1/2 was used as bait in a phage display screening. After four rounds of screening, 20 phages were randomly picked and sequenced. W and Y were found to be highly enriched after screening. There was a common sequence pattern with 2 W (or one W and one Y) separated by 3-6 amino acids. This pattern was strikingly similar to what was found in SND1-interacting MTDH peptide (Guo et al., 2014).

ELISA confirmed that these phages could indeed bind to SN1/2. Six peptides with highest binding affinity towards SN1/2 were selected for further studies. Two out of six peptides could disrupt a 22-mer MTDH peptide from interacting with SN1/2 in ELISA assay. Their relative binding affinity was determined. Peptide 4-2 and peptide 4-8 could compete with 22-mer MTDH binding to SN1/2 with an EC_{50} of 55.4μM and 16.8μM, respectively. Peptide 4-2 could disrupt SND1-MTDH full-length protein interaction in co-immunoprecipitation assay. A diagram of the work flow of this chapter is shown in Figure 2.1.
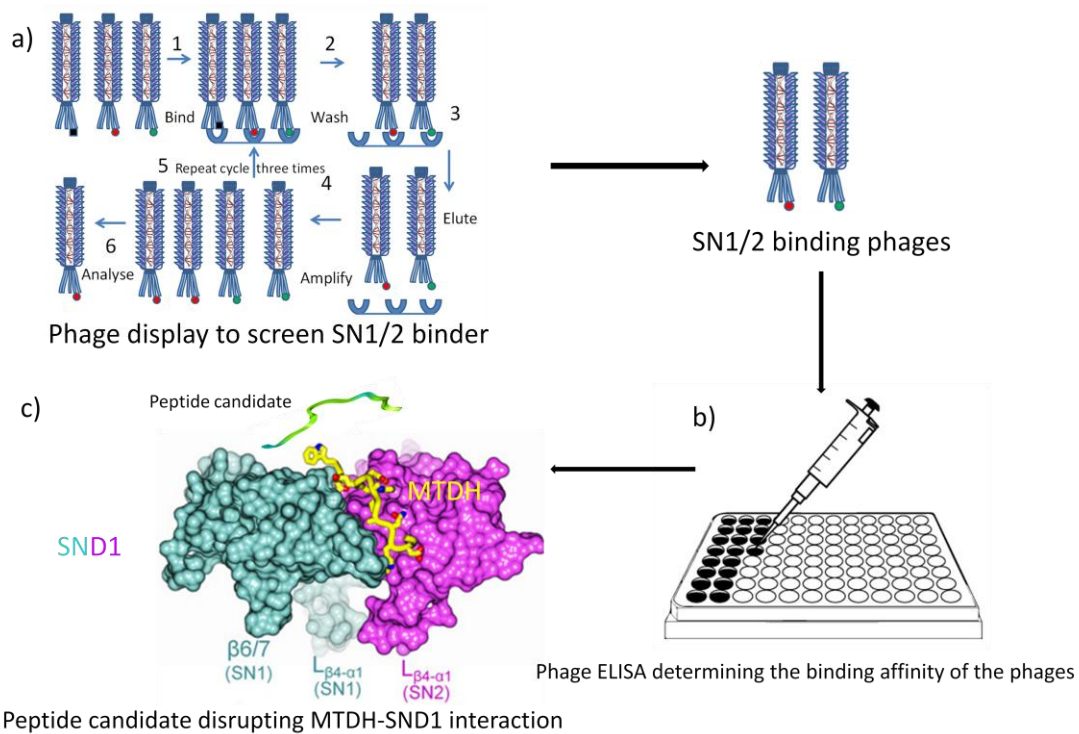
Figure 2.1 Work flow of Chapter 2

a) Phage display was used to identify SN1/2 binders. b) Phage ELISA was performed to determine the binding affinity of SN1/2 binding phages. c) Peptides selected from phage display were tested for their ability in disrupting MTDH-SND1 interaction. The green, purple and yellow structures were the co-crystal structure of SND1-MTDH (PDB: 4QMG) (Guo et al., 2014). The yellow MTDH peptide is nested in the binding groove between SN1 (green) and SN2 (purple) domains of SND1.

2.2 Introduction

2.2.1 Phage display technology

Phage display technology could express a library of short peptides at the end of phages for binding studies. Phage display library was a library of phage particles that expressed unique sequences of peptides which would eventually interact with desired protein targets. Ph.D.-12™ Phage

Display Peptide Library was a commercially-available combinatorial library (NEB) of random 12-mer peptides fused to pIII protein coat of M13 phage. This library consisted of approximately $1\text{X}10^9$ different peptide sequences. Phage display technology was invented by George P. Smith in 1985 by using filamentous M13 phage (Smith, 1985), which was an *Escherichia coli*-specific filamentous bacteriophage with a length of ~1 μm and a diameter of <10 nm.

The phage particle was composed of a single-stranded DNA core inside a protein coat (Marvin, 1998). The pIII protein was positioned at one end of the phage capsid and the C-terminus of pIII was composed of three functional domains (D1, D2 and D3) linked by glycine rich linkers (Stengele et al., 1990). The D1 and D2 domains were mainly used for infecting bacteria. They were usually deleted in most of the phage display systems. The C-terminal D3 domain stayed intact because it was essential for the assembly of phage capsids and phage production (Georgieva and Konthur, 2011). Because the C-terminus of phage pIII coat protein was sometimes modified, peptides were displayed on the N-terminus of pIII. Instead of displaying only one copy of peptide, pentavalent peptides could be displayed on the N-terminal fusion of coat protein pIII (Scott and Smith, 1990).

There were two types of "second-generation" phage display peptide libraries. One was to construct tailor-made phages using the motif

elucidated from a random library, while the other approach was to establish a "biased random mutagenized library" in which the DNA sequence of the originally designed peptidomimetic was 10% "contaminated" by other nucleotides. Using this method, random variants of the original sequence were created (Freund et al., 2009; Ophir and Gershoni, 1995).

2.2.2 SND1-MTDH interaction promoted breast cancer initiation and progression

SND1 interacted with MTDH, an important protein involved in many oncogenic processes (Lee et al., 2013). MTDH was found to be amplified in breast cancer and associated with poor prognosis (Wan et al., 2014). MTDH played an essential role in breast cancer tumorigenesis by stabilizing SND1 (Wan et al., 2014).

A 22-residue MTDH peptide (386-407) was identified as the minimum binding motif of MTDH that could interact with SN1/2 domain of SND1. W394 and W401 were identified as the essential amino acids in MTDH-SND1 interaction. When SND1-MTDH interaction was disrupted by mutating the contact residues, mammosphere formation *in vitro*, tumor initiation and tumor growth *in vivo* were suppressed (Wan et al., 2014).

A co-crystal structure of the SN1/2 domain of SND1 and an 11-residue

MTDH peptide (PDB: 4QMG) revealed the details of SND1-MTDH interaction (Figure 2.2) (Guo et al., 2014). In the co-crystal structure, an 11-residue MTDH peptide occupied an extended groove between SN1 and SN2 domains of SND1 with two tryptophans (W394 and W401) nestled into two well-defined hydrophobic binding pockets (Figure 2.2). The long protruding arms and deep surface valleys at the back side of binding interface on SND1 might also be involved in the interactions with other binding partners (Guo et al., 2014; Wan et al., 2014).
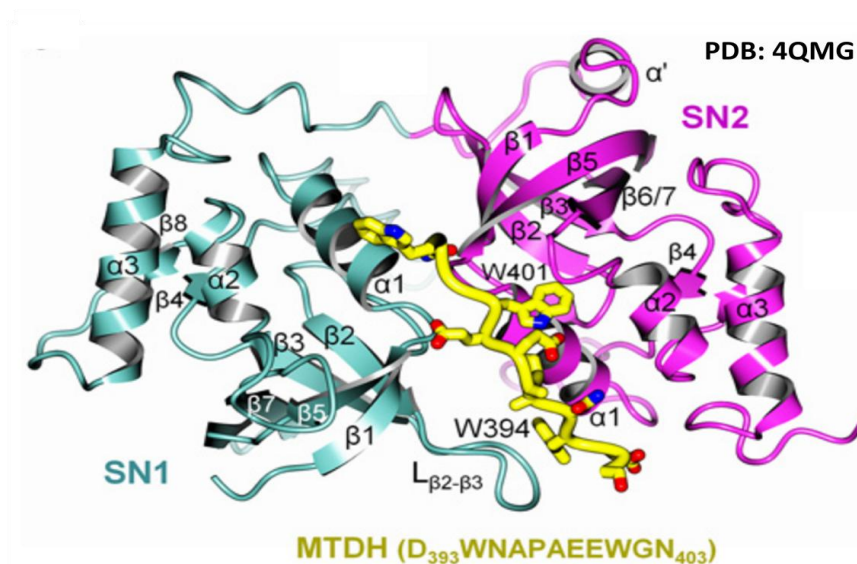
Figure 2.2 Co-crystal structure of SN1/2 domain of SND1 with an 11-residue MTDH peptide (PDB: 4QMG)

Green structure represented SN1 domain of SND1; Purple structure represented SN2 domain of SND1; Yellow linear structure represented MTDH 11-residue peptide (sequence: DWNAPAEEWGN). W394 and W401 of MTDH were the 2 critical amino acids involved in SND1-MTDH interaction. Lβ2-β3 was an essential loop involved in MTDH-SND1 interaction. This loop was the major difference between SN1/2 and SN3/4 domain, which explained why MTDH interacted with SN1/2 instead of SN3/4 domain of SND1. This figure was adapted from (Guo et al., 2014).

2.2.3 Size exclusion chromatography and multi-angle light scattering technology

Size exclusion chromatography (SEC), also known as gel permeation, gel filtration, steric exclusion, or gel chromatography, was an entropically controlled separation technique which separated particles according to the relative size or hydrodynamic volume of a macromolecule with respect to the average pore size of the packing (Barth et al., 1996). Multi-angle light scattering (MALS) was a technology where light was scattered into multiple angles when large particles were irradiated by light to determine both the molecular mass and particle size. In a SEC-MALS system, the molecular weight of a sample was determined by MALS after separation by SEC (Sahin and Roberts, 2012).

2.3 Methodology

2.3.1 Expression and Purification of SN1/2

The cDNA encoding full-length SND1 was purchased from DNASU (https://dnasu.org/DNASU/). The cDNA encoding SN1/2 fragment was obtained by PCR with 5' primer-CGGGATCCGTCCCCACCGTGCAGCGGGGCA and 3' primer-CCGGAATTCTTACTTTTGGTCCAAATTAGCTGTG. SN1/2 cDNA fragment was cloned into glutathione S-transferase (GST)-6xHis

expression vector pET49M.3C and sequenced (Figure 2.3). *E.coli* BL21 competent cells were transformed with pET49M.3C-SN1/2 plasmid, cultured in LB medium supplemented with 50µg/mL kanamycin, and induced with 0.2 mM IPTG at 26°C to express GST-6XHis-SN1/2 recombinant protein.
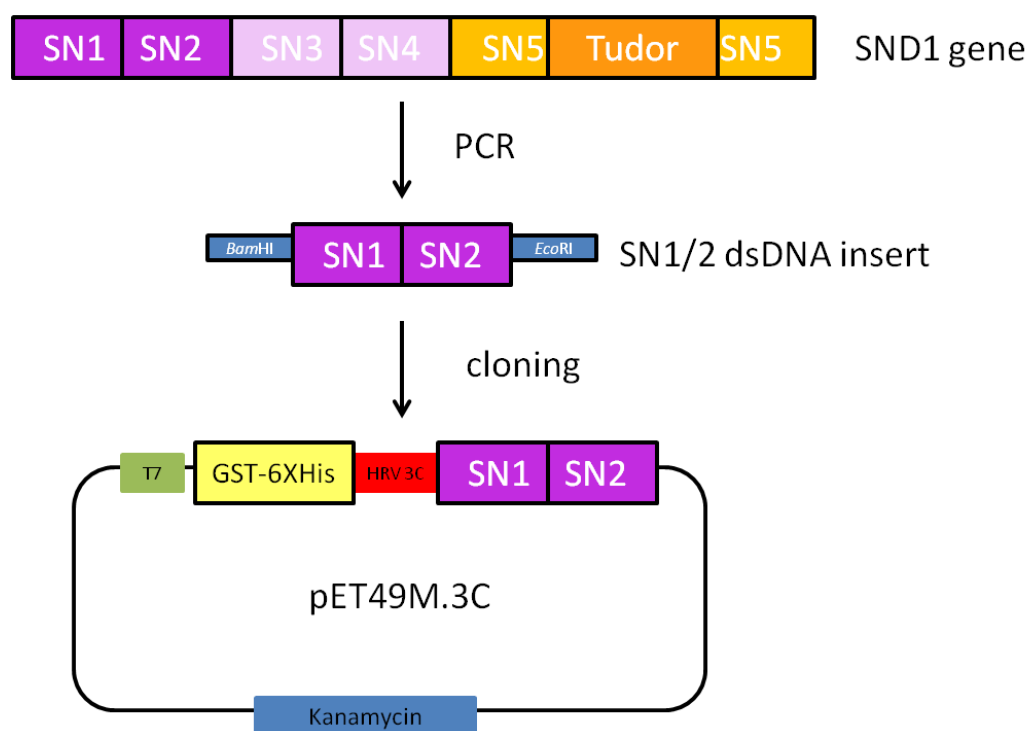
Figure 2.3 Construction of SN1/2 expression vector

SN1/2 dsDNA was obtained from the cDNA of full-length SND1. It was inserted into pET49M.3C vector for expression. The multi-cloning sites used were *Bam*HI and *Eco*RI.

After induction, bacteria culture was centrifuged and pellet was ultrasonicated on ice in His binding buffer (15mM β-ME, 1mM PMSF, 20mM sodium phosphate, 40mM imidazole, 0.5M sodium chloride, pH 7.4) followed by centrifugation at 18,000 rpm at 4°C for 90 min. The

soluble fraction of lysate was purified by HisTrap column (GE Healthcare Life Sciences) using AKTA online purifier and eluted with His elution buffer (20mM sodium phosphate, 500mM imidazole, 0.5M sodium chloride, pH 7.4).

GST-His-SN1/2 protein was digested with human rhinovirus (HRV) 3C protease (self-prepared) at 4°C overnight. The digested protein mixtures (SN1/2 and GST-His tag) was loaded onto HisTrap column and SN1/2 protein was eluted by Tris buffer (50 mM Tris, 150mM NaCl, 10mM KCl and 10 mM MgCl2, PH8). The fraction containing SN1/2 was analyzed by SDS-PAGE. The gel was then stained by Coomassie Brilliant Blue.

2.3.2 Screening of a 12-mer phage display library based on SN1/2

The procedure to screen phage display library was modified according to the manufacturer's instructions (NEB, USA). A petri dish (90x15mm) was coated with SN1/2 before screening. The dish was incubated with 100µg/mL SN1/2 protein at 4°C overnight prior to blocking with 0.1M NaHCO$_3$ (pH8.6) containing 5mg/mL BSA at 4°C for 1 h. Phage display library was then added onto the SN1/2-coated petri dish and incubated at room temperature for 1h. Unbound phages were removed by washing with TBST (TBS + 0.1% [v/v] Tween-20). Subsequently, bound phages were eluted with glycine-HCl (pH 2.2) and amplified. Phages with high

binding affinity to SN1/2 were harvested after four rounds of biopanning. Tween-20 was increased to 0.5% [v/v] in TBST washing buffer in round 2-4.

2.3.3 Phage amplification, titering and sequencing

10ml of LB inoculated with ER2738 (an *E.coli* strain used for M13 phage infection) was incubated for 4-8h until OD_{600} reached ~0.5. Infection of phages to bacteria was accomplished by mixing serial dilutions of phages with bacteria culture for 3 min under room temperature. Top agar was then mixed with phage-infected bacteria and poured onto a pre-warmed LB/IPTG/Xgal plates. Plates were then incubated at 37°C overnight.

For phage titering, plaques on plate were counted (100 plaques per plate were appropriate). For phage sequencing, single phage clone was picked from the blue plaque and then inoculated into ER2738 LB culture (diluting overnight culture of ER2738 at 1:100 into fresh LB.). For phage amplification, LB was firstly inoculated with ER2738 at 37°C with vigorous shaking and followed by infection with phages for another 4.5 hours at 37°C. Amplified phages were collected from the supernatant after centrifugation at 14,000 rpm for 30 seconds. For amplification of single phage clones, phages could be concentrated by adding 20% PEG/2.5M NaCl followed by precipitation at 4°C overnight and resuspended into small volume of TBS.

2.3.4 Phage ELISA and peptide ELISA

For phage ELISA, 96-well plate (Nunc^{TM} 96-well Optical-Bottom Plate) was coated with 100μg/mL SN1/2 protein at 4°C overnight prior to blocking with 0.1M NaHCO$_3$ (pH8.6) containing 5mg/mL BSA at 4°C for 1 h. Background negative control well was only coated with 0.1M NaHCO3 (pH8.6) containing 5mg/mL BSA at 4°C for 1 h. Serial dilutions of single phages were added onto the treated plate for interaction studies. One randomly-picked phage was used as negative control. After incubation at room temperature for 2 hours with agitation, the plate was washed, followed by incubating with HRP-conjugated anti-M13 monoclonal antibody at 0.2μg/mL (Sino Biological, #11973) in blocking buffer at room temperature for 1h with agitation. The plate was washed before the addition of HRP substrate ABTS (Thermo Scientific, #34026) in 50mM sodium citrate, pH4.0. Thirty percent of H$_2$O$_2$ was used as stop solution. Color product was measured at OD$_{410}$.

For direct peptide ELISA, 96-well plate (PerkinElmer Optiplate-96F) was coated with 10μg/mL SN1/2 protein at 4°C overnight prior to blocking with 0.1M NaHCO$_3$ (pH8.6) containing 5mg/mL BSA at 4°C for 1h (For BSA coating negative control plate, only BSA was added to block the plate). Serial dilutions of peptides in binding solution (0.02%TBST) were added onto the plate. After incubation for 1 hour at 37°C, the plate was washed with washing buffer (0.02%TBST) before fluorescent signal was

detected by CLARIOstar microplate reader ($\lambda_{excitation}$=485nm, $\lambda_{emission}$=535nm).

For competitive peptide ELISA, the preparation of 96-well plate was the same as that of direct peptide ELISA. Plates were pre-incubated with serial dilutions of competitive peptides for 1 h at 30°C, followed by thorough washing. 22-mer 5-FAM-MTDH peptide (3.5µM) together with serial dilutions of competitive peptides was added onto the plate for competition for 1h. The plate was washed before fluorescence detection by CLARIOstar microplate reader ($\lambda_{excitation}$=485nm, $\lambda_{emission}$=535nm).

2.3.5 SEC-MALS

The protein particles in the purified SN1/2 sample solution were separated by size exclusion chromatography with a gel filtration column in Tris buffer (50 mM Tris, 150mM NaCl, 10mM KCl and 10 mM MgCl2, PH8) and detected by an online multi-angle light scattering detector to test the aggregation state of SN1/2.

2.3.6 Peptide synthesis

Peptides were synthesized by two peptide companies, Pepmic (Suzhou, China) and Dechi (Shanghai, China) using standard solid-phase peptide synthesis chemistry and purified typically to 95% purity as an acetate form.

The six peptide candidates selected from phage ELISA were synthesized with C-terminus amidation as suggested by Ph.D.-12™ Phage Display Peptide Library Protocol since these peptides were displayed on the N-terminus of pIII phage coat protein. Other peptides were synthesized using the same method in the same purity but with both C-terminus amidation and N-terminus acetylation for better protection against enzymatic degradation and stronger cell penetration ability. 5-FAM-MTDH peptide (5-FAM-SSADPNSDWNAPAEEWGNWVDE) and 5-FAM-MTDH scramble peptide (5-FAM-SNWAESWVAPPGEDSADNEWDN) were synthesized with the same method but with 5-FAM fluorophore labeled on the N-terminus of the peptides.

2.3.7 Co-immunoprecipitation assay

MDA-MB-231-GFP-

Red-FLuc cell lysate was prepared with modified RIPA lysis buffer (10mM Tris, 75mM NaCl, 0.5% NP40, pH7.4) supplemented with 1mM PMSF and 1X protease inhibitor (#11836153001,Roche). After centrifugation at 14,000rpm at 4°C for 10 min, supernatant was collected for co-immunoprecipitation (co-IP) assay. Anti-c-Myc antibody (sc-40) and anti-V5 antibody (#1905424, Invitrogen) were pre-incubated with protein G agarose (sc-2002) for 3h before co-IP. Peptide 4-2 was added to the cell lysate for preincubation at 4°C for 3h. Co-IP was conducted by mixing the

treated beads and cell lysate overnight at 4°C with rotation.

2.4 Results

2.4.1 Expression and purification of GST-6XHis-SN1/2

To produce recombinant SN1/2 as bait for phage display screening, a His-tagged SN1/2 construct was used to produce SN1/2 domain of SND1. Plasmid map was shown in Figure 2.3. SN1/2 domain of SND1 was expressed and purified as described in Methodology. Figure 2.4 showed the chromatogram of purified GST-6XHis-SN1/2 recombinant protein using HisTrap affinity column. Figure 2.5 showed the SDS-PAGE of the eluted fractions of GST-6XHis-SN1/2 recombinant protein (indicated by arrow).
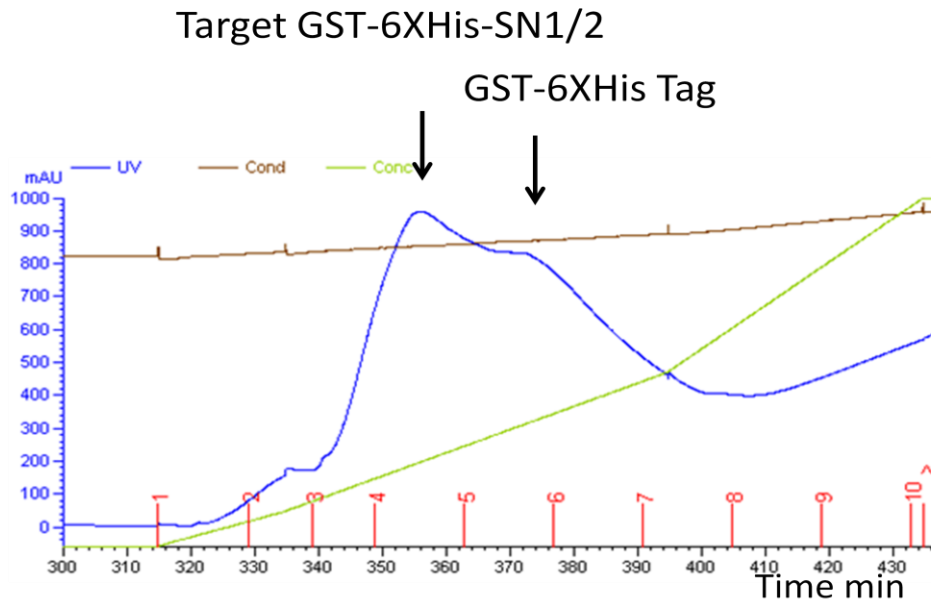
Figure 2.4 FPLC purification of GST-6XHis-SN1/2 recombinant protein

Fast Protein Liquid Chromatography (FPLC) was employed to purify GST-6XHis-SN1/2 using HisTrap affinity column. GST-6XHis-SN1/2 and GST-6XHis were the main protein fractions (indicated by arrows) after expression, which were eluted by gradient elution. The blue line represented UV absorption, the brown line represented conductivity and the green line represented salt concentration (gradient) of the elution buffer. Fraction numbers collected from FPLC were shown on X-axis.
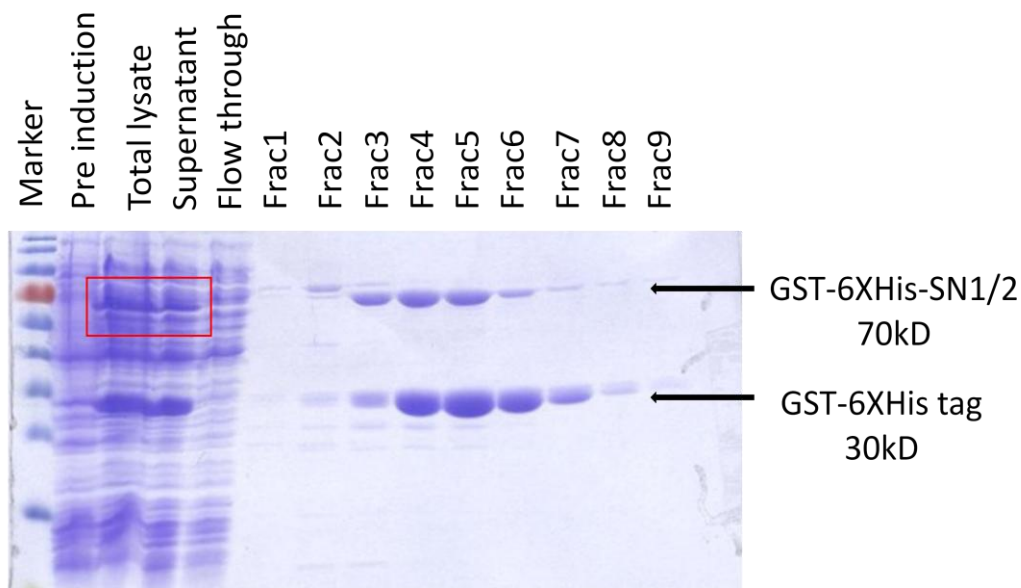
Figure 2.5 Purification of GST-6XHis-SN1/2 recombinant protein

Successful expression of GST-6XHis-SN1/2 recombinant protein was reflected by the presence of a new band corresponding to ~70kD in total lysate. This protein was soluble, which could be demonstrated by the same band in supernatant. GST-6XHis-SN1/2 (~70kD) and GST-6XHis tag (~30kD) are the main components found in fraction 1-9.

After removing the GST-6XHis tag from GST-6XHis-SN1/2 recombinant protein by HRV 3C protease digestion, SN1/2 domain of SND1 was purified using the same method. The results are shown in Figures 2.6 and 2.7. The purity of SN1/2 protein was estimated to be ~90% as indicated by a single band after Coomassie Blue staining (Figure 2.7).
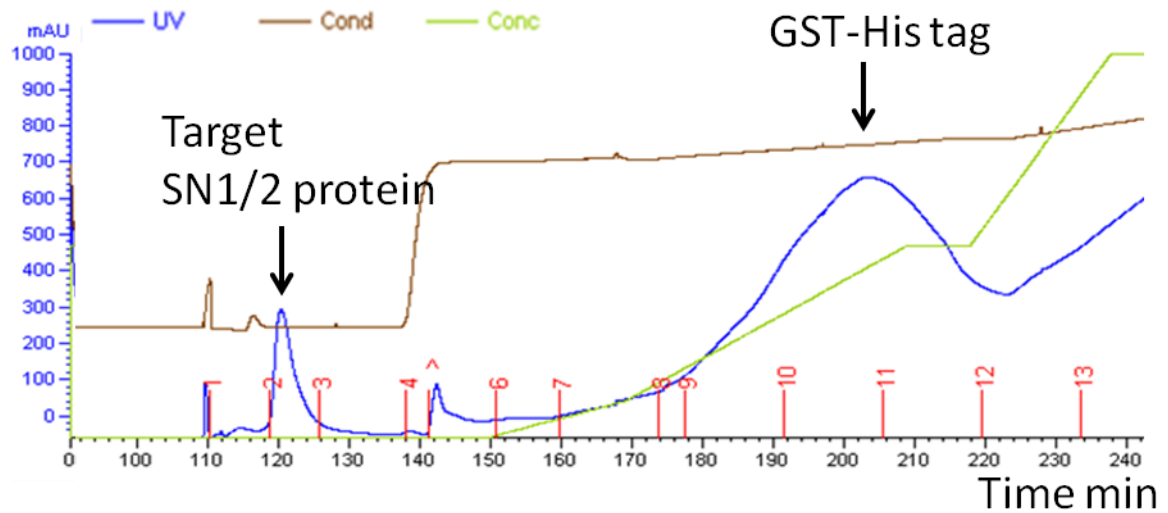
Figure 2.6 FPLC purification of SN1/2 protein after HRV 3C protease digestion

After HRV 3C digestion, GST-6XHis-SN1/2 protein was cleavage into SN1/2 protein and GST-6XHis tag. The purification of SN1/2 protein was achieved by removing GST-His tag using Histrap affinity column. The blue line represented UV absorption, the brown line represented conductivity and the green line represented salt concentration (gradient) of the elution buffer. Fraction numbers collected from FPLC were shown on X-axis.
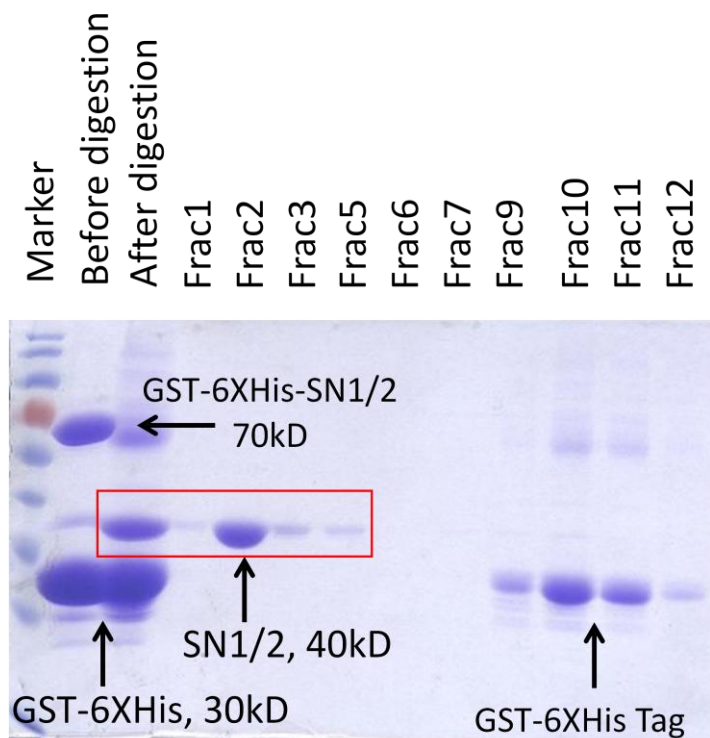
Figure 2.7 Purification of SN1/2 protein after HRV 3C digestion

GST-6XHis-SN1/2 was digested by HRV 3C protease. Pure SN1/2 was obtained by removing GST-6XHis from protein mixture using HisTrap column. Successful cleavage by HRV 3C protease was indicated by the appearance of SN1/2 (40kD) and GST-6XHis (30kD) in lane 3 (after digestion). Since GST-6XHis tag interacted with HisTrap column, SN1/2 was obtained before imidazole gradient elution shown in fraction 2. Bound GST-6XHis tag was eluted by imidazole elution buffer in fraction 9-12.

2.4.2 SEC-MALS confirmed the monomeric status of SN1/2

SEC-MALS was used to measure the aggregation status of SN1/2 domain of SND1. As shown in Figure 2.8, a major peak with average molecular weight ranging from 20kD to 50kD was found. This suggested a monomeric status of SN1/2 domain of SND1 (estimated molecular weight 40kD).
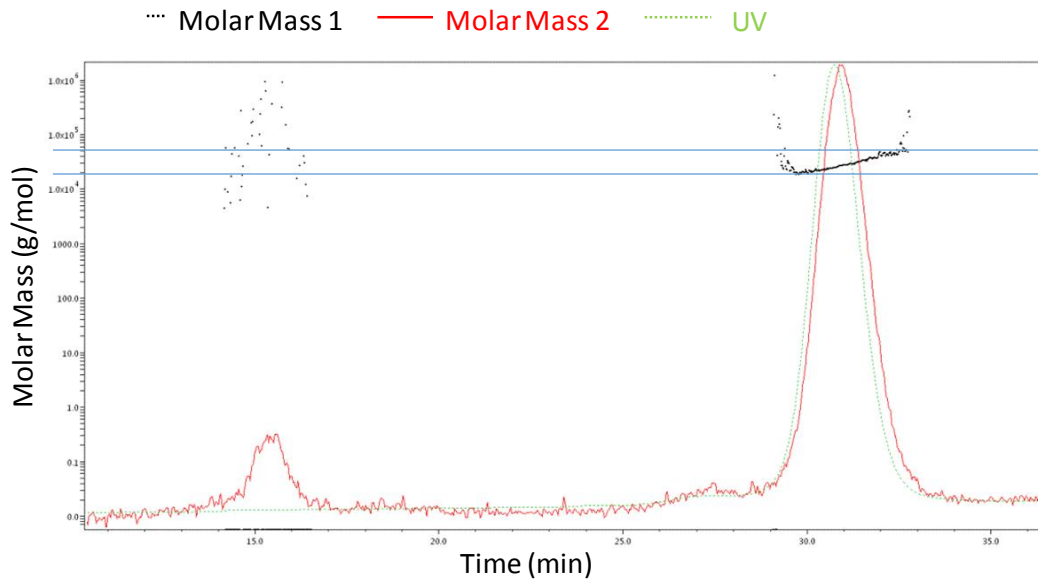
Figure 2.8 SEC-MALS spectrum confirmed the monomeric status of purified SN1/2

A major peak of approximately 20-50kD (corresponding to the molecular weight of SN1/2 of 40kD) was observed in SEC-MALS indicating the monomeric status of SN1/2. A small fraction of unknown identity was also found.

2.4.3 Phage display screening of peptides binding to SN1/2

The above purified SN1/2 was used as bait in phage display screening. A 12-mer phage display library was used to identify SN1/2 binding phages. After 4 rounds of biopanning, phages were isolated and peptide sequences of the phages were determined. As shown in Table 2.1, a total of 20 phages were picked and sequenced. Sequence of peptide 4-1 is repeated in 4-18. Sequence of peptide 4-2 is repeated in 4-3, 4-4, 4-7, 4-9 and 4-10. An unusually high percentage of tryptophan was observed in the peptide sequences. The distance between these tryptophans was

found to be 3-7 amino acids.

Table 2.1 SN1/2 binding peptides identified from phage display

No. of colonies	Peptide sequencing results
4-1	V H W D F R Q W W Q P S
4-2	Q F D Y D H F L M W Y S
4-3	Q F D Y D H F L M W Y S
4-4	Q F D Y D H F L M W Y S
4-5	G H A Y W V D L A S I W
4-6	F H Q P W G Y Y W I S G
4-7	Q F D Y D H F L M W Y S
4-8	W G T I Y Y W E E Y D S
4-9	Q F D Y D H F L M W Y S
4-10	Q F D Y D H F L M W Y S
4-11	D H M P G M K H Y F Y S
4-12	N T H Q Y V G W P I F W
4-13	W Y Y E I D W T S F A L
4-14	S W F S D W D L E L H A
4-15	M W P P S E P R L N Y N
4-16	Y D S R F F L T W W D L
4-17	Y H W H W L D T R D L T
4-18	V H W D F R Q W W Q P S
4-19	W Q W P V R M D W L G S
4-20	H G Y S V W F D S F W L

Twenty SN1/2-binding phages from phage display were picked and sequenced. Repeated phages (4-1 and 4-18; 4-2, 4-3, 4-4, 4-7, 4-9 and 4-10) were highlighted. The unusually high percentage of tryptophan (W) was also highlighted.

2.4.4 Binding affinity of individual phages to SN1/2

Phage ELISA was performed to determine the binding affinity of the phages towards SN1/2. As shown in Figure 2.9, the phages interacted with SN1/2 in a dose-dependent manner. Phages 4-2, 4-5, 4-8, 4-13, 4-16, 4-19 showed high binding affinity towards SN1/2 compared to a randomly picked control (Figure 2.9a). They were selected for further study. Phage 4-2, the sequence of which was most repeated after phage display screening, exhibited medium to high binding affinity among all the phages.

Other phages showing unexpected or low binding affinity towards SN1/2 were suspended for further assays. Phages 4-6, 4-17 and 4-20 showed decreased binding at high concentrations for unknown reasons. Phage 4-1, 4-11, 4-12, 4-14, and 4-15 showed low binding affinity towards SN1/2 compared with the random control (Figure 2.9b).
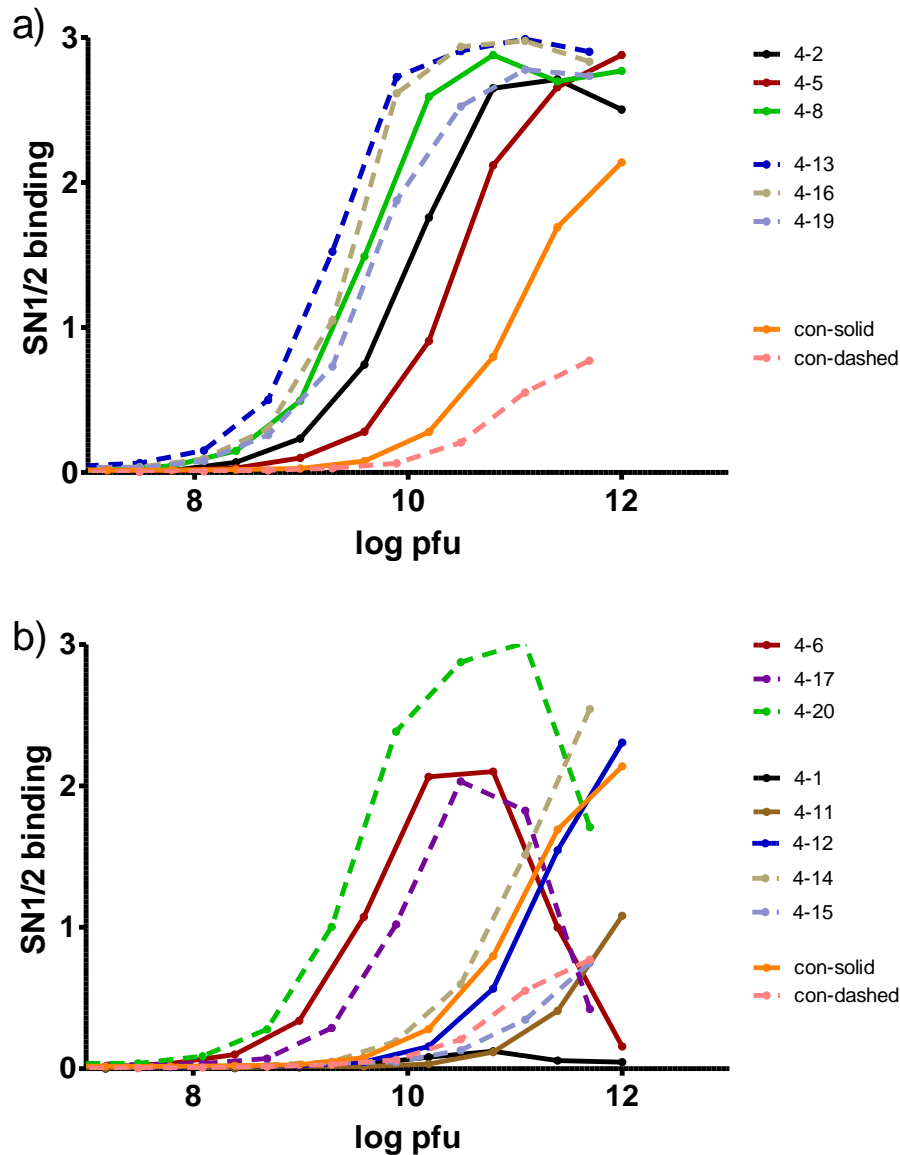
Figure 2.9 Determination of binding affinity of phages towards SN1/2 using ELISA

a) Phage ELISA validated the high SN1/2 binding affinity of the 6 single phage clones compared to a randomly-picked control. b) Phage ELISA showed decreased binding at high concentrations or low binding affinity of the phages to SN1/2. The experiments were conducted in two sets. Con-solid was the control phage used in solid line group. Con-dashed was the control used in dashed line group. Con-solid and con-dashed were the same single phage control clone. Phages binding to SN1/2 were recognized by anti-M13 phage antibody, which also catalyzed ABTS for color detection (OD_{410}).

2.4.5 22-mer 5-FAM-MTDH peptide binding to SN1/2

It has been demonstrated that SN1/2 domain of SND1 could interact with MTDH and SND1-MTDH interaction could induce the initiation and progression of breast cancer (Wan et al., 2014). Here, such interaction was studied using a fluorescently-labeled 22-mer 5-FAM-MTDH peptide (Wan et al., 2014).

As shown in Figure 2.10 a), 5-FAM-MTDH peptide showed a higher binding affinity towards SN1/2 compared to 5-FAM-MTDH scrambled control. Neither MTDH nor scrambled control showed any binding towards BSA. 5-FAM-MTDH scr binding to SN1/2 was subtracted from 5-FAM-MTDH binding to SN1/2 to generate the specific binding of 5-FAM-MTDH to SN1/2 (Figure 2.10 b).
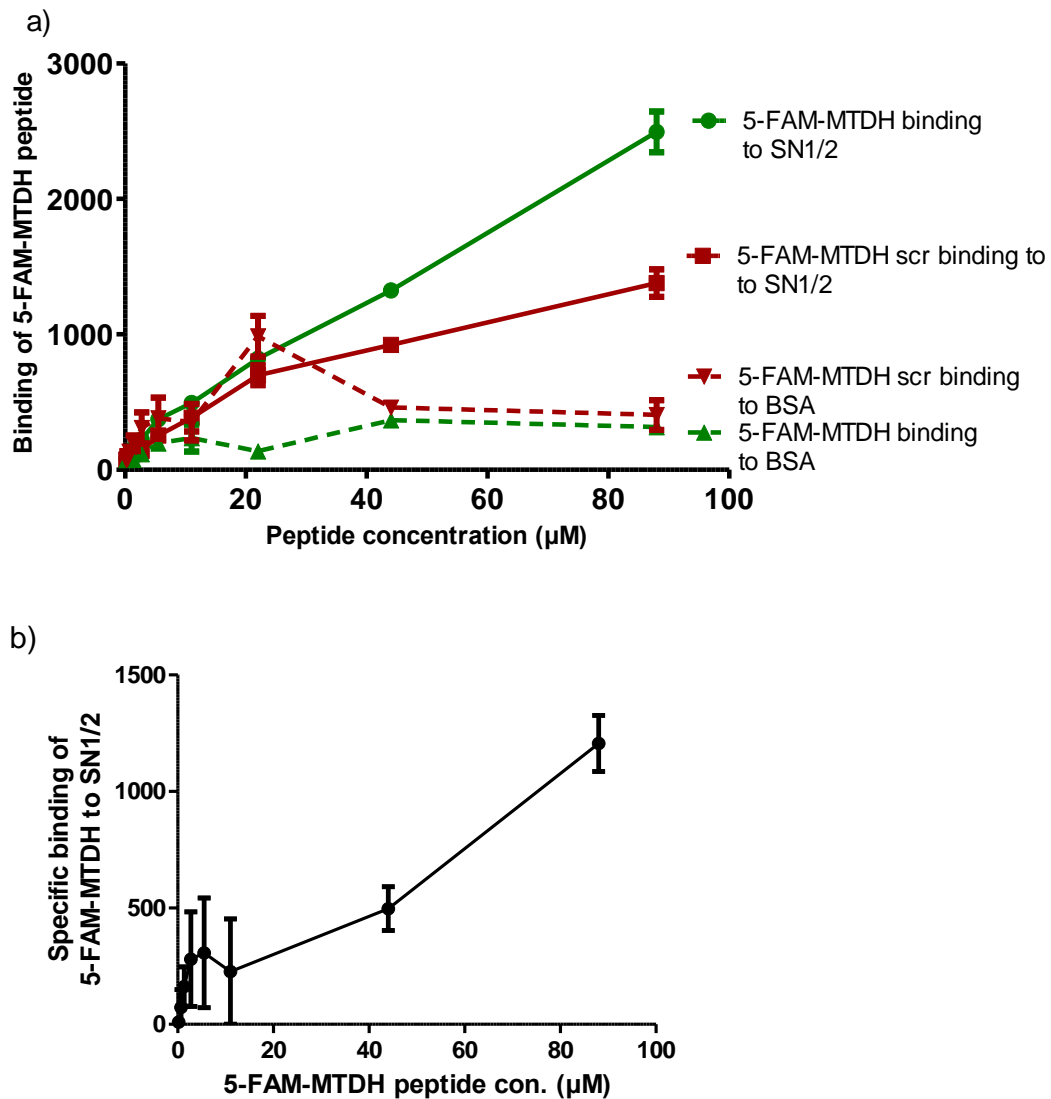
Figure 2.10 ELISA study of 5-FAM-MTDH peptide binding to SN1/2

a) ELISA plate was coated with either SN1/2 or BSA. Increasing concentrations of peptides (5-FAM-MTDH or 5-FAM-MTDH scrambled peptides) were added to the plate. Fluorescence of 5-FAM was measured after washing. b) 5-FAM-MTDH scr binding to SN1/2 was subtracted from 5-FAM-MTDH binding to SN1/2 in a) to generate the specific binding of 5-FAM-MTDH to SN1/2. The mean ±S.D. of fluorescence is shown (n=3).

2.4.6 Peptide candidates competed with MTDH binding to SN1/2

Here the SN1/2 binding peptides identified from phage display (4-2, 4-5, 4-8, 4-13, 4-16 and 4-19) were investigated for their ability to compete with 5-FAM-MTDH binding to SN1/2 (Figure 2.12).
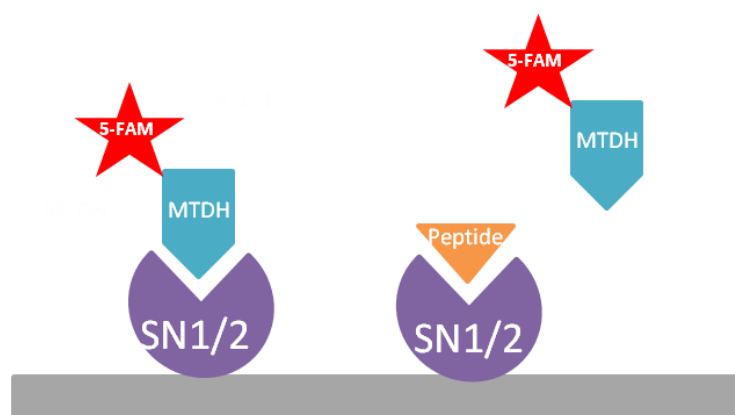
Figure 2.11 ELISA study of peptides competed with 5-FAM-MTDH peptide binding to SN1/2

Peptide 4-2, 4-5, 4-8, 4-13, 4-16 and 4-19 (triangle) competed with 5-FAM-MTDH peptide binding to SN1/2 coated on the plate. Successful binding of peptides to SN1/2 would result in lowered 5-FAM-MTDH binding.

As shown in Figure 2.12, peptides 4-2 and 4-8 could compete with 5-FAM-MTDH peptide binding to SN1/2 with EC_{50}s of 55.4μM and 16.8μM, respectively. 4-13 could compete with 5-FAM-MTDH binding to SN1/2 at low concentrations but unexpectedly enhance this binding at high concentrations. Unexpectedly, the remaining three peptides: 4-5, 4-16 and 4-19 were found to enhance the binding of MTDH peptide to SN1/2 for unknown reasons (Figures 2.13 and 2.14).
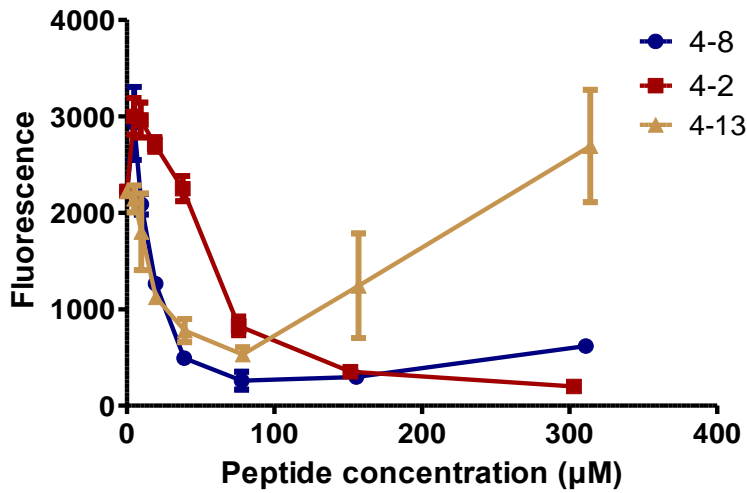
Figure 2.12 Peptide 4-2, 4-8 and 4-13 disrupted 5-FAM-MTDH-SN1/2 interaction

Peptides 4-2 and 4-8 disrupted 5-FAM-MTDH-SN1/2 interaction in a dose-dependent manner. Peptide 4-13 disrupted 5-FAM-MTDH-SN1/2 interaction only at low concentrations. The mean ±S.D. of fluorescence is shown (n=3).
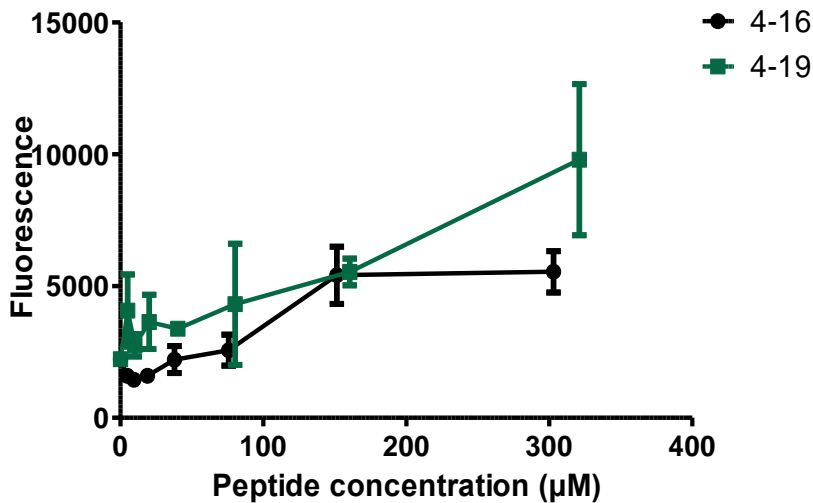
Figure 2.13 Peptide 4-16 and 4-19 enhanced 5-FAM-MTDH-SN1/2 interaction

Disruption study was the same as that in Figure 2.12 but with peptides 4-16 and 4-19. The mean ±S.D. of fluorescence is shown (n=3).
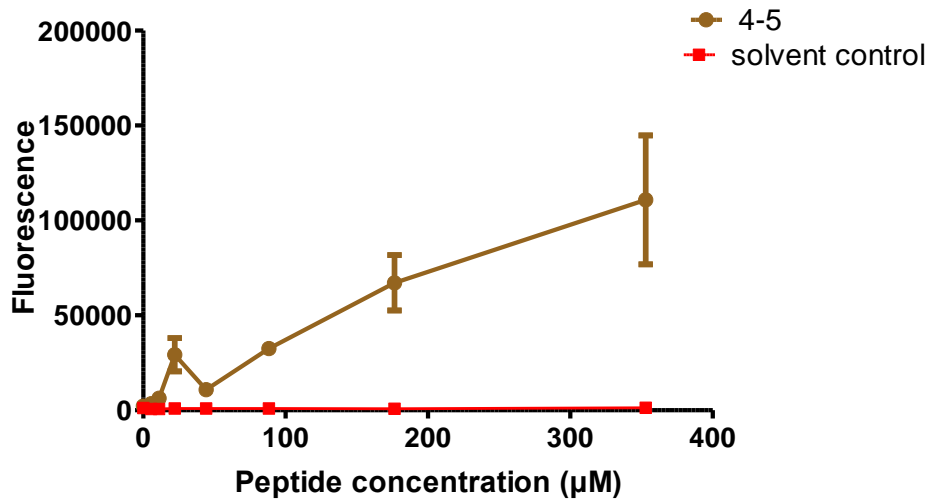
Figure 2.14 Peptide 4-5 enhanced 5-FAM-MTDH-SN1/2 interaction

Disruption study was the same as that in Figure 2.12. Peptide 4-5 was dissolved in DMF-water mixture. The mean ±S.D. of fluorescence is shown (n=3).

2.4.7 Peptide 4-2 disrupted full-length SND1-MTDH complex

Peptide 4-2 was shown to disrupt MTDH-SND1 interaction in ELISA assay, it would be important to test if peptide 4-2 could also disrupt SND1-MTDH full-length protein interaction. Since peptide 4-8 could induce precipitation after fusing with cell penetrating peptide, it was suspended from this stage.

Here c-Myc-tagged SND1 was overexpressed in MDA-MB-231-GFP-Red-FLuc cells. Co-Immunoprecipitation experiment showed that SND1 could pull down MTDH (Figure 2.15 and 2.16) suggesting that SND1 could interact with MTDH. Peptide 4-2 could disrupt SND1-MTDH interaction (Figure 2.16).
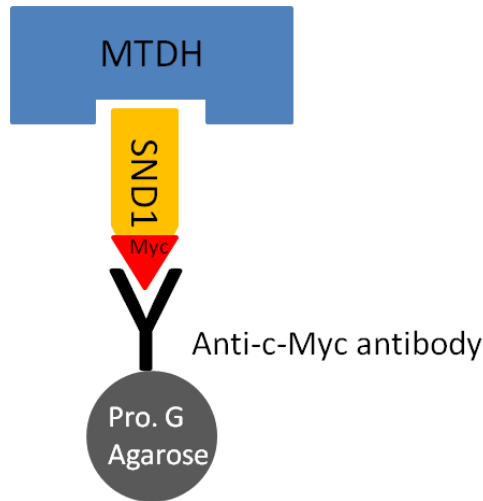
Figure 2.15 co-IP of MTDH by c-Myc-SND1 using c-Myc antibody
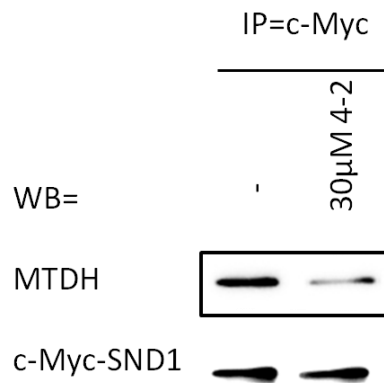
Figure 2.16 Disruption of full-length SND1-MTDH complex by peptide 4-2 (c-Myc co-IP)

Co-IP was conducted with c-Myc antibody using cell lysate from MDA-MB-231-GFP-Red-FLuc-SND1-c-Myc-DDK cells. 30µM of peptide 4-2 could disrupt SND1-MTDH interaction. Each experiment was conducted for more than 3 times and result from one trial is shown here.

Another approach to test SND1/MTDH interaction was to pull down MTDH (instead of SND1 as shown above). V5-tagged MTDH was overexpressed in MDA-MB-231-GFP-Red-FLuc cells. MTDH could pull down SND1 (Figure 2.17 and 2.18) suggesting that MTDH could interact

with SND1. Peptide 4-2 could disrupt SND1-MTDH interaction (Figure 2.18).
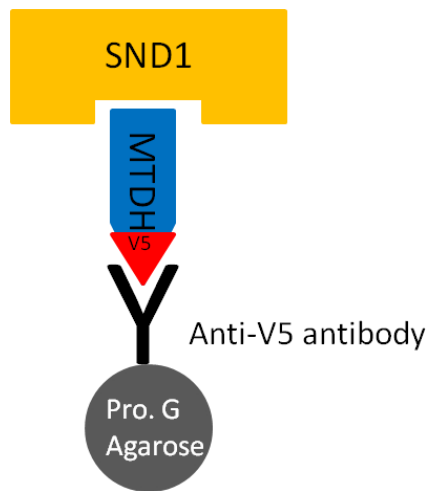
Figure 2.17 co-IP of SND1 by V5-MTDH using V5 antibody
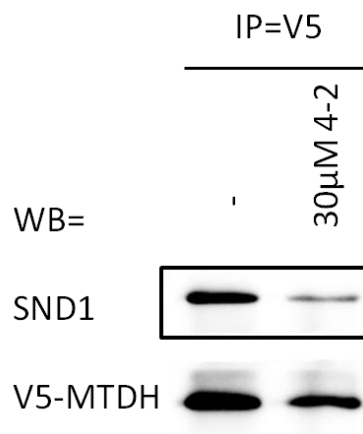
Figure 2.18 Disruption of full-length SND1-MTDH complex by peptide 4-2 (V5 co-IP)

Pull-down was conducted with V5 antibody using cell lysate from MDA-MB-231-GFP-Red-FLuc-MTDH-V5 cells. 30μM of peptide 4-2 could disrupt SND1-MTDH interaction. The experiment was conducted for more than 3 times and result from one trial is shown here.

2.5 Discussion

2.5.1 Unusually high percentage of tryptophan in SN1/2 binding peptides

After four rounds of screening, 20 single phage clones with strong binding affinity to SN1/2 were identified. These phages displayed an unusually higher percentage of tryptophan (Table 2.1). Tryptophan was rare amino acid in nature (Siemion, 1994). Interestingly, there were two important tryptophans (W394, W401) in MTDH occupying the groove of the binding interface of SND1-MTDH complex (Guo et al., 2014) (Figure 2.2). These two tryptophans in MTDH were critical in interacting with SND1 and promoting tumor initiation (Guo et al., 2014). One could speculate that the tryptophans found in the SN1/2 binding peptides might play a similar role with the 2 tryptophans in MTDH in binding to SND1.

2.5.2 Peptide 4-2 could disrupt SND1-MTDH interaction

Peptide 4-2, which was the most repeated peptide after phage display screening, showed high binding affinity to SN1/2 in ELISA assay. Peptide 4-2 could also disrupt 22-mer MTDH peptide from interacting with SN1/2 in ELISA assay and could also disrupt SND1-MTDH full-length protein interaction in co-IP assay, indicating that peptide 4-2 might bind to the

binding interface of SND1-MTDH. The sequence of peptide 4-2 had 5 amino acids between one Y and one W, indicating that peptide 4-2 might be a MTDH-like peptide, which could disrupt SND1-MTDH interaction.

2.5.3 Peptide binding affinity towards SN1/2 (phage ELISA) corresponded to the ability of disrupting 5-FAM-MTDH-SN1/2 interaction

Phages 4-8 and 4-13 showed a higher binding affinity towards SN1/2 compared to phage 4-2 (Figure 2.9a). Interestingly, peptides 4-8 and 4-13 also competed with 5-FAM-MTDH peptide binding to SN1/2 with lower EC_{50}s compared to peptide 4-2 (Figure 2.12). This suggested that the peptides identified from phage display were binding to the interface of SND1-MTDH interaction.

Peptide 4-5, 4-16 and 4-19 could bind to SN1/2 with high binding affinity (Figure 2.9a), but they could not disrupt MTDH-SND1 interaction. Unexpectedly, they could recruit MTDH to bind to SND1 in a dose dependent manner (Figure 2.13 and 2.14). One possible reason might be that these peptides could on one hand interact with SN1/2 but on the other hand also interact with MTDH, forming a sandwich-like structure.

2.5.4 5-FAM-MTDH scrambled peptide showed mild binding affinity towards SN1/2 domain of SND1

5-FAM-MTDH 22-mer scrambled peptide was designed online by a peptide design tool. Our 5-FAM-MTDH scrambled peptide showed mild binding affinity towards SN1/2. Two consecutive prolines in the scramble peptide (SNWAESWVA**PP**GEDSADNEWDN) might be the reason why this peptide showed mild binding affinity towards SN1/2. Proline was an anomalous amino acid whose nitrogen atom was covalently locked within a ring structure, resulting in a constrained phi angle in this amino acid (Morgan and Rubenstein, 2013). Consecutive prolines might facilitate the formation of the secondary structures of proteins or peptides. The two consecutive prolines in 5-FAM-MTDH scrambled peptide might form bent structure, which probably resulted in the strange binding mode of this peptide compared with the fully flexible linear scrambled peptides. After subtracting MTDH scramble peptide binding to SN1/2 from MTDH peptide binding to SN1/2, specific binding of MTDH peptide to SN1/2 was shown.

Chapter 3 Cytotoxic effect of CPP-4-2 to breast cancer cells and its potential mechanism

3.1 Abstract

CPP-4-2 was constructed by fusing a RR-TAT cell penetrating peptide at the N-terminus of peptide 4-2 to facilitate its penetration into mammalian cells. CPP-4-2 preferentially killed breast cancer cell line MDA-MB-231-GFP-Red-FLuc, MCF7 and MDA-MB-468 compared to other cancer type SKOV3, A549-Red-FLuc, QGY-7703 or mouse fibroblast L929. CPP-4-2 killed breast cancer cell by inducing apoptosis. These results indicated that CPP-4-2 affected a specific survival-associated pathway in breast cancer cell but not in other cancer types or normal cell.

Essential amino acids of CPP-4-2 were investigated through mutagenesis. W and Y were selected for mutagenesis since they were highly enriched in the peptides after phage display screening. Simultaneous mutation of Y4, W10 and Y11 to A (producing CPP-4-2AAA) abolished the cytotoxicity of CPP-4-2 to breast cancer cell. W10A mutation alone abolished the cytotoxicity, whereas Y4A mutation or Y11A mutation did not. This result suggested that W10 was essential in the cytotoxicity of CPP-4-2, whereas Y4 and Y11 were not.

The mechanism of CPP-4-2 mediating cytotoxicity in breast cancer cells was investigated. CPP-4-2 peptide, which could disrupt SND1-MTDH interaction, could downregulate SND1 in breast cancer cells. The overexpression of SND1 reduced the cytotoxicity of CPP-4-2 to breast cancer cells, indicating that CPP-4-2 mediated downregulation of SND1 might be the reason for breast cancer cell death.

For SND1 downstream pathway investigation, CPP-4-2, CPP-4-2Y4A and CPP-4-2Y11A could affect Akt pathway in breast cancer cells by upregulating p-Akt S473 and degrading Akt, whereas CPP-4-2AAA and CPP-4-2W10A could not. The degradation of Akt by CPP-4-2 was proteasome-dependent and was partially contributed by the phosphorylation of Akt at S473. Proteomics study indicated that CPP-4-2 affected several important cell survival pathways such as tRNA charging, protein ubiquitination. Among the differentially expressed proteins, the transcription of NF-κB2 was confirmed to be significantly enhanced by CPP-4-2 but not CPP-4-2AAA or CPP-4-2W10A.

The essential amino acid of peptide 4-2 in SND1-interaction was investigated. Peptide 4-2, 4-2Y4A and 4-2Y11A could disrupt biotinylated peptide 4-2 interacting with SND1 but 4-2W10A could not. A detailed molecular docking study revealed that peptide 4-2 interacted with SN1/2 near the binding interface of SND1-MTDH complex.

In summary, peptide 4-2 selectively killed breast cancer cells by inducing

apoptosis probably by interacting with SND1, disrupting SND1-MTDH interaction and inducing SND1 degradation. Peptide 4-2 could also affect SND1 downstream targets, Akt and NF-κB2 by degrading Akt and enhancing the transcription of pro-apoptotic NF-κB2, which probably lead to breast cancer cell death. W10 rather than Y4 or Y11 was the essential amino acid in the activities of peptide 4-2.

3.2 Introduction

SND1 as a multifunctional protein was found to be overexpressed in many types of cancers. After identifying the SND1 binding peptides, we were interested in testing their effects on breast cancer cells by fusing them with a cell penetrating peptide. Multiple pathways were reported to be the downstream of SND1 including Akt pathway (Rajasekaran et al., 2016b) and NF-κB signaling (Santhekadur et al., 2012). We were interested in investigating if SND1 interacting peptide could affect these pathways, which might lead to breast cancer cell death.

3.2.1 Cell-penetrating peptides

Cell-penetrating peptides (CPPs) were short peptides that could pass through tissue and cell membrane via energy-dependent or independent mechanisms. They were widely used to carry a variety of biologically active conjugates (cargoes) into cells (Guidotti et al., 2017). A number of peptides with the ability to be internalized into cells were discovered as shown in Table 3.1. Although there were many ways to classify these CPP peptides, they were usually classified according to their physical-chemical properties. All of the newly discovered CPPs fell into one of the following categories: cationic, amphipathic, or hydrophobic CPPs (Table 3.1) (Guidotti et al., 2017).

Table 3.1 Examples of CPPs and their sequences, origins, and physical–chemical properties

CPP name	Sequence	Origin	Class
HIV-1 TAT protein, TAT$_{48-60}$	GRKKRRQRRRPPQ	HIV-1 TAT protein	Cationic
HIV-1 TAT protein, TAT$_{49-57}$	RKKRRQRRR	HIV-1 TAT protein	Cationic
Penetratin, pAntp(43–58)	RQIKIWFQNRRMKWKK	Antennapedia *Drosophila melanogaster*	Cationic
Polyarginines	Rn	Chemically synthesized	Cationic
DPV1047	VKRGLKLRHVRPRVTRMDV	Chemically synthesized	Cationic
MPG	GALFLGFLGAAGSTMGAWSQPKKKRKV	HIV glycoprotein 41/SV40 T antigen NLS	Amphipathic
Pep-1	KETWWETWWTEWSQPKKKRKV	Tryptophan-rich cluster/SV40 T antigen NLS	Amphipathic
pVEC	LLIILRRRIRKQAHAHSK	Vascular endothelial cadherin	Amphipathic
ARF(1–22)	MVRRFLVTLRIRRACGPPRVRV	p14ARF protein	Amphipathic
BPrPr(1–28)	MVKSKIGSWILVLFVAMWSDVGLCKKRP	N terminus of unprocessed bovine prion protein	Amphipathic
MAP	KLALKLALKALKAALKLA	Chemically synthesized	Amphipathic
Transportan	GWTLNSAGYLLGKINLKALAALAKKIL	Chimeric galanin–mastoparan	Amphipathic
p28	LSTAADMQGVVTDGMASGLDKDYLKPDD	Azurin	Amphipathic
VT5	DPKGDPKGVTVTVTVTGKGDPKPD	Chemically synthesized	Amphipathic
Bac 7 (Bac $_{1-24}$)	RRIRPRPPRLPRPRPRPLPFPRPG	Bactenecin family of antimicrobial peptides	Amphipathic
C105Y	CSIPPEVKFNKPFVYLI	α1-Antitrypsin	Hydrophobic
PFVYLI	PFVYLI	Derived from synthetic C105Y	Hydrophobic
Pep-7	SDLWEMMMVSLACQY	CHL8 peptide phage clone	Hydrophobic

CPPs were classified into three categories: cationic, amphipathic and hydrophobic CPPs. TAT was the most-studied CPPs and it was selected in this project to direct peptides into cells. This table was adapted from (Guidotti et al., 2017).

The most-studied category of CPP was cationic CPP, which included TAT-derived peptides, penetratin, polyarginines, and Diatos peptide vector 1047 (Guidotti et al., 2017). TAT was first identified as CPP in transcription transactivating protein of HIV-1 (Vives et al., 1997). It was found that the 15-mer peptide containing the protein transduction domain of TAT was capable of directing biologically active fusion protein into all tissues, even into brain (Schwarze et al., 1999).

TAT was the most studied CPP and it showed comparably low cytotoxicity (El-Andaloussi et al., 2007). Here TAT was fused with peptide 4-2 to internalize it into cells for functional studies. As the number and the order of amino acids (especially lycines and arginines) within TAT were critical in determining the transduction properties (Tuunnemann et al., 2008; Wender et al., 2000), a hybrid CPP, RR-TAT was also used in this project to further increase the cell penetrating efficiency and also increase the solubility of the fused peptide in cell culture medium.

3.2.2 Akt signaling

Akt (also known as protein kinase B, PKB) was reported to be the downstream of SND1 (Rajasekaran et al., 2016b). It played an important role in cell metabolism, growth, proliferation, and survival (Hemmings and Restuccia, 2012). In 1991, the initial identification of Akt was accomplished by three different groups based on its homology to

protein kinase A (Coffer and Woodgett, 1991) and protein kinase C (Jones et al., 1991) and as the cellular homolog to the retroviral oncogene viral Akt (Bellacosa et al., 1991). Three isoforms of Akt were found in mammalian cells, Akt1, Akt2 and Akt3 (Song et al., 2005a).

3.2.2.1 Activation of Akt signaling

The activation of Akt was controlled by a multi-step process involving phosphoinositide-3-kinase (PI3K) (Hemmings and Restuccia, 2012). PI3K was a lipid kinase that could generate phosphatidylinositol 3-phosphate (PIP_3), recruiting many downstream proteins to plasma membrane. Class 1A and Class 1B of PI3K involved in the activation of Akt pathway were activated by tyrosine kinase (RTK) and G-protein-coupled receptors (GPCR), respectively (Wymann et al., 2003). When these receptors were activated by ligands, PI3K was first recruited to the plasma membrane, converting PIP_2 to PIP_3 (Figure 3.1). Phosphatases such as PTEN could convert PIP_3 back to PIP_2 (Hemmings and Restuccia, 2012; Song et al., 2005b). PIP_3 recruited Akt via its lipid-binding PH domain to the plasma membrane, changing Akt's conformation and allowing an access of Akt to phosphoinositide-dependent protein kinase 1 (PDK1) for subsequent phosphorylation (Song et al., 2005b).

There were two major phosphorylation sites related to the activation of Akt1, T308 in the activation, or T-loop of the catalytic protein kinase core

and S473 in a C-terminal hydrophobic motif (Alessi et al., 1996). The corresponding residues in Akt2 and Akt3 were located at T309 and S474, and T305 and S472, respectively (Manning and Toker, 2017). PDK1 phosphorylated AKT1 at T308 site, which was necessary for AKT activity at a basal level as shown in Figure 3.1 (Alessi et al., 1997). Full activation of AKT required phosphorylation at S473 in the hydrophobic motif. Mechanistic target of rapamycin (mTOR) complex 2 (mTORC2) was the kinase that phosphorylates Akt at S473 for its maximal activation as shown in Figure 3.1 (Sarbassov et al., 2005). Akt activation could positively regulate cell survival, cell proliferation, cell metabolism or cell growth through multiple downstream pathways (Manning and Toker, 2017).
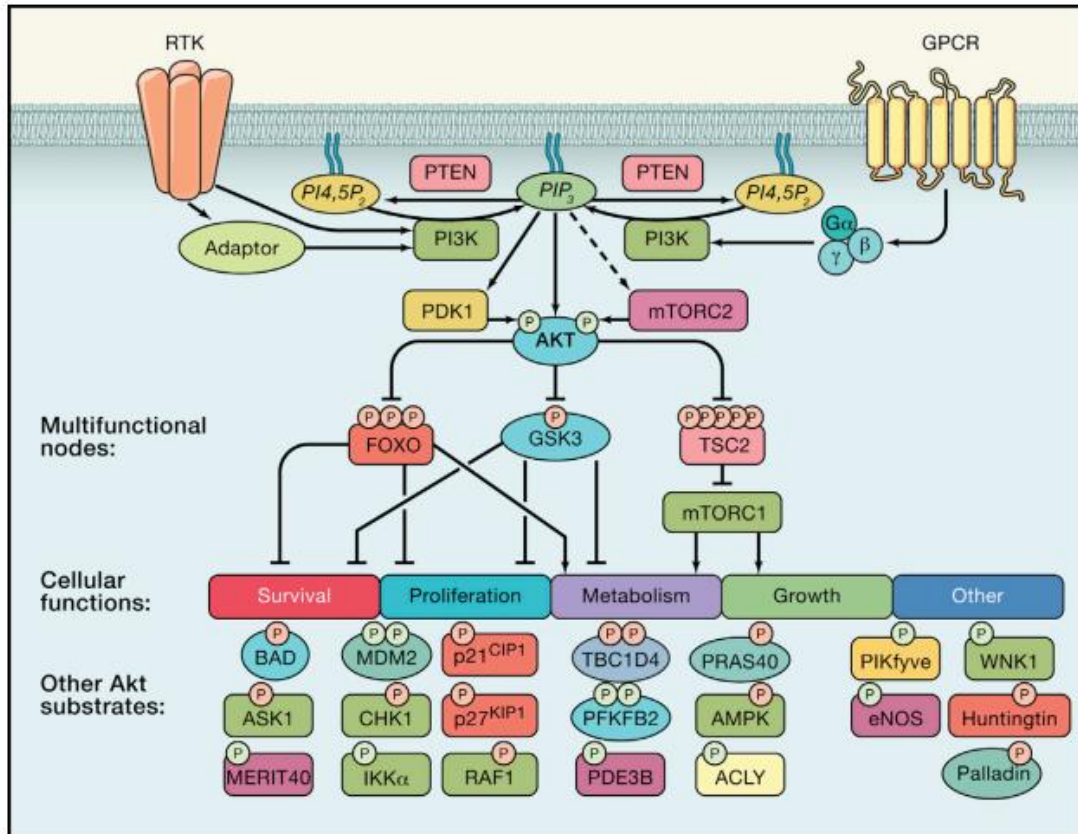
Figure 3.1 Molecular mechanisms of Akt regulation

Activation of Akt pathway was a muti-step process. When RTK and GPCR were activated, PI3K was recruited to the membrane and became activated. PIP_2 ($PI4,5P_2$) was converted into PIP_3 ($PI4,5P_3$) under tight regulation of PI3K and PTEN. Akt was recuited to the membrane by PIP_3 and phosporylated by PDK1 at T308, after which Akt was further phosphorylated by mTORC2 at S473 for full activation. There were several multi-functional nodes at the downstream of Akt such as FOXO, GSK3 and TSC2. A number of Akt substrates were also shown at the bottom of this figure. This diagram was adapted from (Manning and Toker, 2017).

RTK: Tyrosine kinase receptor; GPCR: G-protein-coupled receptors; PIP_3: phosphatidylinositol 3-phosphate; PIP_2: phosphatidylinositol 2-phosphate; PDK1: phosphoinositide-dependent protein kinase 1; mTORC2: mechanistic target of rapamycin complex 2

3.2.2.2 Akt degradation pathways

There were three major protein degradation pathways in mammalian cells: proteasome, lysosome and autophagosome degradation pathways. Akt signaling was linked to two important protein degradation systems in mammalian cells: the ubiquitin–proteasome system and autophagy system (Noguchi et al., 2014).

There were two types of ubiquitinylation that are associated with Akt: K48-linked and K63-linked ubiquitinlyation. K48-linked ubiquitinylation controls proteasomal degradation of Akt and the subsequent downstream signals, whereas K63-linked polyubiquitination of Akt served as a regulatory mechanism to promote plasma membrane recruitment of Akt to facilitate its activation (Mukhopadhyay and Riezman, 2007; Reyes-Turcu et al., 2009). TT3, BRCA1, and MULAN were three different proteins found to be involved in the K48-linked uniquitinylation of Akt.

Tetratricopeptide repeat domain 3 (TTC3) was an E3 ubiquitin ligase, which interacted preferentially with phosphorylated Akt at T308 to induce the polyubiquitination and subsequent degradation of AKT in the nucleus of mammalian cells. It was also reported that overexpression of wild-type TTC3 could significantly inhibit cell proliferation while on the other hand, suppression of TTC3 by siRNA could augment cellular proliferation in HT1080 cells (Suizu et al., 2009).

In addition, Akt was demonstrated to directly interact with MULAN, an E3 ubiquitin ligase which ubiquitinated Akt *in vitro* and *in vivo* (Bae et al., 2012). Phosphorylated Akt was a binding partner and a ubiquitination substrate of MULAN in the cytoplasm of mammalian cells. Moreover, the MULAN-induced degradation of Akt could suppress cell proliferation and viability in HeLa cells (Bae et al., 2012). The discovery of these ubiquitin ligases or protein factors which could regulate the ubiquitinylation and the subsequent degradation-related survival suppression suggested a novel activation-induced suicidal degradation mechanism of Akt (Bae et al., 2012).

The breast cancer susceptibility gene 1 (*BRCA1*) was a suppressor gene in different types of cancers including breast cancer and ovary cancer (Silver and Livingston, 2012). It was reported that *BRCA1* deficiency was able to activate Akt signaling pathway. Phosphorylation and kinase activity of Akt were enhanced in BRCA1 mutants. The interaction between BRCA1-BRCT domains and pAkt S473 would lead to the ubiquitination of Akt toward protein degradation in the nucleus. BRCA1 mutant cells with *BRCT* repeats deficiency could accumulate nuclear pAkt S473 and therefore inactivate the transcription functions of FOXO3a, a major nuclear target of pAKT (Xiang et al., 2008).

3.2.3 NF-κB signaling

NF-κB (nuclear factor-kappaB) was a collective name for inducible dimeric transcription factors which was composed of Rel family of DNA-binding proteins (Karin and Ben-Neriah, 2000). It was an essential gene involved in the activation of large numbers of genes responding to infection, inflammation and cell survival (Karin and Ben-Neriah, 2000). NF-κB family contained 5 members of transcription factors, NF-κB1/p105/p50, NF-κB2/p100/p52, RelA/p65, RelB and c-Rel. They could form heterodimers or homodimers and subsequently bound to consensus DNA sequences at promoter regions of responsive genes (Xia et al., 2014). Under normal condition, NF-κB was localized in the cytoplasm of non-stimulated cells but when NF-κB pathway was activated, it was translocated into the nucleus for transcriptional activation of downstream genes (Karin and Ben-Neriah, 2000). The activation of NF-κB through molecular translocation was controlled by the phosphorylation and subsequent degradation of inhibitors of kappa B (IκB) (Baldwin, 1996).

NF-κB played a very important role in cancer initiation, development, metastasis and chemo-resistance (Xia et al., 2014). NF-κB was known to promote cell survival by upregulating many anti-apoptotic genes, such as Bcl-2 homologues A1/Bfl-1 and Bcl-xL, IEX-1 and XIAP (Baldwin, 2001). Interestingly, NF-κB also showed pro-apoptotic activity depending on the

stimulus given (Kaltschmidt et al., 2000).

NF-κB2/p100

NF-κB2 was the most frequently mutated NF-κB member in human lymphoma (Rayet and Gelinas, 1999). NF-κB2/p100 could undergo proteolytic cleavage to generate a 52k polypeptide (p52) which corresponded to the N-terminal half of p100 (Xiao et al., 2001). P100 protein was composed of Rel homology domain, ankyrin repeats and death domain, whereas P52 was only composed of Rel homology domain after proteolytic processing (Figure 3.2) (Xiao et al., 2001). The C-terminal ankyrin repeats contained intrinsic IκB activity (Senftleben et al., 2001). The Rel homology domain was required for dimerization, DNA binding, interaction with IκBs, and nuclear translocation (Oeckinghaus and Ghosh, 2009).
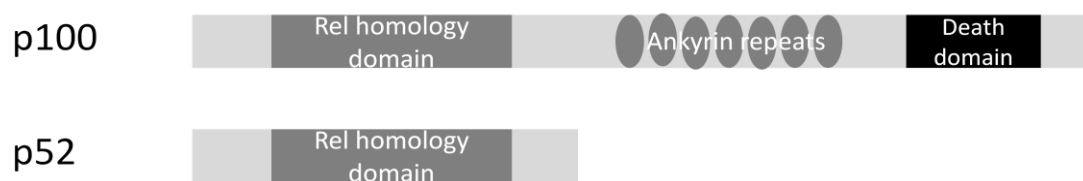
Figure 3.2 Secondary structures of p100 and p52

NF-κB2/p100 was consisted of Rel homology domain, Ankyrin repeats and Death domain. NF-κB2/P52 contained only Rel homology domain (Xiao et al., 2001). The Rel homology domain was responsible for dimerization, DNA binding, interaction with IκBs, and nuclear translocation (Oeckinghaus and Ghosh, 2009).

The death domain of p100 might play a pro-apoptotic function in cancer cells. A selective activation of p52 was detected in human breast cancer tissue (Cogswell et al., 2000). Moreover, C-terminal deletions of NF-κB2 gene and subsequent generation of p100 mutants without the death domain were found in human lymphoid tumors (Rayet and Gelinas, 1999). This information indirectly suggested p100 played a pro-apoptotic function, which was opposite to the commonly known anti-apoptotic function of p52 in cancer cells.

The pro-apoptotic function of p100 and anti-apoptotic function of p52 were further investigated. The death domain at the C-terminus of p100 was found to be absent from all known tumor-derived mutants. It was found to inhibit cell growth and was essential for the pro-apoptotic activity of p100. It could also mediate the recruitment of p100 into death machinery complexes after ligand stimulation. Interestingly, colony formation assay of mouse fibroblast with activated Ras suggested p100 and p52 had anti- and pro-oncogenic activities, respectively. Caspase-8 was revealed to be essential in mediating the anti-oncogenic function of p100 (Wang et al., 2002).

Myc oncoproteins were found to be activated in approximately 70% of human malignancies (Boxer and Dang, 2001). It was reported to transactivate genes through binding to consensus '-CACGTG-3' or E box. It could also suppress transcription by inhibiting gene initiator (Dang,

1999). The NF-κB pathway was found to be suppressed in Myc-driven human Burkitt lymphoma (Dave et al., 2006). Myc oncoprotein could suppress the transcription of *NF-κB2*. The loss of NF-κB2 was able to accelerate Myc-induced lymphomagenesis by impairing apoptosis in Eμ-*Myc* transgenic mice (Keller et al., 2010).

3.3 Methodology

3.3.1 Cell seeding, peptide treatment and MTS assay

A total of 5000-8000 cells were seeded per well into a 96-well tissue culture plate for attachment for 24h in RPMI medium, after which peptides were diluted into series dilutions and added onto cells for incubation. After 72h, medium was removed followed by the addition of MTS, PMS, and medium solution (prepared according to the instruction of Promega). Cells were then incubated for another 1h at 37°C before OD_{490} was measured by a micro-plate reader.

3.3.2 Cell culture, peptide treatment and cell transfection

MDA-MB-231-GFP-Red-FLuc, MCF7, MDA-MB-468, L929, QGY-7703, A549-Red-FLuc and SKOV3 cell lines were cultured in RPMI Medium 1640 (gibco) supplemented with antibiotics P/S (100U/mL penicillin, 100μg/mL Streptomycin) and 10% fetal bovine serum (FBS, HyClone) at 37°C with 5% CO_2. Subculture was performed when the cell density

reached approximately 80-90% confluent.

For testing the effect of CPP-4-2 on Akt pathway, MDA-MB-231-GFP-Red-FLuc cells were seeded and grown to 80-90% confluent before peptide treatment. Cells were incubated with CPP-4-2 and its mutant peptides for 24h before lysis for western blot analysis.

Stable transfection of MDA-MB-231-GFP-Red-FLuc cell line with pCMV6-Entry-SND1-cMyc-DDK plasmid (#RC200059, Origene) and pLX304-MTDH-V5 plasmid (HsCD00438838, DNASU) (Figure 3.3) was conducted using lipofectamine 3000 reagent (Thermo Fisher) according to the manufacturer's instruction. After transfection, MDA-MB-231-GFP-Red-FLuc cells were selected with G418 at the concentration of 2mg/mL or blasticidin at the concentration of 10μg/mL for 2 weeks.
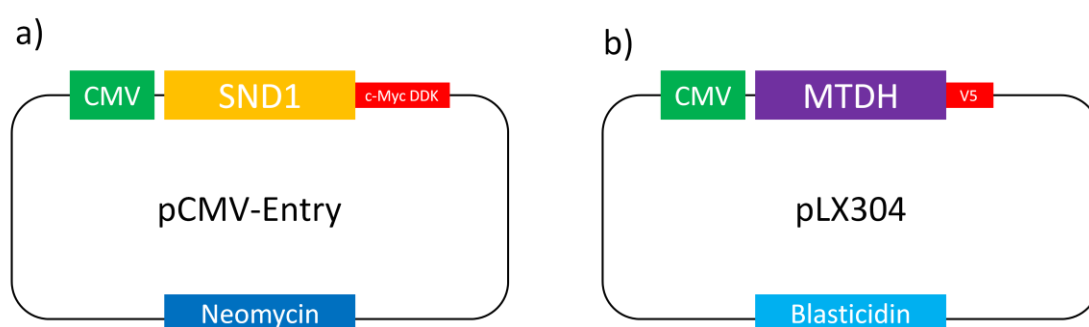
Figure 3.3 Maps of pCMV6-Entry-SND1-cMyc-DDK plasmid and pLX304-MTDH-V5 plasmid

pCMV6-Entry-SND1-cMyc-DDK plasmid and pLX304-MTDH-V5 plasmid were used in the construction of MDA-MB-231-GFP-Red-FLuc transgenic cell lines.

3.3.3 Biotinylated 4-2 peptide pull-down assay

MDA-MB-231-GFP-Red-FLuc and SKOV3 cell lysate was prepared with modified RIPA lysis buffer (10mM Tris, 75mM NaCl, 0.5% NP40, pH7.4) supplemented with 1mM PMSF and 1X protease inhibitor (#11836153001,Roche). After centrifugation at 14,000rpm at 4°C for 10 min, supernatant was collected for pull down assay. For peptide pull-down assay, 20 nmoles of biotinylated 4-2 peptide was pre-incubated with streptavidin agarose breads (Thermo Fisher) for 3h before IP. For pull-down assay with competitive peptides, 40 nmoles of 4-2 and its mutant peptides were added to cell lysate for preincubation at 4°C for 3h. Pull down assay were conducted by mixing the treated beads and cell lysate overnight at 4°C with rotation.

3.3.4 Peptide synthesis

Peptides used here were synthesized using the same method as described in Chapter 2. Biotinylated 4-2 peptide was synthesized with biotinylation at the N-terminus of peptide 4-2.

3.3.5 Western blot

Protein samples with SDS loading dye were loaded onto 10% polyacrylamide gel for separation and then transferred to a PVDF Immobilon P membrane (MilliPore). The membrane was blocked by

incubation in TBST (10mM Tris-HCl; pH 7.6, 150mM NaCl, 0.05% Tween20) containing 5% non-fat milk at room temperature for 1 hour with agitation. After blocking, the membrane was washed 3 times with TBST, each for 5 minutes with agitation, and then incubated with 1:1000-3000 primary antibody, anti-MTDH antibody (#40-6500, Invitrogen), anti-SND1 antibody (sc-271590), anti-β-actin antibody (sc-47778), anti-p-Akt S473 antibody (#9271, Cell Signailing) and anti-Akt antibody (#4691, Cell Signailing) in TBST overnight at 4°C with agitation. The membrane was then thoroughly washed as mentioned above, followed by incubation with 1:3000 secondary antibody, goat anti-rabbit or rabbit anti-mouse IgG-HRP (Santa Cruz Biotechnology Inc.) in TBST for 1 hour at room temperature with agitation. After washing with TBST, the membrane was incubated with the SuperSignal Substrate Western Blot kit (Pierce) before chemiluminescence signal detection by the Azure C600 western blot imaging system.

3.3.6 In silico docking of peptide 4-2 to SN1/2

3.3.6.1 Determination of the binding pockets on SN1/2

ICMPocketFinder Tool (PMID: 15757999) identified potential pockets in SN1/2 (PDB: 4QMG) using ICM-Pro (Miller et al., 2011). Five tentative pockets were chosen for further study. For each pocket, a box space region was drawn around it. Two more boxes were defined, one (Boxi)

around the interface of MTDH peptide and SN1/2 and the other one (Boxno) as a big box containing the whole structure of SN1/2.

3.3.6.2 Peptide sampling using Monte Carlo method

The 7 boxes mentioned above were used to fit peptide 4-2. Peptide 4-2 was sampled in the potential map ensembles through biased probability Monte Carlo method with W10 restrained to each of the 7 boxes to optimize peptide 4-2 (W10 has been proved to be the essential amino acid in interacting with SN1/2). After the presampling of peptide 4-2, 16 top conformations were saved as starting conformations for next step peptide docking. Each starting conformation was further flipped to generate 4 principal starting poses, which were sampled through biased probability Monte Carlo method to optimize the positional and internal variables with W10 (in peptide 4-2) restrained in the tentative binding site.

After docking, 50 top ranking conformations were saved for each starting pose for further analysis. Docking score ≤-190 was chosen as a criterion to select the conformations of the highest possibility to bind to SN1/2.

3.3.7 Proteomics analysis

MDA-MB-231 cells were cultured as described above. Cells were harvested and lysed in cell lysis buffer (10mM Tris pH 7.4, 75mM NaCl,

0.1%SDS). Soluble proteins were collected in the supernatant of cell lysate after centrifugation at 12,000g for 10min. Protein concentration was determined by Bradford (Bio-Rad).

100µg of soluble proteins of each samples were digested with trypsin and then analyzed by mass spectrometry. The digested peptide mixture was analyzed by Bruker amaZon speed ESI-ion trap-ETD mass spectrometer (Thermo Fisher Scientific) coupled with LC-MS/MS by an EASY-nLC system (Thermo Fisher Scientific) through a nanoelectrospray ion source. Samples were concentrated and desalted online with a pre-column (2cm; 100µm ID; 5µm C18-A1; Thermo). Separation was conducted using Acclaim PepMap 100 C18 column (10cm; 75µm ID; 3µm C18-A2; Thermo). A linear gradient of A and B buffers (buffer A: A = 0.1% formic acid; Buffer B = 99% ACN, 0.1% formic acid) from 1% to 50% buffer B for a total of 77 min at a flow rate of 0.3 µL/min was used to elute peptides into the mass spectrometer. Mass spectra were obtained in the positive-ion mode over the range m/z 400-1500. Proteins were identified by identifying at least 3 unique peptides in one protein. Pathway analysis of the differentially expressed proteins was performed by IPA (Ingenuity Pathway Analysis, QIAGEN).

3.3.8 RNA extraction and Real-time PCR

mRNA was extracted from cell pellets using the Trizol Reagent (Life

Technologies). cDNA synthesis was performed by incubating with 2µg RNA with RT Buffer, dNTP, RT random primers and Reverse Transcriptase using High Capacity cDNA Reverse Transcription Kit (Thermo Fisher Scientific) at 25 °C for 10min, 37°C for 120min followed by 85°C for 5min. cDNA (0.5µL RT reaction buffer) was amplified in 10µL real-time PCR buffer containing 4pmol of each primer and 5µL SsoFast EvaGreen Supermix with Low ROX (BIO-RAD). Primers used were listed as follows, ITGB4 primers: 5'-GCAGCCCCATCTCCTAGC-3', 5'-ATCCTCTTCCTCCCTCTCC C-3'; EP400 primers: 5'-ACAGTGAGGACGCAGTGATG-3', 5'-CATCCTCTCGCGTGTAGGTC-3'; NF-κB2 primers: 5'-TGGCCGGGACAAGAGAAAAG-3', 5'-CATCCAGACCTGGGTTGTAGC-3'; NF-κB1 primers: 5'-CCAACAGATGGCCCATACCT-3', 5'-AACCTTTGCTGGTCCCACAT-3'; BCL2 primers: 5'-CAGGATAACGGAGGCTGGGATG-3', 5'-GACTTCACTTGTGGCCCAGAT-3'; Bax primers: 5'-AAACTGGTGCTCAAGGCCC-3', 5'-AAAGTAGGAGAGGAGGCCGT-3'; β-actin primers: 5'-CTCTTCCAGCCTTCCTTCCT-3', 5'-AGCACTGTGTTGGCGTACAG-3'. Real-time PCR was performed with 1 cycle at 95°C for 30s, 35 cycles at 95°C for 10s and 60°C for 30s, and 81 cycles at 55°C for 30s.

3.3.9 5-FAM-CPP-4-2 accumulation assay and flow cytometry

Different cell lines were detached and washed with PBS before

incubating with 10μM 5-FAM-CPP-4-2 (5-FAM-YGRKKRRQRRRQFDYDHFLMWYS-NH$_2$) in 37°C for 2h in RPMI medium with shaking. Cells were then washed with PBS and suspended in FACS flow cytometry buffer (1% BSA, 1mM EDTA in PBS). Peptide accumulation in different cell lines was detected with BD FACSVia cell analyzer.

3.3.10 Apoptosis assay and Flow cytometry

MDA-MB-231-GFP-Red-FLuc cells were seeded for 3 days to 70-80% confluence, followed by incubation with peptides for 24h before detachment. Annexin V and PI staining (#556419, BD Pharmingen) was performed according to the instructions of manufacturer. Annexin V and PI signals was detected with BD FACSVia cell analyzer.

3.4 Results

3.4.1 CPP-4-2 preferentially killed breast cancer cells

CPP-4-2 was constructed by fusing RR-TAT, a hybrid CPP at the N-terminus of peptide 4-2 to facilitate the penetration of peptide 4-2 into mammalian cells. Another SND1 interacting peptide 4-8 was found to precipitate significantly in tissue culture media after fusing with CPP so it was suspended. As shown in Figure 3.4, CPP-4-2 exhibited preferential cytotoxicity towards breast cancer cell lines MDA-MB-231-GFP-Red-FLuc, MCF7 and MDA-MB-468 with an IC_{50} of 22.4±1.0μM, 18.7±0.2μM and 15.9±6.2μM, respectively (Table 3.2). On the other hand, CPP-4-2 was much less toxic to other cancer types including SKOV3, QGY-7703, A549-Red-FLuc, and L929 (mouse SND1 was highly similar to human SND1 with only several difference of residues) under the same condition.

Different killing effects of CPP-4-2 towards different cell lines might be due to different cell penetrating efficiency. CPP-4-2 accumulation in different cell line was tested by flow cytometry. Comparable amount of 5-FAM-CPP-4-2 was detected in all the cell lines except MDA-MB-468, which accumulated 2-3 folds of CPP-4-2 (Figure 3.5). To summarize, CPP-4-2 preferentially killed breast cancer but not other cancer types or normal cell. The mechanism of the cytotoxicity of CPP-4-2 was tissue specific.
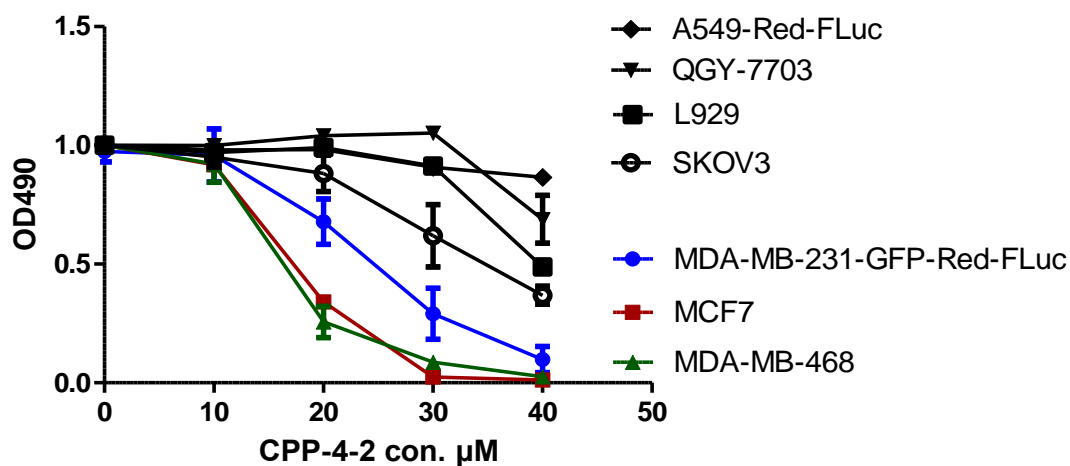
Figure 3.4 CPP-4-2 preferentially killed breast cancer cell lines

Different cell lines were incubated with serial dilutions of CPP-4-2 in RPMI medium for 72h before MTS assay. The mean ±S.D. of OD is shown (n=3).

Table 3.2 IC$_{50}$s of CPP-4-2 of different cell lines

Cell line	Cancer type	IC50 (µM, n≥3)
QGY-7703	Hela derivative	>40
A549-Red-FLuc	Lung	>40
L929	Fibroblast (mouse)	>40
SKOV3	Ovarian	32.4±6.7
MDA-MB-231-GFP-Red-FLuc	Breast	22.4±1.0
MCF7	Breast	18.7±0.2
MDA-MB-468	Breast	15.9±6.2

IC$_{50}$s of CPP-4-2 of different cell lines were calculated according to the data from Figure 3.4.
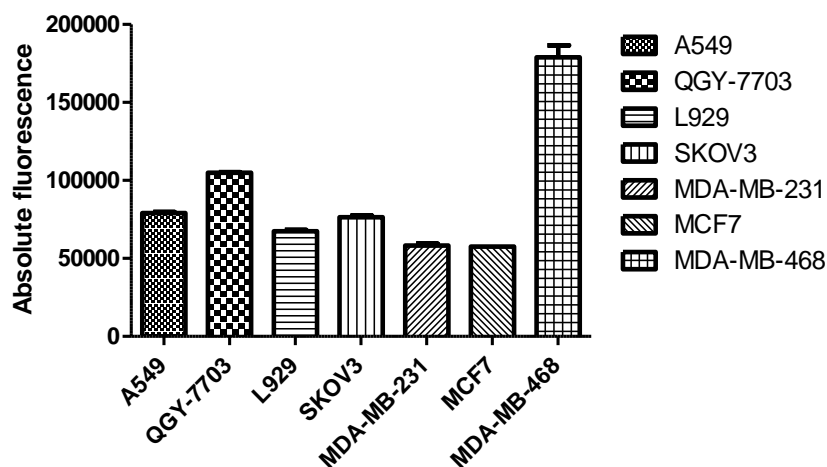
Figure 3.5 CPP-4-2 accumulated equally among different cell lines

Different cell lines were incubated with 10μM of 5-FAM-CPP-4-2 for 2h before flow cytometry analysis. Absolute fluorescence was obtained by subtracting untreated control from peptide treatment group. The mean ±S.D. of absolute fluorescence of 5-FAM-CPP-4-2 is shown (n=2).

Since CPP-4-2 showed preferential cytotoxicity towards breast cancer cell lines, the expression of SND1 in different cell lines were investigated. Endogenous expression of SND1 in different cell lines was shown in Figure 3.6. The cytotoxicity of CPP-4-2 towards different cell lines was irrelevant to the endogenous level of SND1.
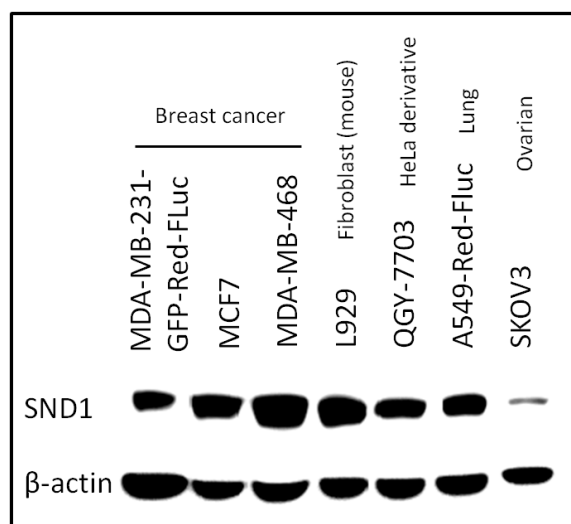
Figure 3.6 Expression level of SND1 in different cell lines

Expression of endogenous SND1 in different cell lines was shown. SND1 expression was normalized to β-actin. Western blot experiment was conducted for more than 3 times and result from one trial is shown in a).

3.4.2 Investigation of the essential amino acids of CPP-4-2 in cytotoxicity

Essential amino acids of CPP-4-2 in its cytotoxicity were investigated. Y and W were selected for mutagenesis since they were highly enriched after phage display screening. A series of mutants of CPP-4-2 (Table 3.3) were synthesized. Figure 3.7 showed that cell penetrating peptide CPP was not toxic to breast cancer cell. CPP-4-2 was highly toxic to MDA-MB-231-GFP-Red-FLuc cell line with an IC_{50} of 23.6±2.5µM compared to CPP-4-2AAA and CPP-4-2W10A (IC_{50}>40µM, Table 3.3). CPP-4-2Y4A and CPP-4-2Y11A were equally toxic as CPP-4-2 with IC_{50}s of 23.9±2.5 and 22.2±1.6µM, respectively (Table 3.3). This result suggested that W10 was the essential amino acid in CPP-4-2 in its cytotoxicity to

MDA-MB-231-GFP-Red-FLuc cells while Y4 and Y11 were not.

Table 3.3 Cytotoxicity of CPP-4-2 and its mutants on MDA-MB-231-GFP-Red-FLuc cells

Peptide Name	Sequence	IC50 (µM, n≥3)
CPP	RRRKKRRQRRR	>40
CPP-4-2	RRRKKRRQRRRQFDYDHFLMWYS	23.6±2.5
CPP-4-2Y4A	RRRKKRRQRRRQFDADHFLMWYS	23.9±2.5
CPP-4-2W10A	RRRKKRRQRRRQFDYDHFLMAYS	>40
CPP-4-2Y11A	RRRKKRRQRRRQFDYDHFLMWAS	22.2±1.6
CPP-4-2AAA	RRRKKRRQRRRQFDADHFLMAAS	>40

The suspected essential amino acids in CPP-4-2 peptide were mutated into alanine (labeled in red). IC_{50}s of these peptides to MDA-MB-231-GFP-Red-FLuc cells were calculated according to the data from Figure 3.7.
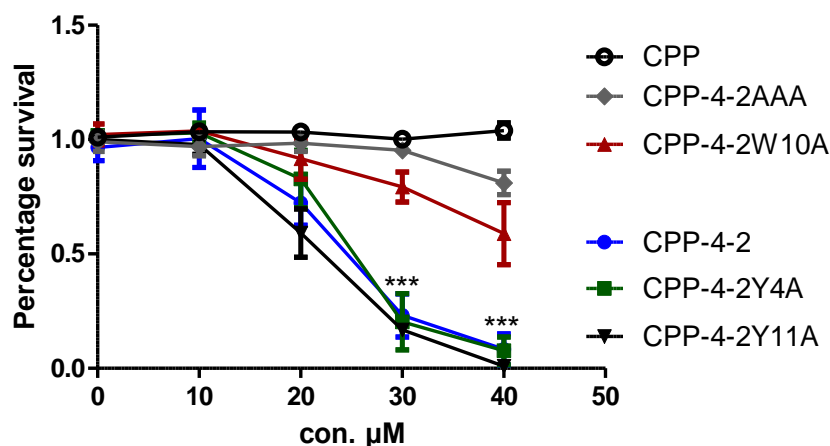
Figure 3.7 Cytotoxicity of CPP-4-2 and its mutants on MDA-MB-231-GFP-Red-FLuc cells

MDA-MB-231-GFP-Red-FLuc cells were incubated with serial dilutions of CPP-4-2 in RPMI medium for 72h before MTS assay. The mean ±S.D. of OD is shown (n=3).

3.4.3 CPP-4-2 killed breast cancer cells by inducing apoptosis

Since CPP-4-2 could kill breast cancer cell MDA-MB-231-GFP-Red-FLuc, we wanted to investigate if the cytotoxicity of CPP-4-2 to breast cancer cells was due to CPP-4-2 mediated apoptosis. Figure 3.8 showed that CPP-4-2 could induce early (34.1%) and late apoptosis (12.4%) on MDA-MB-231-GFP-Red-FLuc cells when compared to CPP-4-2AAA (20.4% early apoptosis, 0.4% late apoptosis) and untreated control (13.2% early apoptosis, 0.0% late apoptosis). This result suggested that CPP-4-2 killed breast cancer cell MDA-MB-231-GFP-Red-FLuc by inducing apoptosis.
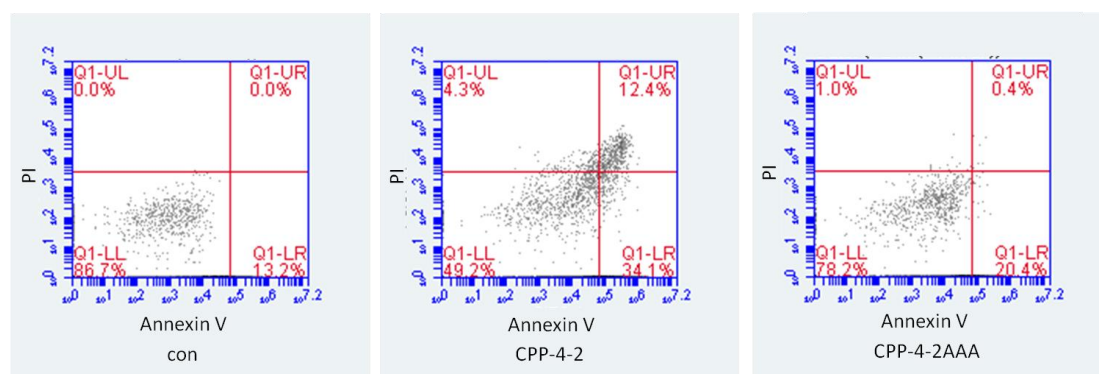
Figure 3.8 CPP-4-2 induces apoptosis of breast cancer cells

MDA-MB-231-GFP-Red-FLuc cells were treated with 30μM of peptides in RPMI medium for 4h before Annexin V and PI staining followed by flow cytometry analysis. Peptide treatment and flow cytometry analysis were conducted for more than 2 times and result from one trial is shown.

3.4.4 Biotinylated 4-2 peptide pulled down full-length SND1

In order to prove the interaction of peptide 4-2 and SND1, a biotinylated 4-2 peptide was synthesized and used to pull down SND1 from cell lysate. It was found that biotinylated 4-2 peptide could pull down SND1 from MDA-MB-231-GFP-Red-FLuc cells (Figure 3.9 and 3.10). Excess unlabeled 4-2 peptide could successfully compete for the pull down, demonstrating the specificity. Interestingly, biotinylated 4-2 peptide could not pull down SND1 from SKOV3 cell lysate, probably due to the low endogenous expression level of SND1 in such cell line.
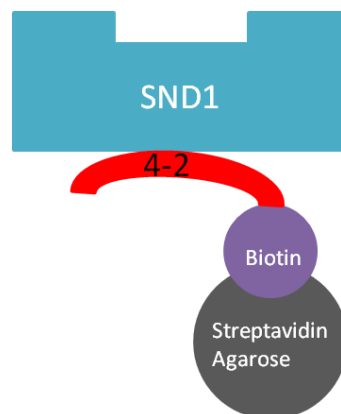
Figure 3.9 Biotinylated 4-2 peptide pulled down SND1 (diagram)

SND1 was pulled down by biotinylated 4-2 peptide using streptavidin agarose beads.
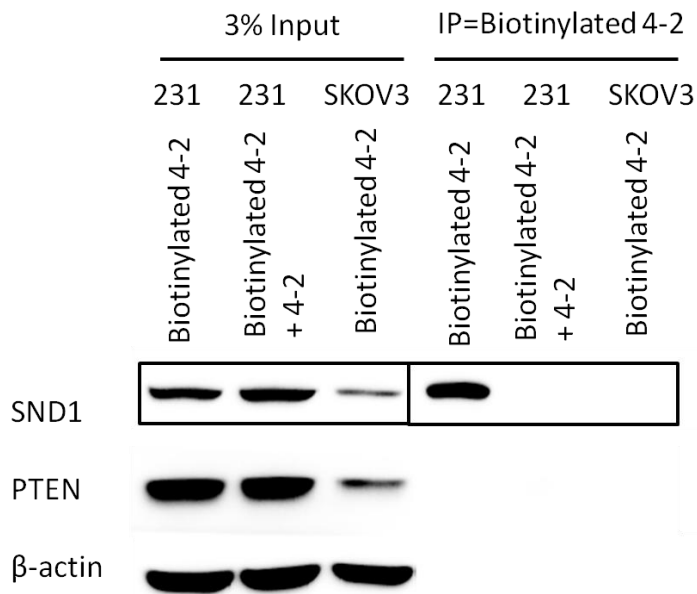
Figure 3.10 Biotinylated 4-2 peptide pulled down SND1

Pull down assay was conducted with cell lysate from MDA-MB-231-GFP-Red-FLuc or SKOV3 cells using biotinylated 4-2 peptide (20μM). SKOV3 expressed relatively low level of SND1 compared with MDA-MB-231-GFP-Red-FLuc. PTEN and β-actin were used as unrelated negative controls. Excess peptide 4-2 (40μM) was used in competition assay. The experiment was conducted for more than 3 times and result from one trial is shown here.

3.4.5 Investigation of the essential amino acids of peptide 4-2 in SND1 interaction

To investigate the essential amino acids of peptide 4-2 in SND1 interaction, a series of mutants of peptide 4-2 were synthesized as shown in Table 3.4. These peptides showed different cytotoxic effect towards MDA-MB-231-GFP-Red-FLuc cells as investigated before (Figure 3.7).

Table 3.4 Sequences and cytotoxicity of peptide 4-2 and its mutants

Peptide Name	Sequences	Cytotoxicity to MDA-MB-231-GFP-Red-FLuc
4-2	QFDYDHFLMWYS	+
4-2Y4A	QFDADHFLMWYS	+
4-2W10A	QFDYDHFLMAYS	-
4-2Y11A	QFDYDHFLMWAS	+

Hydrophobic amino acids (W and Y) of peptide 4-2 were mutated into alanine (labeled in red). The cytotoxic effect of these peptides towards MDA-MB-231-GFP-Red-FLuc cells (Figure 3.7) was shown in the last column.

Pull down assays of SND1 by biotinylated 4-2 peptide was conducted in the presence of competing peptides (Figure 3.11). Figure 3.12 showed that 4-2, 4-2Y4A and 4-2Y11A could compete with the pull-down of SND1 by biotinylated 4-2 whereas 4-2W10A could not. This result suggested that W10 was an essential amino acid of peptide 4-2 in interacting with SND1 whereas Y4 or Y11 were not. The ability of the peptides to interact with SND1 was consistent with the cytotoxicity of these peptide (Table 3.5), suggesting that the cytotoxicity of the peptides was dependent on their interaction with SND1.
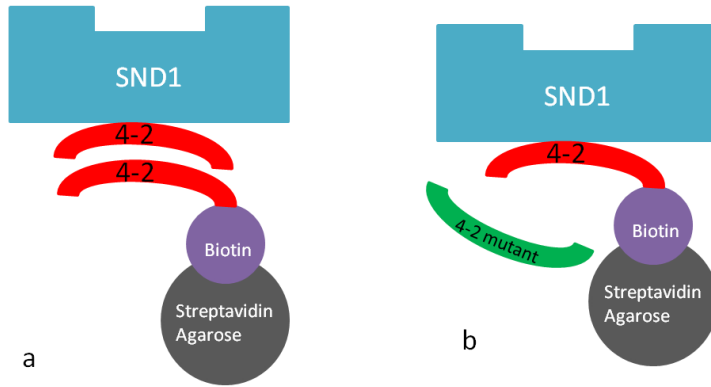
Figure 3.11 4-2 and its mutant peptides competed with the pull down of SND1 by biotinylated 4-2 peptide (diagram)

SND1 was pulled down by biotinylated 4-2 peptide using streptavidin agarose beads. Biotinylated 4-2 peptide pulled down SND1 in the presence of competing peptide 4-2 (a) or non-competing peptide 4-2 mutant (b).
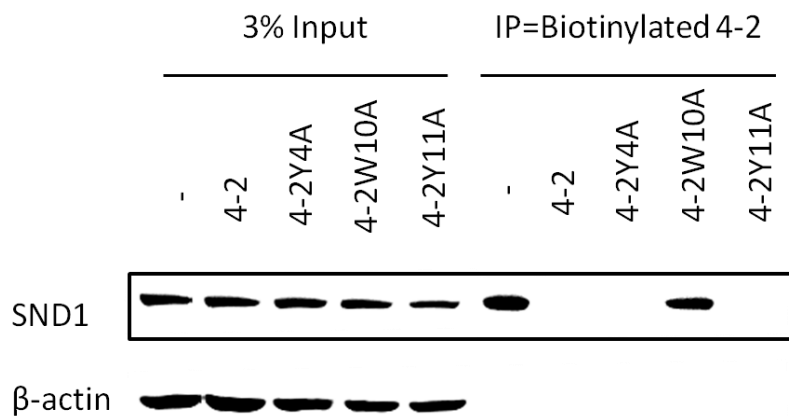
Figure 3.12 W10 was the essential amino acid in SND1-interaction

Pull-down assay was conducted using biotinylated 4-2 peptide and cell lysate from MDA-MB-231-GFP-Red-FLu with or without competing peptides. 4-2, 4-2Y4A and 4-2Y11A (80µM) could compete with the pulling down of SND1 by biotinylated 4-2 (40µM) while 4-2W10A (80µM) could not. β-actin was used as unrelated negative control; The experiment was conducted for more than 3 times and result from one trial is shown here.

Table 3.5 Cytotoxicity and SND1 binding ability of peptide 4-2 and its mutants

Peptide Name	Cytotoxicity to MDA-MB-231-GFP-Red-FLuc	SND1 interaction
4-2	+	+
4-2Y4A	+	+
4-2W10A	-	-
4-2Y11A	+	+

Cytotoxicity of the peptides towards MDA-MB-231-GFP-Red-FLuc cells and their ability to interact with SND1 in MDA-MB-231-GFP-Red-FLuc cell lysate were summarized in this table.

3.4.6 CPP-4-2 downregulated SND1 of breast cancer cells

CPP-4-2 preferentially killed breast cancer cell compared to other cancer types or normal cell. The mechanism of CPP-4-2 preferentially killing breast cancer cells was investigated. As shown in Figure 3.13 and Table 3.6, at 30µM CPP-4-2, CPP-4-2Y4A and CPP-4-2Y11A could downregulate SND1 of MDA-MB-231-GFP-Red-FLuc cells whereas CPP-4-2W10A and CPP-4-2AAA could not.

To summarize, CPP-4-2 could downregulate SND1 in MDA-MB-231-GFP-Red-FLuc cells. W10 was the essential amino acid of CPP-4-2 in SND1 downregulation whereas Y4 and Y11 were not.
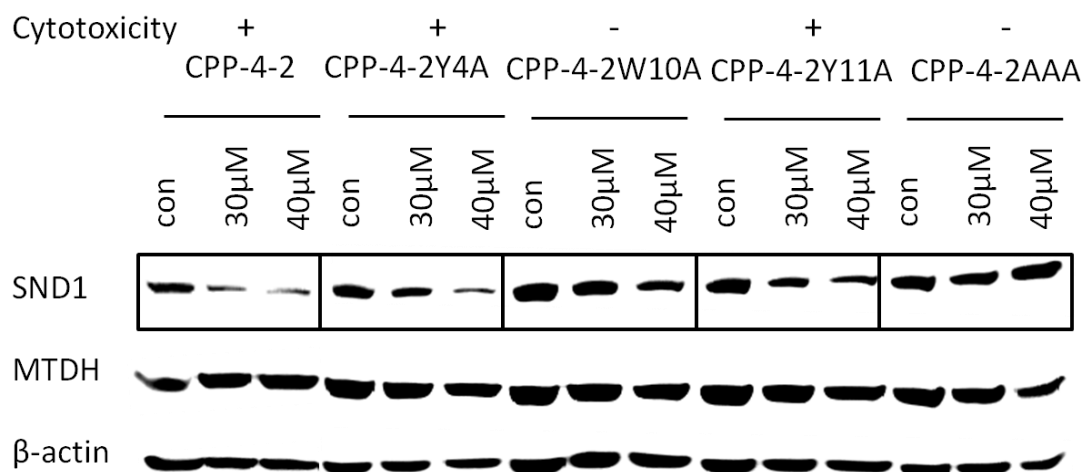
Figure 3.13 CPP-4-2 downregulated SND1 in MDA-MB-231-GFP-Red-FLuc cells

MDA-MB-231-GFP-Red-FLuc cells were treated with CPP-4-2 and its mutant peptides for 24h. The experiment was conducted for more than 3 times and result from one trial is shown here.

Table 3.6 Cytotoxicity of peptides and their ability to interact with SND1 or downregulate SND1

Peptide	Interaction with SND1	Cytotoxicity to MDA-MB-231 -GFP-Red-FLuc	SND1 downregulation (at 30μM)
CPP-4-2	+	+ + +	+
CPP-4-2Y4A	+	+ + +	+
CPP-4-2W10A	-	- -	-
CPP-4-2Y11A	+	+ + +	+
CPP-4-2AAA	NA	- - -	-

Cytotoxicity of 4-2 and its mutant peptides towards MDA-MB-231-GFP-Red-FLuc cells, their ability to interact with SND1 or downregulate SND1 were summarized in this table. NA: not available

Since CPP-4-2 could downregulate SND1 in MDA-MB-231-GFP-Red-FLuc cells, we tested the effect of CPP-4-2 on other breast cancer cell lines. Figure 3.14 showed that CPP-4-2 could downregulate SND1 in all of the 3 breast cancer cell lines MDA-MB-231-GFP-Red-FLuc, MCF7 and MDA-MB-468.
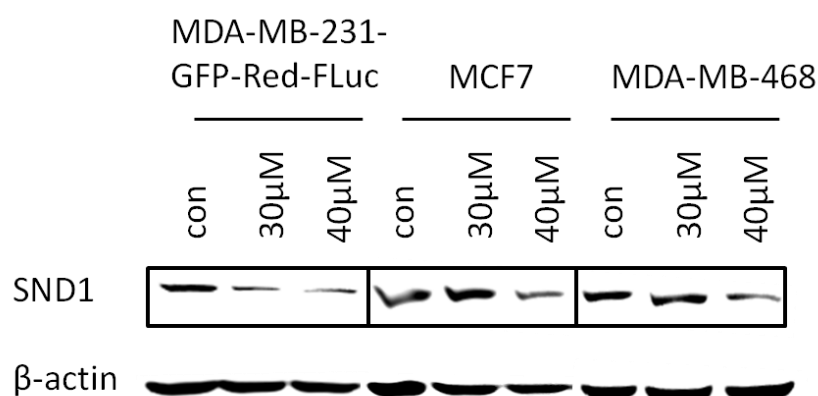
Figure 3.14 CPP-4-2 downregulated SND1 in breast cancer cells

Different cell lines were treated with CPP-4-2 for 24h. The experiment was conducted for more than 3 times and result from one trial is shown here.

3.4.7 Overexpression of SND1 reduced the cytotoxicity of CPP-4-2 to breast cancer cells

Since CPP-4-2 could downregulate SND1 of breast cancer cells and was toxic to breast cancer cells, we wanted to investigate if the downregulation of SND1 by CPP-4-2 was the reason for breast cancer cell death. SND1 was overexpressed in breast cancer cell line MDA-MB-231-GFP-Red-FLuc (Figure 3.15). When SND1 was overexpressed, the cytotoxicity of CPP-4-2 to breast cancer cells was

reduced (Figure 3.16) indicating that CPP-4-2 mediated SND1 downregulation was the possible reason for breast cancer cell death.
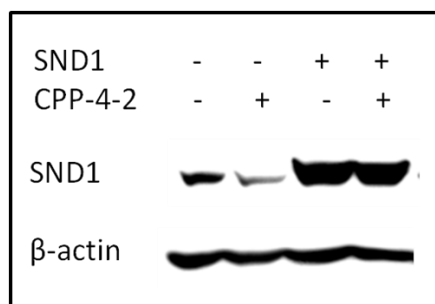
Figure 3.15 Overexpression of SND1 in MDA-MB-231-GFP-Red-FLuc cell

SND1 was overexpressed in MDA-MB-231-GFP-Red-FLuc cells according to the method in methodology. pCMV6-Entry-SND1-cMyc-DDK plasmid was used to transfect MDA-MB-231-GFP-Red-FLuc cells using lipofectamine 3000. The experiment was conducted for more than 3 times and result from one trial is shown here.
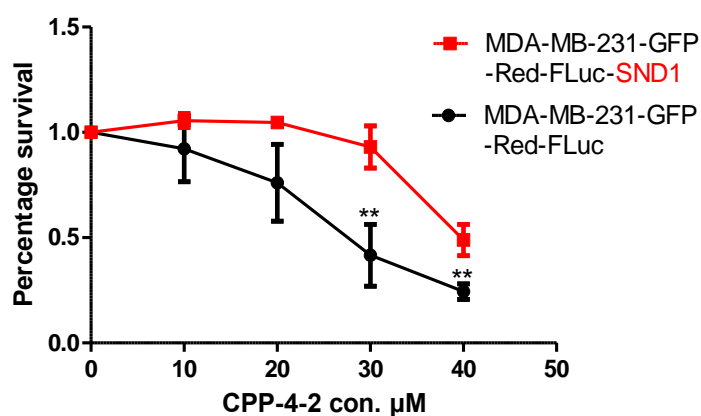
Figure 3.16 SND1 overexpression reduced the cytotoxicity of CPP-4-2 to MDA-MB-231-GFP-Red-FLuc cells

SND1 was overexpressed in MDA-MB-231-GFP-Red-FLuc cells according to the method in methodology. pCMV6-Entry-SND1-cMyc-DDK plasmid was used to transfect MDA-MB-231-GFP-Red-FLuc cells using lipofectamine 3000. Cells were incubated with serial dilutions of CPP-4-2 in RPMI medium for 72h before MTS assay. The mean ±S.D. of OD is shown (n=3).

3.4.8 CPP-4-2 affected Akt pathway by upregulating p-Akt and downregulating Akt

CPP-4-2 could downregulate SND1 in breast cancer cells. Since Akt pathway was reported to be the downstream of SND1 (Rajasekaran et al., 2016b), the effect of CPP-4-2 on Akt pathway was investigated.

As shown in Figure 3.17, 3.18 and Table 3.7, CPP-4-2, CPP-4-2Y4A and CPP-4-2Y11A could upregulate p-Akt s473 and downregulate total Akt in MDA-MB-231-GFP-Red-FLuc cells. CPP-4-2W10A and CPP-4-2AAA could not upregulate p-Akt s473. The downregulation of total Akt by CPP-4-2W10A and CPP-4-2AAA was not as significant as the other 3 peptides.

CPP-4-2 could specifically affect Akt pathway in MDA-MB-231-GFP-Red-FLuc cells. W10 was the essential amino acid of CPP-4-2 in affecting Akt pathway whereas Y4 and Y11 were not.
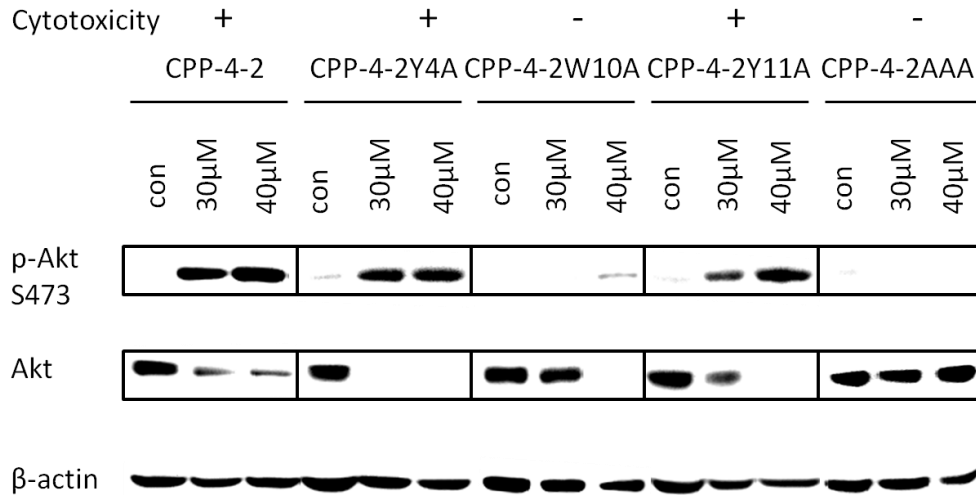
Figure 3.17 CPP-4-2 specifically affected Akt pathway by upregulating p-Akt s473 and downregulating total Akt in MDA-MB-231-GFP-Red-FLuc cells

MDA-MB-231-GFP-Red-FLuc cells were treated with CPP-4-2 and its mutant peptides for 24h. The experiment was conducted for more than 3 times and result from one trial is shown here.
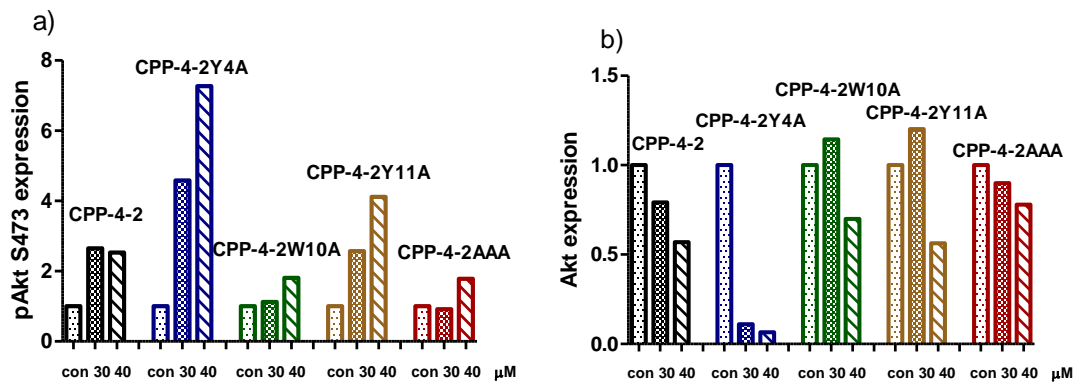
Figure 3.18 Quantization of pAkt S473 and Akt expression after treatment with CPP-4-2

Quantization of pAkt S473 (a) and Akt (b) was performed according to the western blot results in Figure 3.15. The expression levels of SND1, pAkt S473 and Akt were normalized to β-actin.

Table 3.7 Cytotoxicity of peptides and their ability to interact with SND1, downregulate SND1 or affect Akt pathway

Peptide	Interaction with SND1	Cytotoxicity to MDA-MB-231-GFP-Red-FLuc	SND1 downregulation (at 30µM)	Upregulation of pAkt S473	Downregulation of total Akt
CPP-4-2	+	+ + +	+	↑↑	↓↓
CPP-4-2Y4A	+	+ + +	+	↑↑↑	↓↓↓
CPP-4-2W10A	-	- -	-	↑	↓
CPP-4-2Y11A	+	+ + +	+	↑↑	↓↓
CPP-4-2AAA	NA	- - -	-	↑	↓

Cytotoxicity of 4-2 and its mutant peptides towards MDA-MB-231-GFP-Red-FLuc cells, their ability to interact with SND1, upregulate pAkt S473 or downregulate total Akt were summarized in this table. NA: not available

After CPP-4-2 treatment, the expression of p-Akt S473 and total Akt of different cell lines were tested (Figure 3.19). It was found that CPP-4-2 could upregulate p-Akt s473 and downregulate total Akt in MDA-MB-231-GFP-Red-FLuc, MCF7, MDA-MB-468 and QGY-7703 cell lines. In ovary cancer cell line SKOV3, only downregulation of total Akt was observed. In lung cancer cell line A549-Red-FLuc, only downregulation of pAkt S473 was observed. For mouse fibroblast L929, Akt pathway was not affected.

The above data demonstrated that CPP-4-2 preferentially killed breast cancer compared to other cancer types and normal cells. Here we also found that Akt pathway in the 3 breast cancer cell lines were all affected

by CPP-4-2 whereas less sensitive cell lines such as L929 was not affected by CPP-4-2. These results suggested that CPP-4-2 preferentially killed breast cancer cells probably by affecting Akt pathway.
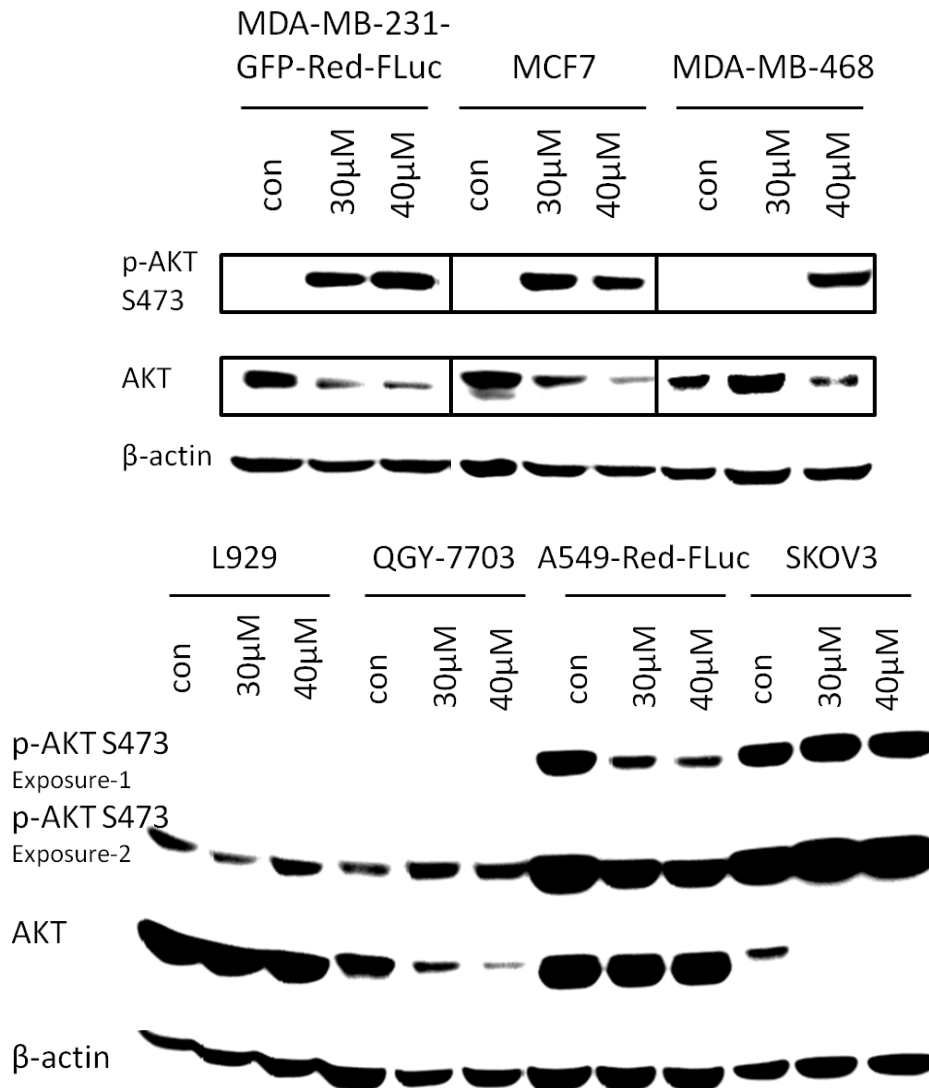
Figure 3.19 CPP-4-2 specifically affected Akt pathway in breast cancer cells

Different cell lines were treated with CPP-4-2 for 24h before Western blot analysis. The experiment was conducted for 3 times and result from one trial is shown here.

3.4.9 The activation of Akt by CPP-4-2 was transient

CPP-4-2 was found to enhance the phosphorylation of Akt, which might lead to the activation of its downstream survival promoting pathways. For this concern, we detect the phosphorylation of Akt by CPP-4-2 in details. As shown in Figure 3.20, the upregulation of p-Akt S473 was transient and in long term, there should be no activation of Akt.
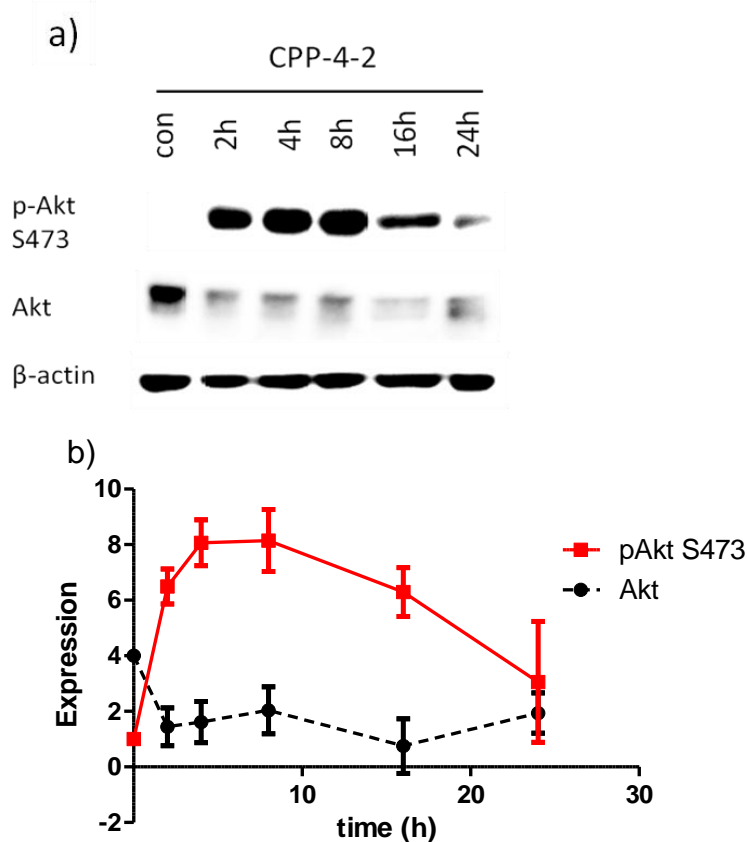
Figure 3.20 The activation of Akt by CPP-4-2 was transient

a) MDA-MB-231-GFP-Red-FLuc cells were treated with CPP-4-2 for different time before Western blot analysis. The experiment was conducted for 3 times and result from one trial is shown here. b) Quantization of pAkt S473 and Akt was performed according to the western blot results in a). The expression levels of SND1, pAkt S473 and Akt were normalized to β-actin.

3.4.10 The activation of Akt by CPP-4-2 was not transmitted to its downstream target mTORC1

Since Akt was a very important hallmark of cell survival and it was activated after CPP-4-2 treatment. mTORC1 was reported to be one of the downstream targets of Akt (Manning and Toker, 2017). We wanted to investigate if the activation of Akt was transmitted to its downstream target mTORC1. Figure 3.21 showed that there was no significant change of p-mTOR S2448 after CPP-4-2 treatment, which indicated that the activation of Akt by CPP-4-2 was not transmitted to its downstream target mTORC1.
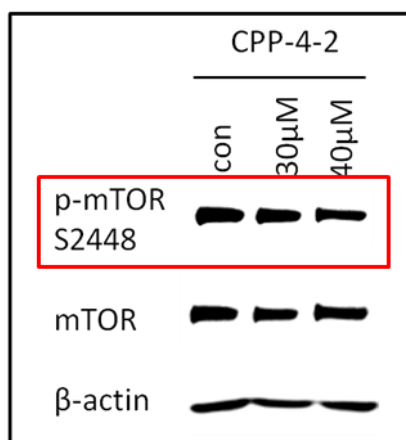
Figure 3.21 CPP-4-2 did not activate mTORC1

MDA-MB-231-GFP-Red-FLuc cells were treated with CPP-4-2 for 24h before Western blot analysis. The experiment was conducted for 3 times and result from one trial is shown here.

3.4.11 CPP-4-2 mediated degradation of Akt was proteasome-dependent, the phosphorylation of Akt partially contributed to the degradation of Akt

Since CPP-4-2 could downregulate SND1 and Akt, we wanted to investigate if the downregulation of SND1 and Akt by CPP-4-2 was due to proteasome degradation. Figure 3.22 showed that proteasome inhibitor MG132 could rescue CPP-4-2 mediated degradation of Akt whereas MG132 could not rescue CPP-4-2 mediated downregulation of SND1. Interestingly, when Akt degradation was rescued by MG132, the phosphorylation of Akt induced by CPP-4-2 was also suppressed, which indicated that the phosphorylation of Akt might be a feedback of Akt degradation.

To summarize the degradation of Akt induced by CPP-4-2 was proteasome dependent whereas the downregulation of SND1 induced by CPP-4-2 was not. The phosphorylation of Akt might be a feedback of Akt degradation induced by CPP-4-2.
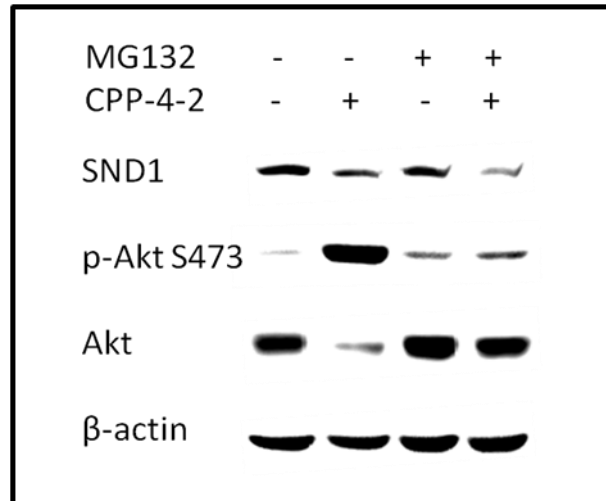
Figure 3.22 CPP-4-2 induced proteasome-dependent degradation of Akt

MDA-MB-231-GFP-Red-FLuc cells were pre-incubated with 5μM of MG132 for 24h before co-incubation with 30μM of CPP-4-2 peptide in RPMI medium for 24h before western blot analysis. β-actin was shown as loading control. Cell treatment and western blot were conducted for 3 times. Result from one trial is shown.

CPP-4-2 could mediate proteasome degradation of Akt and phosphorylation of Akt in breast cancer cells. We wanted to investigate the mechanism of Akt degradation. It was reported that p-Akt was a more preferred substrate for proteasome degradation than Akt (Bae et al., 2012). PI3K inhibitor LY294002 was used to inhibit the phosphorylation of Akt (Figure 3.23). When the phosphorylation of Akt was suppressed by LY294002, Akt degradation was partially rescued, indicating that the degradation of Akt induced by CPP-4-2 was partially contributed by the phosphorylation of Akt at S473.
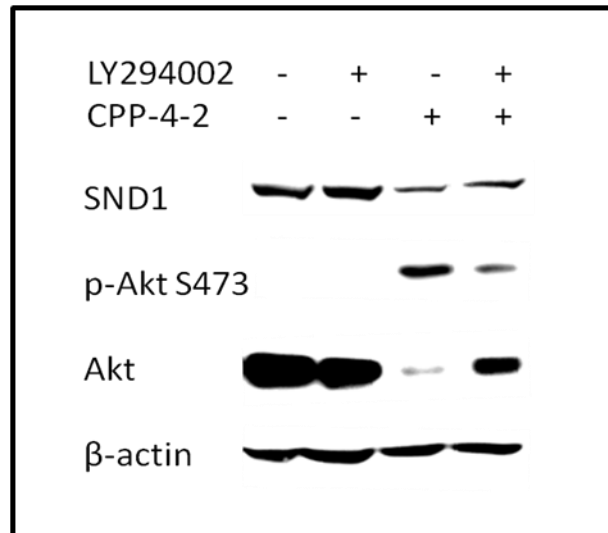
Figure 3.23 Akt degradation induced by CPP-4-2 was partially contributed by the phosphorylation of Akt at S473

MDA-MB-231-GFP-Red-FLuc cells were pre-incubated with 10μM of LY294002 for 2h before co-incubation with 30μM of CPP-4-2 peptide in RPMI medium for 24h before western blot analysis. β-actin was shown as loading control. Cell treatment and western blot were conducted for 3 times. Result from one trial is shown.

3.4.12 CPP-4-2 affected important cell survival pathway of MDA-MB-231-GFP-Red-FLuc cells in proteomics study

In order to study the global effect of CPP-4-2, a proteomics study was performed to identify the differentially expressed proteins after CPP-4-2 treatment in MDA-MB-231-GFP-Red-FLuc cells. There were 1860 proteins found to be differentially expressed after treating with CPP-4-2, CPP-4-2W10A or CPP-4-2AAA. A total of 372 proteins were found to be differently expressed when comparing CPP-4-2 vs. untreated, CPP-4-2AAA and CPP-4-2W10A group with a P value <0.05. The top 30 (the most upregulated) and bottom 30 (the most downregulated) proteins were shown in Table 3.8 after ranking (according to the fold change of the proteins in CPP-4-2 group vs. untreated group). Most of the proteins were found to be involved in basic cellular functions such as cytoskeleton formation, mRNA processing, Acetyl-CoA metabolism and cell migration. Three promising SND1 downstream targets, NF-κB2, p400 and ITGB4 were selected for further validation (Table 3.8). NF-κB signaling was reported to be the downstream of SND1 (Santhekadur et al., 2012). P400, E1A-binding protein p400, a tumor suppressor gene (Samuelson et al., 2005) was found to be upregulated after CPP-4-2 treatment. Sequence of peptide 4-2 showed high similarity to that of ITGB4 (Integrin, beta 4) (Figure 3.24).

Table 3.8 Proteomics study of differentially-expressed proteins after treatment with CPP-4-2 and its mutants

	Gene accession	Fold change CPP-4-2/untreated	$P_{CPP-4-2 \text{ vs. untreated}}$	$P_{CPP-4-2 \text{ vs. CPP-4-2AAA}}$	$P_{CPP-4-2 \text{ vs. CPP-4-2W10A}}$	Peptide count
1	CC125	220.4452	0.0109	0.0107	0.0126	13
2	TSP1	44.7043	0.0011	0.0013	0.0028	9
3	AAMP	36.9075	0.0221	0.0210	0.0241	4
4	H1T	36.2005	0.0081	0.0091	0.0089	5
5	MTCL1	26.8343	0.0003	0.0003	0.0005	23
6	CO3	25.6535	0.0027	0.0026	0.0044	24
7	CAPR2	24.5095	0.0080	0.0089	0.0136	3
8	PRP8	23.8686	0.0210	0.0210	0.0269	31
9	CARF	21.7133	0.0041	0.0038	0.0047	10
10	HBA	18.8369	0.0002	0.0002	0.0014	7
11	CPSF1	18.6850	0.0040	0.0080	0.0443	15
12	ACTN3	18.6073	0.0018	0.0016	0.0015	18
13	LIPA1	17.9625	0.0102	0.0134	0.0367	24
14	NFKB2	17.4986	0.0011	0.0010	0.0010	7
15	ACACA	16.2168	0.0039	0.0040	0.0055	28
16	DVL2	14.6437	0.0000	0.0000	0.0000	8
17	PXDN	13.6041	0.0166	0.0185	0.0194	8
18	GOLP3	12.9939	0.0028	0.0029	0.0084	4
19	NU160	12.9299	0.0002	0.0002	0.0008	12
20	SMTN	12.6924	0.0015	0.0012	0.0012	13
21	UBR5	12.1336	0.0000	0.0000	0.0001	22
22	SRCAP	11.6398	0.0005	0.0005	0.0011	23
23	PIEZ1	11.1430	0.0028	0.0024	0.0029	17
24	ATP7A	11.1043	0.0000	0.0001	0.0033	15
25	DSG2	11.0559	0.0062	0.0056	0.0075	10
26	ROCK2	10.9489	0.0067	0.0065	0.0243	22
27	TCPW	10.7468	0.0058	0.0084	0.0248	11
28	ARAP3	10.5210	0.0019	0.0024	0.0053	11
29	EP400	10.2308	0.0003	0.0002	0.0004	21
30	IF4G3	10.0832	0.0037	0.0028	0.0049	19
...	...					
188	SND1	0.3630	0.0002	0.0033	0.0022	22
...	...					
212	ITB4	0.3138	0.0370	0.0304	0.0132	17
...	...					

343	BDP1	0.1216	0.0161	0.0003	0.0355	25
344	PRDX1	0.1213	0.0222	0.0121	0.0095	13
345	GEMI5	0.1206	0.0063	0.0001	0.0088	11
346	TCPD	0.1176	0.0032	0.0452	0.0027	20
347	HAP28	0.1173	0.0425	0.0008	0.0376	6
348	HNRPF	0.1165	0.0006	0.0030	0.0071	13
349	CYBP	0.1164	0.0014	0.0054	0.0056	9
350	DPP3	0.1134	0.0007	0.0002	0.0001	5
351	RM12	0.1118	0.0018	0.0017	0.0417	7
352	DCTN2	0.1065	0.0088	0.0047	0.0245	9
353	SYK	0.1060	0.0139	0.0160	0.0359	11
354	CPIN1	0.1011	0.0117	0.0012	0.0024	6
355	HSPB1	0.0949	0.0008	0.0034	0.0044	7
356	P5CS	0.0891	0.0050	0.0069	0.0093	10
357	DUS12	0.0832	0.0004	0.0012	0.0256	4
358	CCAR2	0.0797	0.0013	0.0011	0.0116	8
359	CALR	0.0764	0.0193	0.0304	0.0044	13
360	HNRPR	0.0737	0.0047	0.0249	0.0058	13
361	GAK6	0.0730	0.0248	0.0083	0.0306	8
362	ACTZ	0.0712	0.0063	0.0265	0.0155	6
363	RPR1B	0.0684	0.0001	0.0153	0.0286	7
364	THOC4	0.0637	0.0048	0.0185	0.0024	12
365	SYDC	0.0605	0.0123	0.0271	0.0019	18
366	TOM70	0.0445	0.0181	0.0138	0.0147	9
367	AAAS	0.0342	0.0000	0.0163	0.0107	3
368	AL7A1	0.0335	0.0027	0.0109	0.0007	10
369	UBP2L	0.0287	0.0035	0.0079	0.0410	8
370	PPIB	0.0231	0.0394	0.0007	0.0328	6
371	EIF3M	0.0149	0.0010	0.0283	0.0003	7
372	EIF3L	0.0135	0.0035	0.0210	0.0008	9

MDA-MB-231-GFP-Red-FLuc cells were incubated with 30μM of CPP-4-2, CPP-4-2W10A or CPP-4-2AAA for 24h before proteomics study. A total of 372 proteins were found to be differentially expressed ($P_{CPP-4-2\ vs.\ untreated} < 0.05$, $P_{CPP-4-2\ vs.\ CPP-4-2AAA} < 0.05$ and $P_{CPP-4-2\ vs.\ CPP-4-2W10A} < 0.05$). The 372 proteins were ranked according to the fold change of the proteins in CPP-4-2 group vs. untreated group. The top 30 (most upregulated) and bottom 30 (most downregulated) proteins were shown in this table. The highlighted proteins were promising SND1 downstream targets and SND1 which were selected for further validation.

```
4-2        3    DYDHFLMWYS 12
                DYD FLM YS
ITGB4   1377    DYDSFLM-YS 1385
```

Figure 3.24 Sequence alignment of peptide 4-2 to ITGB4

Sequence alignment of peptide 4-2 was conducted with NCBI BLAST. ITGB4 showed highest similarity to peptide 4-2 among proteins from mammalian cells. Sequence ID of ITGB4 isoform X1 (Homo sapiens): XP_006721929.1.

Among the 372 differentially expressed proteins, pathway analysis was conducted to cluster these proteins. The top 8 pathways that were most probably affected by CPP-4-2 were shown in Figure 3.25. These pathways were all essential cell-survival associated pathways, including tRNA charging, actin cytoskeleton signaling, .regulation of eIF4 and p70S6K signaling, protein ubiquitination pathway, EIF2 signaling, sirtuin signaling pathway, mTOR signaling and caveolar mediated endocytosis signaling.
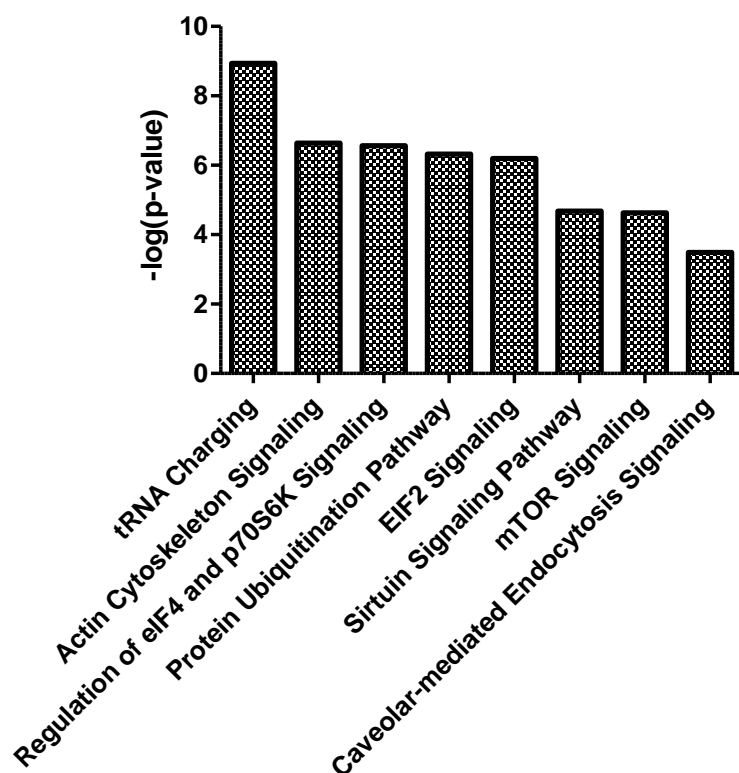
Figure 3.25 Top 8 pathways most probably affected by CPP-4-2 determined by proteomics study

MDA-MB-231-GFP-Red-FLuc cells were incubated with 30μM of CPP-4-2, CPP-4-2W10A or CPP-4-2AAA for 24h before proteomics study. A total of 372 proteins were found to be differentially expressed ($P_{CPP-4-2\ vs.\ untreated}<0.05$, $P_{CPP-4-2\ vs.\ CPP-4-2AAA}<0.05$ and $P_{CPP-4-2\ vs.\ CPP-4-2W10A}<0.05$). After pathway analysis with IPA, the top 8 pathways most probably affected by CPP-4-2 were shown. −log (p-value) represented the probability of one pathway affected by CPP-4-2. Cell treatment with peptides was conducted in triplicate. Mass spectrometry analysis was conducted in triplicate.

3.4.13 CPP-4-2 upregulated pro-apoptotic NF-κB2 but did not affect EP400 or ITGB4

Among the 372 differentially expressed proteins, ITGB4, EP400 and NF-κB2, as promising downstream targets of SND1 were selected for further validation. Real-time PCR was performed to determine the mRNA level of these genes. No significant difference was detected in the mRNA level of ITGB4 or EP400 after CPP-4-2 treatment (Figure 3.26). The protein levels of EP400 and ITGB4 remained unknown.
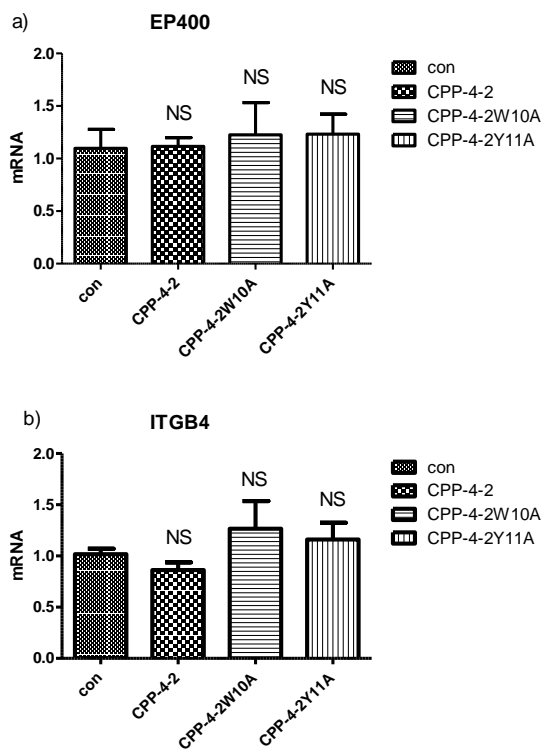
Figure 3.26 CPP-4-2 did not change the mRNA levels of EP400 or ITGB4

MDA-MB-231-GFP-Red-FLuc cells were treated with 30μM of CPP-4-2 or its mutant peptides for 24h before RNA extraction. mRNA levels of EP400 and ITGB4 were determined by real-time PCR. The mean ±S.D. of fold change of mRNA is shown here (n=3). NS: not significant, $p > 0.05$.

Interestingly, NF-κB2 mRNA was significantly upregulated after CPP-4-2 treatment compared with untreated control, CPP-4-2W10A or CPP-4-2AAA (Figure 3.27a). The cytotoxic mutant, CPP-4-2Y4A could also enhance the transcription of NF-κB2 to the similar extent as CPP-4-2, whereas the other cytotoxic mutant CPP-4-2Y11A could not.

Since NF-κB2 was a member of NF-κB family, the expression of other NF-κB family members NFkB1 and RelA was also tested. Even though both NF-κB1 and RelA genes showed similar trend as NF-κB2 after peptide treatment, there was no statistically significant difference of the mRNA levels of NF-κB1 and RelA among different peptide treatment groups (Figure 3.27b and c).
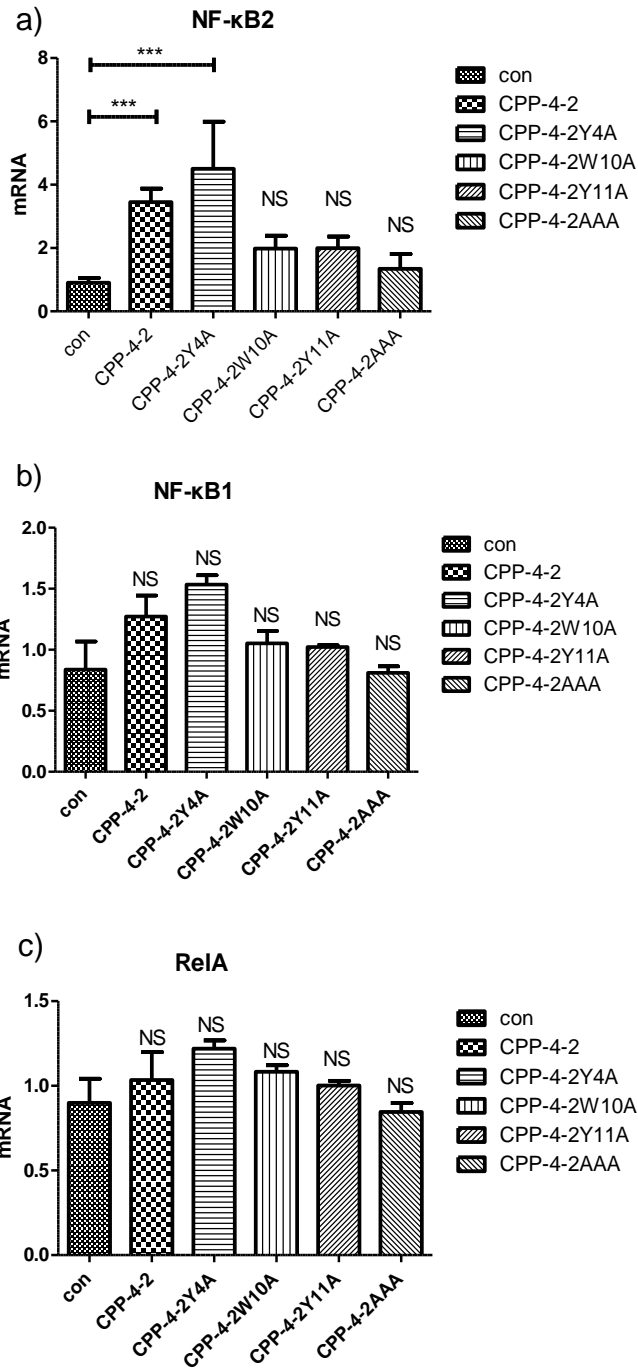
Figure 3.27 CPP-4-2 upregulated mRNA levels of NF-κB2 and its family members

MDA-MB-231-GFP-Red-FLuc cells were treated with 30μM of CPP-4-2 or its mutant peptides for 24h before RNA extraction. mRNA levels of NF-κB2, NF-κB1 and RelA were determined by real-time PCR. The mean ±S.D. of fold change of mRNA is shown here (n=3). ***p<0.001 compared with control; NS: not significant, p>0.05.

Since CPP-4-2 peptide could induce apoptosis in flow cytometry assay, we investigated if CPP-4-2 induced apoptosis through Bax/BCL2 signaling. As shown in Figure 3.28 a, no significant difference was observed in the mRNA levels of Bax after CPP-4-2 treatment. The mRNA level of BCL2 was found to be upregulated by CPP-4-2, which was opposite to the expected results (Figure 3.28 b). The protein levels of Bax and BCL2 remained unknown.
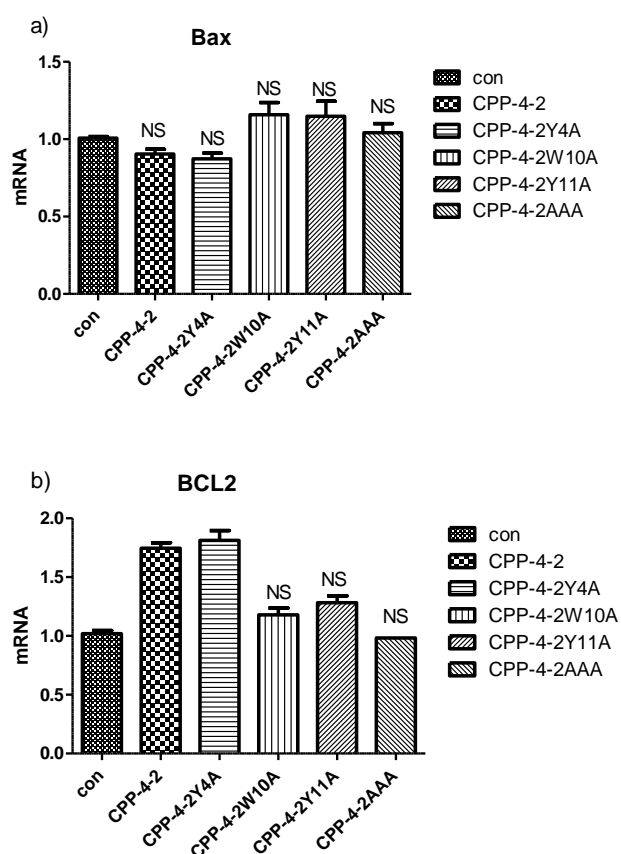
Figure 3.28 mRNA levels of Bax and BCL2 after peptide treatment

MDA-MB-231-GFP-Red-FLuc cells were treated with 30µM of CPP-4-2 or its mutant peptides for 24h before RNA extraction. mRNA levels of Bax and BCL2 were determined by real-time PCR. The mean ±S.D. of fold change of mRNA is shown here (n=3). NS: not significant, p>0.05.

3.4.14 In silico docking of peptide 4-2 to SN1/2

In silico docking of peptide 4-2 to SN1/2 was conducted in Prof. Ruben Abagyan's lab using ICM (Internal Coordinate Mechanics) (Abagyan and Totrov, 1994). Sincere thanks are given to Prof. Ruben Abagyan and his PhD student Mr. Da Shi.

Five tentative binding sites (colored spaces) on SN1/2 identified by PocketFinder were shown in Figure 3.29. One box, Box1 was demonstrated as an example of the box space region around Pocket1 (Figure 3.29).
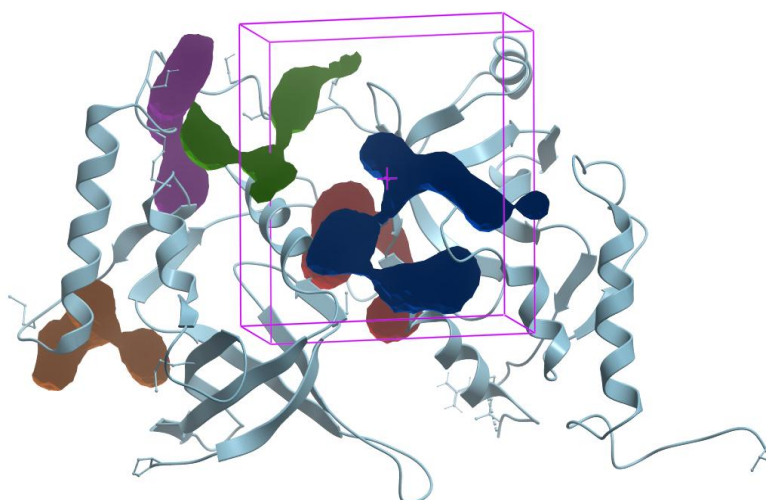
Figure 3.29 Five tentative binding sites on SN1/2 and Box1

Tentative binding sites (the 5 colored spaces) on SN1/2 were identified by PocketFinder. Box1, defined as box space region around Pocket1 was shown as an example. The blue helix protein structure was the crystal structure of SN1/2 domain of SND1 (PDB: 4QMG).

In silico docking of peptide 4-2 was performed with W10 (the essential amino acid in the activity of CPP-4-2) restrained in Box1-5, Boxi and

Boxno, respectively. As a result, 3200 conformations in each box were output as possible conformations of 4-2 interacting with SN1/2.

The docking scores of 2 conformations in Box1, 1 conformation in Box4, 3 conformations in Boxno and 15 conformations in Boxi were ≤-190 (Table 3.9). There were 3 very similar conformations of peptide 4-2 (overlapping helix-like structures in Figure 3.30 b) identified from Boxi (Figure 3.30 a), besides which no other conformations of any similarities were identified among the 21 conformations (Table 3.9). As a result, the overlapping helix-like structure shown in Figure 3.24b was the most possible conformation of peptide 4-2 interacting with SN1/2.

Table 3.9 Possible conformations of peptide 4-2 binding to SN1/2

Box No.	No. of conformations with docking score ≤-190	Features of the conformations with docking score ≤-190
Box1	2	ADC
Box2	0	ADC
Box4	1	ADC
Box5	0	ADC
Box6	0	ADC
Boxno	3	ADC
Boxi	15	SC*3

Lower docking score meant better binding in ICM. ADC: all different conformations; SC: similar conformations.
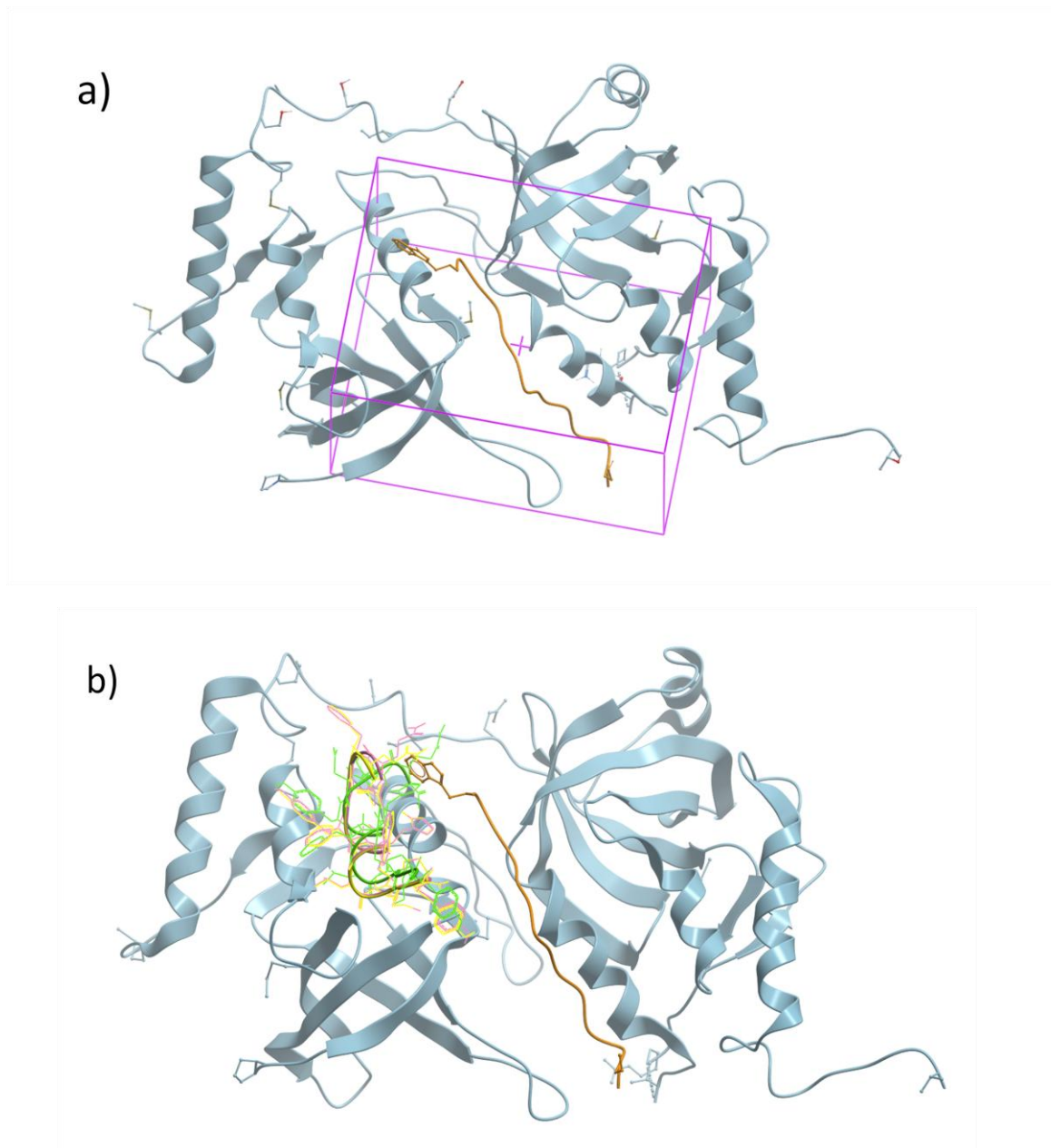
Figure 3.30 Most possible conformation of 4-2 interacted with SN1/2

The orange linear peptide structure was MTDH 11-mer peptide nested in the binding groove of SND1-MTDH interface; The big blue structure was SN1/2 domain of SND1 (PDB: 4QMG). a) The purple box was boxi encompassing the space region around SND1-MTDH interface; b) The yellow, pink and green overlapping helix-like structure was the most possible conformation of peptide 4-2 interacting with SN1/2;

3.5 Discussion

3.5.1 Construction of CPP-4-2 peptide

TAT CPP was selected for directing 4-2 and 4-8 peptides into mammalian cells because it had high cell penetrating efficiency and low cytotoxicity. Unfortunately, TAT-4-2 and TAT-4-8 peptides induced precipitation in cell culture medium probably due to their low isoelectric point (pI) values. As a consequence, two more arginines were added before TAT to produce a hybrid CPP, RR-TAT to solve the problem of solubility by increasing pI while to increase cell penetrating efficiency.

However, RR-TAT-4-8 peptide still induced great precipitation in tissue culture medium. This peptide was suspended for further assay.

3.5.2 In silico docking of peptide 4-2 to SN1/2

SND1-interacting peptide 4-2 could disrupt SND1-MTDH interaction. W10 was found to be the essential amino acid in the activity of peptide 4-2, including cytotoxicity, SND1 interaction, SND1 downregulation, Akt degradation and activation of NF-κB2. In silico docking of peptide 4-2 to SN1/2 was performed to explain the importance of W10 in SND1 interaction. We wanted to predict the binding site of 4-2 on SN1/2 and also to know if the binding site was SND1-MTDH interface.

There were 3 very similar conformations of peptide 4-2 identified in Boxi

(Figure 3.30b, helix-like structure), besides which no other conformations of any similarities were identified in the 21 conformations with docking score≤-190. This result suggested that the helical structure of peptide 4-2 was close to but not at the interface of SND1-MTDH, which might explain the inconsistency of the disruption of MTDH-SND1 by peptide 4-2 in different assays.

Docking study suggested that peptide 4-2 adopted a helical structure and interacted with SN1/2 near the binding interface of SND1-MTDH complex. The peptide motif shown in the co-crystal structure of SND1-MTDH was an 11-mer MTDH peptide motif (Figure 2.2, PDB: 4QMG), which was shorter than the 22-mer MTDH peptide which was used in the peptide ELISA assay and much shorter than the MTDH full-length protein. This indicated that there was unknown structure of MTDH, which might be disrupted by peptide 4-2.

3.5.3 MTS, Flow cytometry and high content screening

MTS and flow cytometry methods were used in this project to measure the cytotoxicity of peptides to breast cancer cells. MTS is a standard method through measuring the metabolic activity of the cells to represent the number of viable cells. Flow cytometry is another standard method to measure the flip of phosphatidylserine from the inner surface of cell membrane to the outer surface and also cell permeability to

represent the viability of living cells. These two methods are two standard methods but with different principles, which are used in this project to double confirm the cytotoxicity of peptide 4-2 to breast cancer cells.

More powerful methods for drug screening have been developed such as high content screening. In order to test the activity of thousands of compounds, high-content screening is a better choice. The microscope can capture the image of cells and output multiple phenotypes of cells at one time. Thousands of compounds can be tested in parallel for their activity at the same time. So high content screening is very efficient and powerful for high-throughput screening.

3.5.4 CPP-4-2 preferentially killed breast cancer cells but not other cancer types or mouse fibroblast

There are different subtypes of breast cancer according to different classification criteria as introduced in the introduction. According to the receptor status, breast cancer can be classified into luminal, HER2 overexpression, basal and normal-like subtypes of breast cancer (Dai et al., 2015). Basal subtype or triple negative breast cancer was the most difficult to treat due to the missing of ER, PR and HER2 receptors. In our study, we chose 2 triple negative breast cancer cell line, MDA-MB-231 and MDA-MB-468 to represent triple negative breast cancer (Subik et al.,

2010). We also used MCF7, which had ER and PR receptors to represent luminal A subtype of breast cancer (Subik et al., 2010) to further expand the scope of our study. In our initial thought, we used QGY-7703 to represent liver cancer cell line, which was found to be Hela derivative, warning us of proper choosing of cell lines for cancer study and drug screening.

CPP-4-2 peptide preferentially killed breast cancer cells, MDA-MB-231-GFP-Red-FLuc, MCF7 and MDA-MB-468 but not ovary cancer cell SKOV3, Hela derivative QGY-7703, lung cancer cell A549 or mouse fibroblast L929. One possible reason was that CPP-4-2 had different cell penetration efficiency in these cell lines. Peptide accumulation assay indicated that peptide accumulation in different cell lines were similar. More likely, CPP-4-2 affected a unique SND1-dependent pathway which was specific and essential to the survival of breast cancer cells probably the SND1-dependent Akt pathway. Targeting SND1 and its potential binding partner by CPP-4-2 might be a treatment specific to breast cancer.

3.5.5 CPP-4-2 mediated SND1-dependent cytotoxicity in MDA-MB-231-GFP-Red-FLuc cells

Y and W were the hydrophobic amino acids enriched in the peptide sequences after phage display screening. Y4 and W10 in peptide 4-2 had

a distance of 5 (Y4 and Y11 had the distance of 6) amino acids in between, which corresponded to the sequence pattern of MTDH peptide that interacted with SND1. Results from mutagenesis experiments confirmed that W10 of peptide 4-2 was essential in mediating cytotoxicity and interacting with SND1. Mutation of W to A in position 10 (CPP-4-2W10A) abolished its cytotoxicity and its ability to interact with SND1. This result suggested that CPP-4-2 mediated an SND1-dependent cytotoxicity in MDA-MB-231-GFP-Red-FLuc cells.

3.5.6 Peptide 4-2 mediated disruption of SND1-MTDH interaction and subsequent degradation of SND1 might be the reason for breast cancer cell death

Peptide 4-2 was demonstrated to compete with the binding of 22-mer MTDH peptide to SN1/2 domain of SND1. Peptide 4-2 could also disrupt full-length SND1-MTDH complex in co-IP assay (Chapter 2). It was reported that the disruption of SND1-MTDH interaction by mutagenesis would result in the suppression of mammosphere formation *in vitro* and tumor initiation *in vivo* (Wan et al., 2014). And the mechanism was proposed to be when MTDH-SND1 interaction was disrupted, MTDH could no longer protect SND1, which resulted in the degradation of SND1 (Wan et al., 2014). In our result, peptide 4-2 could disrupt SND1-MTDH interaction, which probably lead to the degradation of SND1. Besides,

overexpression of SND1 could reduce the cytotoxicity of peptide 4-2 to breast cancer cells. These results suggested that the disruption of SND1-MTDH interaction and subsequent degradation of SND1 by peptide 4-2 might be the reason for breast cancer cell death (Figure 3.31).

3.5.7 CPP-4-2 might kill breast cancer cells by affecting Akt pathway or by enhancing NF-κB2 transcription

The abilities of CPP-4-2 and its mutant peptides in exerting cytotoxicity, interacting with SND1, downregulating SND1, affecting Akt pathway and upregulating NF-kB2 were summarized in Table 3.10. CPP-4-2, CPP-4-2Y4A and CPP-4-2Y11A were found to be toxic to breast cancer cell MDA-MB-231-GFP-Red-FLuc. Consistently, they were also demonstrated to affect Akt pathway, upregulate NF-κB2 and interact with SND1 (the upregulation of NF-κB2 by CPP-4-2Y11A was not significant). CPP-4-2W10A, which was found to be non-toxic to MDA-MB-231-GFP-Red-FLuc could not affect Akt pathway, interact with SND1 or upregulate NF-kB2.

Table 3.10 A summary of the characteristics of CPP-4-2 and its mutants

Peptide	Interacting with SND1 (Peptide pull-down assay)	Cytotoxicity to MDA-MB-231 -GFP-Red-FLuc	SND1 downregulation (at 30μM)	Affecting Akt pathway	NF-kB2 regulation
CPP-4-2	+	+	+	+	+
CPP-4-2Y4A	+	+	+	+	+
CPP-4-2W10A	-	-	-	-	-
CPP-4-2Y11A	+	+	+	+	-
CPP-4-2AAA	NA	-	-	-	-

This table summarized the ability of CPP-4-2 and its mutant peptides to interact with SND1, kill MDA-MB-231-GFP-Red-FLuc cells, affect Akt pathway and upregulate NF-κB2. The SND1-interacting ability of the peptides was determined by peptide pull-down assay. NA: not available

3.5.7.1 CPP-4-2 induced cytotoxicity probably through Akt pathway

Akt pathway was reported to be the downstream of SND1 (Rajasekaran et al., 2016b). Since Akt pathway played a very essential role in cell survival, the significant downregulation of total Akt might be one of the reasons for cell death. Akt could be degraded by ubiquitin proteasome-dependent pathway, caspase-mediated cleavage, or caspase-dependent ubiquitination (Liao and Hung, 2010). Interestingly, pAkt S473 was a more preferred substrate than Akt for ubiquitination by E3 ubiquitin ligase MULAN. The degradation of Akt by MULAN could

suppress cell proliferation and viability (Bae et al., 2012). In our result, peptide 4-2 induced degradation of Akt, which was partially contributed by the phosphorylation of Akt. The degradation of Akt might be mediated by E3 ubiquitin ligase MULAN. And MULAN-mediated degradation of Akt might be the reason for breast cancer cell death induced by peptide 4-2.

Besides, X-linked inhibitor of apoptosis protein (XIAP) regulated apoptosis through PI3K/Akt pathway, which involved caspase cleavage (Asselin et al., 2001). Caspase-dependent cleavage of many specific proteins might turn off survival pathways including PI3K/Akt pathway, which might otherwise interfere with the apoptotic response (Widmann et al., 1998). As a result, the downregulation of Akt induced by CPP-4-2 in breast cancer cells might be the reasons for cell death (Figure 3.31).

3.5.7.2 CPP-4-2 killed breast cancer cells probably by enhancing the transcription of NF-κB2

NF-κB2/p100 was reported to promote apoptosis through its death domain. When p100 lost its death domain by being processed to p52, the tumorigenic activity was elevated (Wang et al., 2002). This suggested a pro-apoptotic role of p100 (not p52) in promoting cancer cell death. NF-κB2 was considered as a direct activator of programmed cell death (Hacker and Karin, 2002). The expression of p100 profoundly sensitized

cells to death-receptor-mediated apoptosis through an IκB-independent pathway (Wang et al., 2002).

In our experiments, significant upregulation of NF-κB2 instead of NF-κB1 or RelA by CPP-4-2 indicated a specific activation of NF-κB2 gene instead of the whole NF-κB pathway. The elevated pro-apoptotic activity of the death domain of p100 induced by CPP-4-2 peptide might lead to the death of the cells. It was possible that the acute accumulation of p100, which was not processed into p52 might lead to the death of breast cancer cells. This hypothesis could be validated through detecting both of the protein levels of p100 and p52 after CPP-4-2 treatment in the future experiments. NF-κB2 was reported to induce apoptosis through activating caspase-8 (Wang et al., 2002) and probably subsequent caspase-3. To summarize, CPP-4-2 might induce apoptosis of breast cancer cells by enhancing the transcription of NF-κB2 (Figure 3.31).

Besides, Akt has already been demonstrated to be a direct substrate of caspase in apoptotic cells. The Asp-462 of Akt1 was determined as the primary cleavage site and a 43kD cleaved product (N-terminal of Akt product) was produced (Xu et al., 2002). Unfortunately, the Akt antibody used in our experiments could only recognize the C-terminal of Akt protein, which could not recognize the possible cleaved Akt product. The signigicant degradation of total Akt induced by CPP-4-2 peptide might be due to the NF-κB2 mediated activation of caspase cascade.
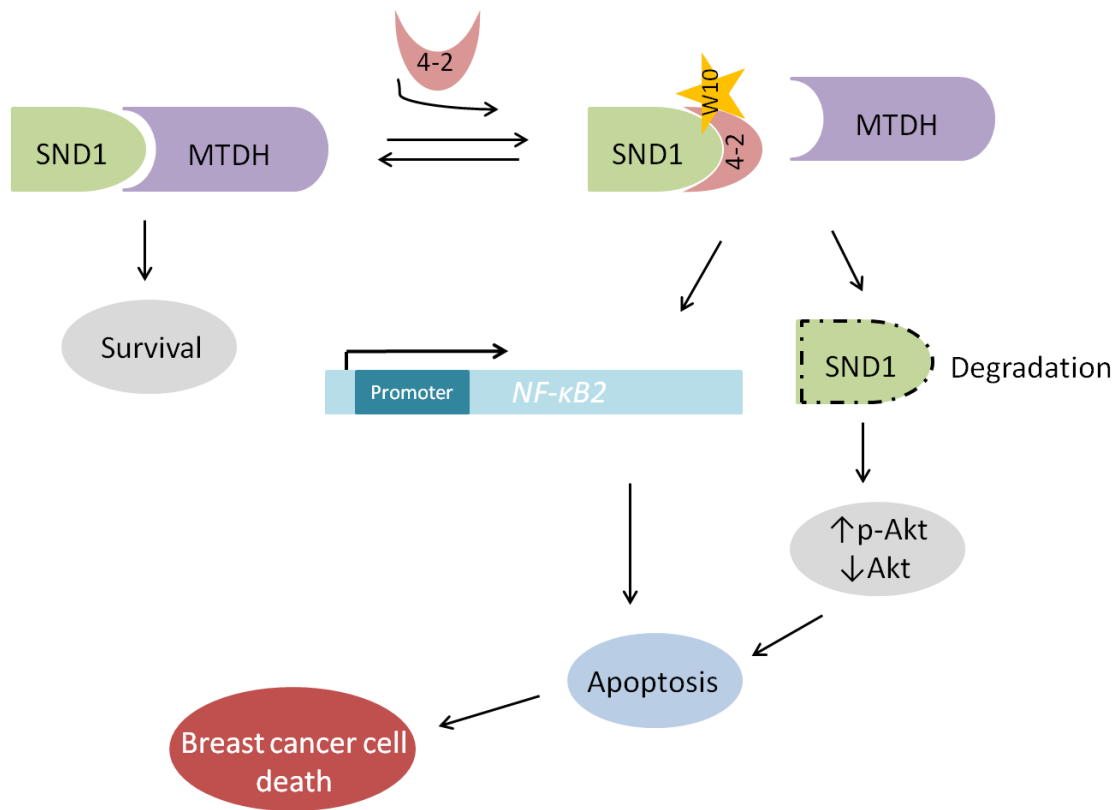
Figure 3.31 A proposed pathway of peptide 4-2 mediating breast cancer cell death

Based on the results in our experiments, we hypothesized a pathway probably through which CPP-4-2 killed breast cancer cells. In untreated breast cancer cells, SND1 can interact with MTDH so breast cancer cell will survive. When peptide 4-2 is added onto breast cancer cells, it will interact with SND1 and disrupts SND1-MTDH interaction, which probably leads to the degradation of SND1. The degradation of SND1 might result in the phosphorylation and degradation of Akt, which leads to the apoptosis of breast cancer cell. On the other hand, the disruption of SND1-MTDH interaction by peptide 4-2 might enhance the transcription of NF-κB2, which leads to the apoptosis of breast cancer cell.

Chapter 4 Limitations and Future perspectives

4.1 A novel SND1-interacting peptide that can disrupt SND1-MTDH interaction

In this study, we identified a novel SN1/2 interacting peptide 4-2 using phage display. We have successfully demonstrated that peptide 4-2 could interact with SND1 and disrupt SND1-MTDH interaction, which probably lead to the degradation of SND1. A novel way to disrupt SND1-MTDH interaction was identified in this study. Besides MTDH there are also many other SND1-interacting partners, which are listed in Table 4.1.

Table 4.1 SND1 binding partners

name	Binding domains in SND1	Functions	Publications
MTDH	SN1/2 domain Binding to 384-407 of MTDH	Oncoprotein	(Wan et al., 2014)
Ago2	SN domian	Essential component of RISC	(Caudy et al., 2003b)
CBP	SN domain binding to 1099-1758 of CBP	Transcriptional coactivator	(Valineva et al., 2005)
STAT6	SN domain binding to TAD domain of STAT6	Transcription factor	(Yang et al., 2002)
G3BP	SN domain	Marker and effector of stress granules	(Gao et al., 2010)
MGLL	SN domain	Monoglyceride lipase, tumor suppressor gene	(Rajasekaran et al., 2016a)
syt11	Binding to N-terminal tandem repeats of syt11C2B	Calcium-sensitive members in the regulation of post-Golgi traffic	(Milochau et al., 2014b)
PC1	Bind to the C-terminus of PC-1	Associated with kidney disease	(Low et al., 2006)
Pim-1	NA	Proto-oncogene	(Leverson et al., 1998)
SAM68	NA	Splicing factor	(Cappellari et al., 2014)

SND1 was reported as a binding partner of multiple proteins. SN1/2 domain of SND1 was used as a bait to screen out SND1 binding peptide in our project. However, SND1 was reported to be interacting with multiple binding partners through SN1/2 domain. NA: not available

SND1 could form complex with many partners, such as MTDH (Wan et al., 2014), Ago2 (Caudy et al., 2003b), CBP (Valineva et al., 2005), STAT6 (Yang et al., 2002), PC1 (Low et al., 2006), Pim-1 (Leverson et al., 1998), G3BP (Gao et al., 2010), SAM68 (Cappellari et al., 2014), syt11 (Milochau et al., 2014a) and MGLL (Rajasekaran et al., 2016b). Publications

reporting the interactions between these binding partners and SND1 were listed in Table 4.1.

In the initial hypothesis of this project, we proposed that the SND1 interacting peptides identified from phage display would disrupt the interaction of SND1 with MTDH. This hypothesis was based on the fact that the bait used in phage display screening was SN1/2 domain of SND1, which was involved in SND1-MTDH interaction. Besides, the binding interface of MTDH to SND1 was well characterized as a binding groove with two hydrophobic binding pockets on SND1 (Guo et al., 2014), and therefore as a potential binding site for interacting with peptide. In fact, SND1 had so many binding partners, which could also be affected by peptide 4-2 (Table 4.1), which became the limitation of this project.

4.2 Peptide 4-2 shows preferential cytotoxicity towards breast cancer cells

The novel SND1-interacting peptide 4-2 is preferentially toxic to breast cancer cells. The IC_{50}s of peptide 4-2 to breast cancer cells are 15.9-22.4µM, which are high for *in vivo* efficacy study. Optimization of peptide 4-2 is necessary before *in vivo* efficacy study. We have identified 1 amino acid W10, which is essential in the cytotoxicity of peptide 4-2. We may change this W to other hydrophobic amino acid to see if it can increase its affinity to SND1 and subsequent cytotoxicity to breast cancer

cells. Other optimization strategy could also be used such as cyclization of peptide 4-2, changing L-form amino acid to D-form amino acid or introducing peptide 4-2 into nanoparticles.

Peptide 4-2 kills breast cancer cells by inducing apoptosis, which is one common mechanism of anti-cancer drug to suppress cancer growth. Another mechanism of inhibiting cancer progression is inducing cell cycle arrest, for example doxorubicin can induce cell cycle arrest by suppressing G2/M transition (Ling et al., 1996). It is better to combine these two mechanisms, inducing apoptosis and cell cycle arrest to treat cancer. As a result, in our future *in vivo* efficacy experiment we can combine the apoptosis-inducing peptide 4-2 with doxorubicin, which can induce cell cycle arrest as a combination therapy to treat breast cancer.

4.3 Mechanisms of the cytotoxicity of peptide 4-2 to breast cancer cells

Mechanism investigation of the cytotoxicity of peptide 4-2 to breast cancer cell suggested that peptide 4-2 could interact with SND1 and disrupt SND1-MTDH interaction, which probably lead to the degradation of SND1. Overexpression of SND1 could reduce the cytotoxicity of peptide 4-2 to breast cancer cells, indicating that the downregulation of SND1 induced by peptide 4-2 was the possible reason for breast cancer cell death. Further investigation on the downstream pathway of SND1

suggested that on one hand, peptide 4-2 could induce the degradation of Akt, which was partially contributed by the phosphorylation of Akt. On the other hand, peptide 4-2 could enhance the transcription of NF-κB2. But whether the degradation of Akt by peptide 4-2 and the enhanced transcription of NF-κB2 by peptide 4-2 are mediated through SND1 are unknown.

It was reported that the overexpression of E3 ubiquitin ligase MULAN could result in the degradation of Akt and suppression of cell proliferation and cell viability (Bae et al., 2012). And it was also reported that NF-κB2/p100 had pro-apoptotic function by inducing apoptosis through activating caspase-8 (Wang et al., 2002). These two are the possible mechanisms which lead to breast cancer cell death. But whether peptide 4-2 mediated death of breast cancer cells are through these two pathways needs further validation. MG132, which could inhibit Akt degradation and caspase-8 inhibitor could be used to top Akt degradation and caspase-8 cascade to protect breast cancer cell from the death induced by peptide 4-2 in future experiments.

4.4 W10 is the essential amino acid in the activity of peptide 4-2

The SND1-interacting peptides showed increased frequency of W and Y after phage display screening. In the subsequent experiments, W10 was

found to be the essential amino acid in cytotoxicity, SND1-interaction, SND1 downregulation, Akt degradation and NF-κB2 activation. We used molecular docking to determine the configuration of peptide 4-2 on SN1/2 and found out that peptide 4-2 bound to a binding site near the binding interface of SND1-MTDH. Moreover, the essential amino acid W10 was facing outward to the binding interface of peptide 4-2 and SN1/2. It was difficult to explain the importance of W10 in the direct interaction of peptide 4-2 with SN1/2. W10 might work as an essential amino acid in maintaining the secondary structure of peptide 4-2 for interacting with SND1. In order to investigate the binding site of peptide 4-2 on SND1, different motif of SN1/2 could be expressed or synthesized to interact with peptide 4-2 in binding assays in the future.

Reference

Abagyan, R., and Totrov, M. (1994). Biased Probability Monte-Carlo Conformational Searches and Electrostatic Calculations for Peptides and Proteins. J Mol Biol *235*, 983-1002.

Abraham, B.K., Fritz, P., McClellan, M., Hauptvogel, P., Athelogou, M., and Brauch, H. (2005). Prevalence of CD44(+)/CD24(-/low) cells in breast cancer may not be associated with clinical outcome but may favor distant metastasis. Clin Cancer Res *11*, 1154-1159.

Agrawal, N., Dasaradhi, P.V.N., Mohmmed, A., Malhotra, P., Bhatnagar, R.K., and Mukherjee, S.K. (2003). RNA interference: Biology, mechanism, and applications. Microbiol Mol Biol R *67*, 657-+.

Aktas, B., Tewes, M., Fehm, T., Hauch, S., Kimmig, R., and Kasimir-Bauer, S. (2009). Stem cell and epithelial-mesenchymal transition markers are frequently overexpressed in circulating tumor cells of metastatic breast cancer patients. Breast Cancer Res *11*.

Al-Hajj, M., Wicha, M.S., Benito-Hernandez, A., Morrison, S.J., and Clarke, M.F. (2003). Prospective identification of tumorigenic breast cancer cells (vol 100, pg 3983, 2003). Proceedings of the National Academy of Sciences of the United States of America *100*, 6890-6890.

Alessi, D.R., Andjelkovic, M., Caudwell, B., Cron, P., Morrice, N., Cohen, P., and Hemmings, B.A. (1996). Mechanism of activation of protein kinase B by insulin and IGF-1. Embo J *15*, 6541-6551.

Alessi, D.R., James, S.R., Downes, C.P., Holmes, A.B., Gaffney, P.R.J., Reese, C.B., and Cohen, P. (1997). Characterization of a 3-phosphoinositide-dependent protein kinase which phosphorylates and activates protein kinase B alpha. Curr Biol *7*, 261-269.

Alphonse Taghian, M.N.E.-G., Sofia D Merajver (2017). Overview of the treatment of newly diagnosed, non-metastatic breast cancer.

Armengol, S., Arretxe, E., Enzunza, L., Llorente, I., Mendibil, U., Navarro-Imaz, H., Ochoa, B., Chico, Y., and Martinez, M.J. (2017). SREBP-2-driven transcriptional activation of human SND1 oncogene. Oncotarget *8*, 108181-108194.

Asselin, E., Mills, G.B., and Tsang, B.K. (2001). XIAP regulates Akt activity and caspase-3-dependent cleavage during cisplatin-induced apoptosis in human ovarian epithelial cancer cells. Cancer Res *61*, 1862-1868.

Badve, S., Dabbs, D.J., Schnitt, S.J., Baehner, F.L., Decker, T., Eusebi, V., Fox, S.B., Ichihara, S., Jacquemier, J., Lakhani, S.R., Palacios, J., Rakha, E.A., Richardson, A.L., Schmitt, F.C., Tan, P.H., Tse, G.M., Weigelt, B., Ellis, I.O., and Reis-Filho, J.S. (2011). Basal-like and triple-negative breast cancers: a critical review with an emphasis on the implications for pathologists and oncologists. Modern Pathol *24*, 157-167.

Bae, S.H., Kim, S.Y., Jung, J.H., Yoon, Y.M., Cha, H.J., Lee, H.J., Kim, K., Kim, J., An, I.S., Kim, J., Um, H.D., Park, I.C., Lee, S.J., Nam, S.Y., Jin, Y.W., Lee, J.H., and An, S.W. (2012). Akt is negatively regulated by the MULAN E3 ligase. Cell research *22*, 873-885.

Baldwin, A.S. (2001). Control of oncogenesis and cancer therapy resistance by the transcription factor NF-kappa B. J Clin Invest *107*, 241-246.

Baldwin, A.S., Jr. (1996). The NF-kappa B and I kappa B proteins: new discoveries and insights. Annual review of immunology *14*, 649-683.

Balic, M., Lin, H., Young, L., Hawes, D., Giuliano, A., McNamara, G., Datar, R.H., and Cote, R.J. (2006). Most early disseminated cancer cells detected in bone marrow of breast cancer patients have a putative breast cancer stem cell phenotype. Clin Cancer Res *12*, 5615-5621.

Balmana, J., Diez, O., Castiglione, M., and Grp, E.G.W. (2009). BRCA in breast cancer: ESMO Clinical Recommendations. Ann Oncol *20*, 19-20.

Balogh, J., Victor, D., Asham, E.H., Burroughs, S.G., Boktour, M., Saharia, A., Li, X., Ghobrial, R.M., and Monsour, H.P. (2016). Hepatocellular carcinoma: a review. J Hepatocell Carcino *3*, 41-53.

Barth, H.G., Boyes, B.E., and Jackson, C. (1996). Size exclusion chromatography. Anal Chem *68*, R445-R466.

Bellacosa, A., Testa, J.R., Staal, S.P., and Tsichlis, P.N. (1991). A retroviral oncogene, akt, encoding a serine-threonine kinase containing an SH2-like region. Science *254*, 274-277.

Bertucci, F., Finetti, P., Cervera, N., Esterni, B., Hermitte, F., Viens, P., and Birnbaum, D. (2008). How basal are triple-negative breast

cancers? Int J Cancer *123*, 236-240.

Blanco, M.A., Aleckovic, M., Hua, Y.L., Li, T., Wei, Y., Xu, Z., Cristea, I.M., and Kang, Y.B. (2011). Identification of Staphylococcal Nuclease Domain-containing 1 (SND1) as a Metadherin-interacting Protein with Metastasis-promoting Functions. J Biol Chem *286*, 19982-19992.

Boxer, L.M., and Dang, C.V. (2001). Translocations involving c-myc and c-myc function. Oncogene *20*, 5595-5610.

Brenton, J.D., Carey, L.A., Ahmed, A.A., and Caldas, C. (2005). Molecular classification and molecular forecasting of breast cancer: Ready for clinical application? Journal of Clinical Oncology *23*, 7350-7360.

Britt, D.E., Yang, D.F., Yang, D.Q., Flanagan, D., Callanan, H., Lim, Y.P., Lin, S.H., and Hixson, D.C. (2004). Identification of a novel protein, LYRIC, localized to tight junctions of polarized epithelial cells. Exp Cell Res *300*, 134-148.

Brown, D.M., and Ruoslahti, E. (2004). Metadherin, a cell surface protein in breast tumors that mediates lung metastasis. Cancer Cell *5*, 365-374.

Buchan, J.R., and Parker, R. (2009). Eukaryotic Stress Granules: The Ins and Outs of Translation. Molecular Cell *36*, 932-941.

Callebaut, I., and Mornon, J.P. (1997). The human EBNA-2 coactivator p100: Multidomain organization and relationship to the staphylococcal nuclease fold and to the tudor protein involved in Drosophila melanogaster development. Biochem J *321*, 125-132.

Cappellari, M., Bielli, P., Paronetto, M.P., Ciccosanti, F., Fimia, G.M., Saarikettu, J., Silvennoinen, O., and Sette, C. (2014). The transcriptional co-activator SND1 is a novel regulator of alternative splicing in prostate cancer cells. Oncogene *33*, 3794-3802.

Caudy, A.A., Ketting, R.F., Hammond, S.M., Denli, A.M., Bathoorn, A.M., Tops, B.B., Silva, J.M., Myers, M.M., Hannon, G.J., and Plasterk, R.H. (2003a). A micrococcal nuclease homologue in RNAi effector complexes. Nature *425*, 411-414.

Caudy, A.A., Ketting, R.F., Hammond, S.M., Denli, A.M., Bathoorn, A.M.P., Tops, B.B.J., Silva, J.M., Myers, M.M., Hannon, G.J., and Plasterk, R.H.A. (2003b). A micrococcal nuclease homologue in RNAi effector complexes. Nature *425*, 411-414.

Cerami, E., Gao, J., Dogrusoz, U., Gross, B.E., Sumer, S.O., Aksoy, B.A., Jacobsen, A., Byrne, C.J., Heuer, M.L., Larsson, E., Antipin, Y., Reva, B., Goldberg, A.P., Sander, C., and Schultz, N. (2012). The cBio cancer genomics portal: an open platform for exploring multidimensional cancer genomics data. Cancer Discov *2*, 401-404.

Chang, J.C., Wooten, E.C., Tsimelzon, A., Hilsenbeck, S.G., Gutierrez, M.C., Tham, Y.L., Kalidas, M., Elledge, R., Mohsin, S., Osborne, C.K., Chamness, G.C., Allred, D.C., Lewis, M.T., Wong, H., and O'Connell, P. (2005). Patterns of resistance and incomplete response to docetaxel by gene expression profiling in breast cancer patients. Journal of Clinical Oncology *23*, 1169-1177.

Chen, W.J., Wang, H., Tang, Y., Liu, C.L., Li, H.L., and Li, W.T. (2010). Multidrug resistance in breast cancer cells during epithelial-mesenchymal transition is modulated by breast cancer resistant protein. Chin J Cancer *29*, 151-157.

Chesneau, O., and Elsolh, N. (1994). Primary Structure and Biological Features of a Thermostable Nuclease Isolated from Staphylococcus-Hyicus. Gene *145*, 41-47.

Coffer, P.J., and Woodgett, J.R. (1991). Molecular-Cloning and Characterization of a Novel Putative Protein-Serine Kinase Related to the Camp-Dependent and Protein-Kinase-C Families. European Journal of Biochemistry *201*, 475-481.

Cogswell, P.C., Guttridge, D.C., Funkhouser, W.K., and Baldwin, A.S. (2000). Selective activation of NF-kappa B subunits in human breast cancer: potential roles for NF-kappa B2/p52 and for Bcl-3. Oncogene *19*, 1123-1131.

Cotton, F.A., Hazen, E.E., Jr., and Legg, M.J. (1979). Staphylococcal nuclease: proposed mechanism of action based on structure of enzyme-thymidine 3',5'-bisphosphate-calcium ion complex at 1.5-A resolution. Proc Natl Acad Sci U S A *76*, 2551-2555.

Cserni, G., Chmielik, E., Cserni, B., and Tot, T. (2018). The new TNM-based staging of breast cancer. Virchows Arch *472*, 697-703.

Cuatrecasas, P. (1970). Topography of the active site of staphylococcal nuclease. Affinity labeling with diazonium substrate analogues. J Biol Chem *245*, 574-584.

Cuatrecasas, P., Wilchek, M., and Anfinsen, C.B. (1969). The action of staphylococcal nuclease on synthetic substrates. Biochemistry *8*, 2277-2284.

Dai, X.F., Li, T., Bai, Z.H., Yang, Y.K., Liu, X.X., Zhan, J.L., and Shi, B.Z. (2015). Breast cancer intrinsic subtype classification, clinical use and future trends. Am J Cancer Res *5*, 2929-2943.

Dang, C.V. (1999). c-myc target genes involved in cell growth, apoptosis, and metabolism. Mol Cell Biol *19*, 1-11.

Dash, A.B., Orrico, F.C., and Ness, S.A. (1996). The EVES motif mediates both intermolecular and intramolecular regulation of c-Myb. Gene Dev *10*, 1858-1869.

Dave, S.S., Fu, K., Wright, G.W., Lam, L.T., Kluin, P., Boerma, E.J., Greiner, T.C., Weisenburger, D.D., Rosenwald, A., Ott, G., Muller-Hermelink, H., Gascoyne, R.D., Delabie, J., Rimsza, L.M., Braziel, R.M., Grogan, T.M., Campo, E., Jaffe, E.S., Dave, B.J., Sanger, W., Bast, M., Vose, J.M., Armitage, J.O., Connors, J.M., Smeland, E.B., Kvaloy, S., Holte, H., Fisher, R.I., Miller, T.P., Montserrat, E., Wilson, W.H., Bahl, M., Zhao, H., Yang, L.M., Powell, J., Simon, R., Chan, W.C., Staudt, L.M., and Profil, L.L.M. (2006). Molecular diagnosis of Burkitt's lymphoma. New Engl J Med *354*, 2431-2442.

David, C.J., and Manley, J.L. (2010). Alternative pre-mRNA splicing regulation in cancer: pathways and programs unhinged. Genes Dev *24*, 2343-2364.

Decker, C.J., and Parker, R. (2012). P-Bodies and Stress Granules: Possible Roles in the Control of Translation and mRNA Degradation. Csh Perspect Biol *4*.

Economopoulou, P., Kaklamani, V.G., and Siziopikou, K. (2012). The Role of Cancer Stem Cells in Breast Cancer Initiation and Progression: Potential Cancer Stem Cell-Directed Therapies. Oncologist *17*, 1394-1401.

El-Andaloussi, S., Jarver, P., Johansson, H.J., and Langel, U. (2007). Cargo-dependent cytotoxicity and delivery efficacy of cell-penetrating peptides: a comparative study. Biochem J *407*, 285-292.

Emdad, L., Lee, S.G., Su, Z.Z., Jeon, H.Y., Boukerche, H., Sarkar, D., and Fisher, P.B. (2009). Astrocyte elevated gene-1 (AEG-1) functions as an oncogene and regulates angiogenesis. P Natl Acad Sci USA *106*, 21300-21305.

Freund, N.T., Enshell-Seijffers, D., and Gershoni, J.M. (2009). Phage display selection, analysis, and prediction of B cell epitopes. Curr Protoc Immunol *Chapter 9*, Unit 9 8.

Gao, J.J., Aksoy, B.A., Dogrusoz, U., Dresdner, G., Gross, B., Sumer, S.O., Sun, Y.C., Jacobsen, A., Sinha, R., Larsson, E., Cerami, E., Sander, C., and Schultz, N. (2013). Integrative Analysis of Complex Cancer Genomics and Clinical Profiles Using the cBioPortal. Sci Signal *6*.

Gao, X.J., Fu, X., Song, J., Zhang, Y., Cui, X.T., Su, C., Ge, L., Shao, J., Xin, L.B., Saarikettu, J., Mei, M., Yang, X., Wei, M.X., Silvennoinen, O., Yao, Z., He, J.Y., and Yang, J. (2015). Poly(A)(+) mRNA-binding protein Tudor-SN regulates stress granules aggregation dynamics. Febs J *282*, 874-890.

Gao, X.J., Ge, L., Shao, J., Su, C., Zhao, H., Saarikettu, J., Yao, X.Y., Yao, Z., Silvennoinen, O., and Yang, J. (2010). Tudor-SN interacts with and co-localizes with G3BP in stress granules under stress conditions. FEBS letters *584*, 3525-3532.

Georgieva, Y., and Konthur, Z. (2011). Design and Screening of M13 Phage Display cDNA Libraries. Molecules *16*, 1667-1681.

Ginestier, C., Hur, M.H., Charafe-Jauffret, E., Monville, F., Dutcher, J., Brown, M., Jacquemier, J., Viens, P., Kleer, C.G., Liu, S.L., Schott, A., Hayes, D., Birnbaum, D., Wicha, M.S., and Dontu, G. (2007). ALDH1 is a marker of normal and malignant human mammary stem cells and a predictor of poor clinical outcome. Cell Stem Cell *1*, 555-567.

Guidotti, G., Brambilla, L., and Rossi, D. (2017). Cell-Penetrating Peptides: From Basic Research to Clinics. Trends Pharmacol Sci *38*, 406-424.

Guo, F., Wan, L.L., Zheng, A.P., Stanevich, V., Wei, Y., Satyshur, K.A., Shen, M.H., Lee, W., Kang, Y.B., and Xing, Y.N. (2014). Structural Insights into the Tumor-Promoting Function of the MTDH-SND1 Complex. Cell reports *8*, 1704-1713.

Gutierrez-Beltran, E., Denisenko, T.V., Zhivotovsky, B., and Bozhkov, P.V. (2016). Tudor staphylococcal nuclease: biochemistry and functions. Cell Death Differ *23*, 1739-1748.

Gyorffy, B., Lanczky, A., Eklund, A.C., Denkert, C., Budczies, J., Li, Q.Y., and Szallasi, Z. (2010). An online survival analysis tool to rapidly assess the effect of 22,277 genes on breast cancer prognosis using microarray data of 1,809 patients. Breast Cancer Res Tr *123*, 725-731.

Hacker, H., and Karin, M. (2002). Is NF-kappa B2/p100 a direct activator of programmed cell death? Cancer cell *2*, 431-433.

Hayes, D.F. (2018). Systemic treatment for metastatic breast cancer: General principles.

Hemmings, B.A., and Restuccia, D.F. (2012). PI3K-PKB/Akt Pathway. Csh Perspect Biol *4*.

Ho, J., Kong, J.W., Choong, L.Y., Loh, M.C., Toy, W., Chong, P.K., Wong, C.H., Wong, C.Y., Shah, N., and Lim, Y.P. (2009a). Novel breast

cancer metastasis-associated proteins. J Proteome Res *8*, 583-594.

Ho, J., Kong, J.W.F., Choong, L.Y., Loh, M.C.S., Toy, W., Chong, P.K., Wong, C.H., Wong, C.Y., Shah, N., and Lim, Y.P. (2009b). Novel Breast Cancer Metastasis-Associated Proteins. Journal of Proteome Research *8*, 583-594.

Hou, Y.B., Yu, L.H., Mi, Y.H., Zhang, J.W., Wang, K., and Hu, L.Y. (2016). Association of MTDH immunohistochemical expression with metastasis and prognosis in female reproduction malignancies: a systematic review and meta-analysis. Sci Rep-Uk *6*.

Hu, G.H., Chong, R.A., Yang, Q.F., Wei, Y., Blanco, M.A., Li, F., Reiss, M., Au, J.L.S., Haffty, B.G., and Kang, Y.B. (2009). MTDH Activation by 8q22 Genomic Gain Promotes Chemoresistance and Metastasis of Poor-Prognosis Breast Cancer. Cancer Cell *15*, 9-20.

Iseri, O.D., Kars, M.D., Arpaci, F., Atalay, C., Pak, I., and Gunduz, U. (2011). Drug resistant MCF-7 cells exhibit epithelial-mesenchymal transition gene expression pattern. Biomed Pharmacother *65*, 40-45.

Jang, J.S., Lee, A., Li, J., Liyanage, H., Yang, Y.A., Guo, L.X., Asmann, Y.W., Li, P.W., Erickson-Johnson, M., Sakai, Y., Sun, Z.F., Jeon, H.S., Hwang, H., Bungum, A.O., Edell, E.S., Simon, V.A., Kopp, K.J., Eckloff, B., Oliveira, A.M., Wieben, E., Aubry, M.C., Yi, E., Wigle, D., Diasio, R.B., Yang, P., and Jen, J. (2015). Common Oncogene Mutations and Novel SND1-BRAF Transcript Fusion in Lung Adenocarcinoma from Never Smokers. Sci Rep-Uk *5*.

Jankowitz, R.C., and Davidson, N.E. (2013). Adjuvant Endocrine Therapy for Breast Cancer: How Long Is Long Enough? Oncology-Ny *27*, 1210-+.

Jariwala, N., Rajasekaran, D., Mendoza, R.G., Shen, X.N., Siddiq, A., Akiel, M.A., Robertson, C.L., Subler, M.A., Windle, J.J., Fisher, P.B., Sanyal, A.J., and Sarkar, D. (2017). Oncogenic Role of SND1 in Development and Progression of Hepatocellular Carcinoma. Cancer Res *77*, 3306-3316.

Jariwala, N., Rajasekaran, D., Srivastava, J., Gredler, R., Akiel, M.A., Robertson, C.L., Emdad, L., Fisher, P.B., and Sarkar, D. (2015a). Role of the staphylococcal nuclease and tudor domain containing 1 in oncogenesis. Int J Oncol *46*, 465-473.

Jariwala, N., Rajasekaran, D., Srivastava, J., Gredler, R., Akiel, M.A., Robertson, C.L., Emdad, L., Fisher, P.B., and Sarkar, D. (2015b). Role of the staphylococcal nuclease and tudor domain containing 1 in oncogenesis (review). International journal of oncology *46*, 465-473.

Jones, P.F., Jakubowicz, T., Pitossi, F.J., Maurer, F., and Hemmings, B.A. (1991). Molecular cloning and identification of a serine/threonine protein kinase of the second-messenger subfamily. Proc Natl Acad Sci U S A *88*, 4171-4175.

Kaltschmidt, B., Kaltschmidt, C., Hofmann, T.G., Hehner, S.P., Droge, W., and Schmitz, M.L. (2000). The pro- or anti-apoptotic function of NF-kappa B is determined by the nature of the apoptotic stimulus. European Journal of Biochemistry *267*, 3828-3835.

Karin, M., and Ben-Neriah, Y. (2000). Phosphorylation meets ubiquitination: the control of NF-[kappa]B activity. Annual review of immunology *18*, 621-663.

Keller, U., Huber, J., Nilsson, J.A., Fallahi, M., Hall, M.A., Peschel, C., and Cleveland, J.L. (2010). Myc suppression of Nfkb2 accelerates lymphomagenesis. Bmc Cancer *10*.

Koren, S., and Bentires-Alj, M. (2015). Breast Tumor Heterogeneity: Source of Fitness, Hurdle for Therapy. Molecular Cell *60*, 537-546.

Kozlowski, J., Kozlowska, A., and Kocki, J. (2015). Breast cancer metastasis - insight into selected molecular mechanisms of the phenomenon. Postep Hig Med Dosw *69*, 447-451.

Kuruma, H., Kamata, Y., Takahashi, H., Igarashi, K., Kimura, T., Miki, K., Miki, J., Sasaki, H., Hayashi, N., and Egawa, S. (2009). Staphylococcal Nuclease Domain-Containing Protein 1 as a Potential Tissue Marker for Prostate Cancer. Am J Pathol *174*, 2044-2050.

Lagadec, C., Vlashi, E., Della Donna, L., Dekmezian, C., and Pajonk, F. (2012). Radiation-Induced Reprogramming of Breast Cancer Cells. Stem Cells *30*, 833-844.

Lee, S.G., Kang, D.C., DeSalle, R., Sarkar, D., and Fisher, P.B. (2013). AEG-1/MTDH/LYRIC, the beginning: initial cloning, structure, expression profile, and regulation of expression. Adv Cancer Res *120*, 1-38.

Leverson, J.D., Koskinen, P.J., Orrico, F.C., Rainio, E.M., Jalkanen, K.J., Dash, A.B., Eisenman, R.N., and Ness, S.A. (1998). Pim-1 kinase and p100 cooperate to enhance c-myb activity. Mol Cell *2*, 417-425.

Li, C.L., Yang, W.Z., Chen, Y.P., and Yuan, H.S. (2008a). Structural and functional insights into human Tudor-SN, a key component linking RNA interference and editing. Nucleic Acids Res *36*, 3579-3589.

Li, J., Yang, L., Song, L., Xiong, H., Wang, L., Yan, X., Yuan, J., Wu, J., and Li, M. (2009). Astrocyte elevated gene-1 is a proliferation promoter in breast cancer via suppressing transcriptional factor FOXO1. Oncogene *28*, 3188-3196.

Li, J., Zhang, N., Song, L.B., Liao, W.T., Jiang, L.L., Gong, L.Y., Wu, J.H., Yuan, J., Zhang, H.Z., Zeng, M.S., and Li, M.F. (2008b). Astrocyte elevated gene-1 is a novel prognostic marker for breast cancer progression and overall patient survival. Clin Cancer Res *14*, 3319-3326.

Li, X., Kong, X., Huo, Q., Guo, H., Yan, S., Yuan, C., Moran, M.S., Shao, C., and Yang, Q. (2011). Metadherin enhances the invasiveness of breast cancer cells by inducing epithelial to mesenchymal transition. Cancer Sci *102*, 1151-1157.

Li, X.X., Lewis, M.T., Huang, J., Gutierrez, C., Osborne, C.K., Wu, M.F., Hilsenbeck, S.G., Pavlick, A., Zhang, X.M., Chamness, G.C., Wong, H., Rosen, J., and Chang, J.C. (2008c). Intrinsic resistance of tumorigenic breast cancer cells to chemotherapy. J Natl Cancer I *100*, 672-679.

Liao, Y., and Hung, M.C. (2010). Physiological regulation of Akt activity and stability. American journal of translational research *2*, 19-42.

Ling, Y.H., el-Naggar, A.K., Priebe, W., and Perez-Soler, R. (1996). Cell cycle-dependent cytotoxicity, G2/M phase arrest, and disruption of p34cdc2/cyclin B1 activity induced by doxorubicin in synchronized P388 cells. Molecular pharmacology *49*, 832-841.

Liu, K., Chen, C., Guo, Y.H., Lam, R., Bian, C.B., Xu, C., Zhao, D.Y., Jin, J., MacKenzie, F., Pawson, T., and Min, J.R. (2010). Structural basis for recognition of arginine methylated Piwi proteins by the extended Tudor domain. P Natl Acad Sci USA *107*, 18398-18403.

Low, S.H., Vasanth, S., Larson, C.H., Mukherjee, S., Sharma, N., Kinter, M.T., Kane, M.E., Obara, T., and Weimbs, T. (2006). Polycystin-1, STAT6, and pathway that transduces P100 function in a ciliary mechanosensation and is activated in polycystic kidney disease. Dev Cell *10*, 57-69.

Lumachi, F., Brunello, A., Maruzzo, M., Basso, U., and Basso, S.M.M. (2013). Treatment of Estrogen Receptor-Positive Breast Cancer. Curr Med Chem *20*, 596-604.

Lumachi, F., Luisetto, G., Basso, S.M.M., Basso, U., Brunello, A., and Camozzi, V. (2011). Endocrine Therapy of Breast Cancer. Curr Med Chem *18*, 513-522.

Makki, J. (2015). Diversity of Breast Carcinoma: Histological Subtypes and Clinical Relevance. Clin Med Insights-Pa *8*.

Mani, S.A., Guo, W., Liao, M.J., Eaton, E.N., Ayyanan, A., Zhou, A.Y., Brooks, M., Reinhard, F., Zhang, C.C., Shipitsin, M., Campbell, L.L., Polyak, K., Brisken, C., Yang, J., and Weinberg, R.A. (2008). The epithelial-mesenchymal transition generates cells with properties of stem cells. Cell *133*, 704-715.

Manning, B.D., and Toker, A. (2017). AKT/PKB Signaling: Navigating the Network. Cell *169*, 381-405.

Marvin, D.A. (1998). Filamentous phage structure, infection and assembly. Curr Opin Struct Biol *8*, 150-158.

Miller, L.J., Chen, Q., Lam, P.C.H., Pinon, D.I., Sexton, P.M., Abagyan, R., and Dong, M.Q. (2011). Refinement of Glucagon-like Peptide 1 Docking to Its Intact Receptor Using Mid-region Photolabile Probes and Molecular Modeling. Journal of Biological Chemistry *286*.

Milochau, A., Lagree, V., Benassy, M.N., Chaignepain, S., Papin, J., Garcia-Arcos, I., Lajoix, A., Monterrat, C., Coudert, L., Schmitter, J.M., Ochoa, B., and Lang, J. (2014a). Synaptotagmin 11 interacts with components of the RNA-induced silencing complex RISC in clonal pancreatic beta-cells. Febs Lett *588*, 2217-2222.

Milochau, A., Lagree, V., Benassy, M.N., Chaignepain, S., Papin, J., Garcia-Arcos, I., Lajoix, A., Monterrat, C., Coudert, L., Schmitter, J.M., Ochoa, B., and Lang, J.C. (2014b). Synaptotagmin 11 interacts with components of the RNA-induced silencing complex RISC in clonal pancreatic beta-cells. FEBS letters *588*, 2217-2222.

Moody, S.E., Perez, D., Pan, T.C., Sarkisian, C.J., Portocarrero, C.P., Sterner, C.J., Notorfrancesco, K.L., Cardiff, R.D., and Chodosh, L.A. (2005). The transcriptional repressor snail promotes mammary tumor recurrence. Cancer Cell *8*, 197-209.

Morgan, A.A., and Rubenstein, E. (2013). Proline: the distribution, frequency, positioning, and common functional roles of proline and polyproline sequences in the human proteome. PloS one *8*, e53785.

Mukhopadhyay, D., and Riezman, H. (2007). Proteasome-independent functions of ubiquitin in endocytosis and signaling. Science *315*,

201-205.

Navarro-Imaz, H., Rueda, Y., and Fresnedo, O. (2016). SND1 overexpression deregulates cholesterol homeostasis in hepatocellular carcinoma. Bba-Mol Cell Biol L *1861*, 988-996.

Ness, S.A. (1996). The Myb oncoprotein: Regulating a regulator. Bba-Rev Cancer *1288*, F123-F139.

Noguchi, M., Hirata, N., and Suizu, F. (2014). The links between AKT and two intracellular proteolytic cascades: Ubiquitination and autophagy. Bba-Rev Cancer *1846*, 342-352.

Oeckinghaus, A., and Ghosh, S. (2009). The NF-kappa B Family of Transcription Factors and Its Regulation. Csh Perspect Biol *1*.

Ophir, R., and Gershoni, J.M. (1995). Biased Random Mutagenesis of Peptides - Determination of Mutation Frequency by Computer-Simulation. Protein Eng *8*, 143-146.

Paget, S. (1989). The distribution of secondary growths in cancer of the breast. 1889. Cancer Metastasis Rev *8*, 98-101.

Pan, H.C., Gray, R., Braybrooke, J., Davies, C., Taylor, C., McGale, P., Peto, R., Pritchard, K.I., Bergh, J., Dowsett, M., Hayes, D.F., and Ebctcg (2017). 20-Year Risks of Breast-Cancer Recurrence after Stopping Endocrine Therapy at 5 Years. New Engl J Med *377*, 1836-1846.

Papaccio, F., Paino, F., Regad, T., Papaccio, G., Desiderio, V., and Tirino, V. (2017a). Concise Review: Cancer Cells, Cancer Stem Cells, and Mesenchymal Stem Cells: Influence in Cancer Development. Stem cells translational medicine *6*, 2115-2125.

Papaccio, F., Paino, F., Regad, T., Papaccio, G., Desiderio, V., and Tirino, V. (2017b). Concise Review: Cancer Cells, Cancer Stem Cells, and Mesenchymal Stem Cells: Influence in Cancer Development. Stem Cell Transl Med *6*, 2115-2125.

Paukku, K., Yang, J., and Silvennoinen, O. (2003). Tudor and nuclease-like domains containing protein p100 function as coactivators for signal transducer and activator of transcription 5. Mol Endocrinol *17*, 1805-1814.

Peng, L., Xu, T., Long, T., and Zuo, H.Q. (2016). Association Between BRCA Status and P53 Status in Breast Cancer: A Meta-Analysis. Med Sci Monitor *22*, 1939-1945.

Peshkin, B.N., Alabek, M.L., and Isaacs, C. (2010). BRCA1/2 mutations and triple negative breast cancers. Breast Dis *32*, 25-33.

Pratt, A.J., and MacRae, I.J. (2009). The RNA-induced Silencing Complex: A Versatile Gene-silencing Machine. J Biol Chem *284*, 17897-17901.

Rabbani, S.A., and Mazar, A.P. (2007). Evaluating distant metastases in breast cancer: from biology to outcomes. Cancer Metast Rev *26*, 663-674.

Rajasekaran, D., Jariwala, N., Mendoza, R.G., Robertson, C.L., Akiel, M.A., Dozmorov, M., Fisher, P.B., and Sarkar, D. (2016a). Staphylococcal Nuclease and Tudor Domain Containing 1 (SND1 Protein) Promotes Hepatocarcinogenesis by Inhibiting Monoglyceride Lipase (MGLL). Journal of Biological Chemistry *291*, 10736-10746.

Rajasekaran, D., Jariwala, N., Mendoza, R.G., Robertson, C.L., Akiel, M.A., Dozmorov, M., Fisher, P.B., and Sarkar, D. (2016b). Staphylococcal Nuclease and Tudor Domain Containing 1 (SND1 Protein) Promotes Hepatocarcinogenesis by Inhibiting Monoglyceride Lipase (MGLL). The Journal of biological chemistry *291*, 10736-10746.

Rayet, B., and Gelinas, C. (1999). Aberrant rel/nfkb genes and activity in human cancer. Oncogene *18*, 6938-6947.

Reck, M., and Rabe, K.F. (2017). Precision Diagnosis and Treatment for Advanced Non-Small-Cell Lung Cancer. N Engl J Med *377*, 849-861.

Reyes-Turcu, F.E., Ventii, K.H., and Wilkinson, K.D. (2009). Regulation and Cellular Roles of Ubiquitin-Specific Deubiquitinating Enzymes. Annu Rev Biochem *78*, 363-397.

Robert, N.J. (1997). Clinical efficacy of tamoxifen. Oncology *11*, 15-20.

Rowinsky, E.K., and Donehower, R.C. (1995). Paclitaxel (taxol). The New England journal of medicine *332*, 1004-1014.

Sahin, E., and Roberts, C.J. (2012). Size-exclusion chromatography with multi-angle light scattering for elucidating protein aggregation mechanisms. Methods Mol Biol *899*, 403-423.

Samarasinghe, B.B. (2013). The Hallmarks of Cancer 6: Tissue Invasion and Metastasis. Scientific American.

Samuelson, A.V., Narita, M., Chan, H.M., Jin, J.P., de Stanchina, E., McCurrach, M.E., Narita, M., Fuchs, M., Livingston, D.M., and Lowe, S.W. (2005). p400 is required for E1A to promote apoptosis. Journal of Biological Chemistry *280*, 21915-21923.

Santhekadur, P.K., Akiel, M., Emdad, L., Gredler, R., Srivastava, J., Rajasekaran, D., Robertson, C.L., Mukhopadhyay, N.D., Fisher, P.B., and Sarkar, D. (2014). Staphylococcal nuclease domain containing-1 (SND1) promotes migration and invasion via angiotensin II type 1 receptor (AT1R) and TGF beta signaling. Febs Open Bio *4*, 353-361.

Santhekadur, P.K., Das, S.K., Gredler, R., Chen, D., Srivastava, J., Robertson, C., Baldwin, A.S., Fisher, P.B., and Sarkar, D. (2012). Multifunction Protein Staphylococcal Nuclease Domain Containing 1 (SND1) Promotes Tumor Angiogenesis in Human Hepatocellular Carcinoma through Novel Pathway That Involves Nuclear Factor kappa B and miR-221. J Biol Chem *287*, 13952-13958.

Sarbassov, D.D., Guertin, D.A., Ali, S.M., and Sabatini, D.M. (2005). Phosphorylation and regulation of Akt/PKB by the rictor-mTOR complex. Science *307*, 1098-1101.

Scadden, A.D. (2005). The RISC subunit Tudor-SN binds to hyper-edited double-stranded RNA and promotes its cleavage. Nat Struct Mol Biol *12*, 489-496.

Schiff, P.B., Fant, J., and Horwitz, S.B. (1979). Promotion of microtubule assembly in vitro by taxol. Nature *277*, 665-667.

Schramm, A., De Gregorio, N., Widschwendter, P., Fink, V., and Huober, J. (2015). Targeted Therapies in HER2-Positive Breast Cancer - a Systematic Review. Breast care *10*, 173-178.

Schwarze, S.R., Ho, A., Vocero-Akbani, A., and Dowdy, S.F. (1999). In vivo protein transduction: Delivery of a biologically active protein into the mouse. Science *285*, 1569-1572.

Scott, J.K., and Smith, G.P. (1990). Searching for Peptide Ligands with an Epitope Library. Science *249*, 386-390.

Senftleben, U., Cao, Y.X., Xiao, G.T., Greten, F.R., Krahn, G., Bonizzi, G., Chen, Y., Hu, Y.L., Fong, A., Sun, S.C., and Karin, M. (2001). Activation by IKK alpha of a second, evolutionary conserved, NF-kappa B signaling pathway. Science *293*, 1495-1499.

Shi, X., and Wang, X. (2015). The role of MTDH/AEG-1 in the progression of cancer. Int J Clin Exp Med *8*, 4795-4807.

Siemion, I.Z. (1994). Compositional Frequencies of Amino-Acids in the Proteins and the Genetic-Code. Biosystems *32*, 163-170.

Silver, D.P., and Livingston, D.M. (2012). Mechanisms of BRCA1 Tumor Suppression. Cancer Discov *2*, 679-684.

Smith, G.P. (1985). Filamentous Fusion Phage - Novel Expression Vectors That Display Cloned Antigens on the Virion Surface. Science *228*, 1315-1317.

Song, G., Ouyang, G., and Bao, S. (2005a). The activation of Akt/PKB signaling pathway and cell survival. J Cell Mol Med *9*, 59-71.

Song, G., Ouyang, G.L., and Bao, S.D. (2005b). The activation of Akt/PKB signaling pathway and cell survival. Journal of Cellular and Molecular Medicine *9*, 59-71.

Sorlie, T., Perou, C.M., Tibshirani, R., Aas, T., Geisler, S., Johnsen, H., Hastie, T., Eisen, M.B., van de Rijn, M., Jeffrey, S.S., Thorsen, T., Quist, H., Matese, J.C., Brown, P.O., Botstein, D., Lonning, P.E., and Borresen-Dale, A.L. (2001). Gene expression patterns of breast carcinomas distinguish tumor subclasses with clinical implications. P Natl Acad Sci USA *98*, 10869-10874.

Spano, D., Heck, C., De Antonellis, P., Christofori, G., and Zollo, M. (2012). Molecular networks that regulate cancer metastasis. Semin Cancer Biol *22*, 234-249.

Steeg, P.S. (2006). Tumor metastasis: mechanistic insights and clinical challenges. Nat Med *12*, 895-904.

Stengele, I., Bross, P., Garces, X., Giray, J., and Rasched, I. (1990). Dissection of Functional Domains in Phage Fd Adsorption Protein - Discrimination between Attachment and Penetration Sites. J Mol Biol *212*, 143-149.

Subik, K., Lee, J.F., Baxter, L., Strzepek, T., Costello, D., Crowley, P., Xing, L., Hung, M.C., Bonfiglio, T., Hicks, D.G., and Tang, P. (2010). The Expression Patterns of ER, PR, HER2, CK5/6, EGFR, Ki-67 and AR by Immunohistochemical Analysis in Breast Cancer Cell Lines. Breast cancer : basic and clinical research *4*, 35-41.

Suizu, F., Hiramuki, Y., Okumura, F., Matsuda, M., Okumura, A.J., Hirata, N., Narita, M., Kohno, T., Yokota, J., Bohgaki, M., Obuse, C., Hatakeyama, S., Obata, T., and Noguchi, M. (2009). The E3 Ligase TTC3 Facilitates Ubiquitination and Degradation of Phosphorylated Akt. Dev Cell *17*, 800-810.

Sunil R. Lakhani, I.O.E., Stuart J. Schnitt, Puay Hoon Tan, Marc J. van de Vijver (2012). WHO Classification of Tumours of the Breast. International Agency for Research on Cancer *4*.

Sutherland, H.G., Lam, Y.W., Briers, S., Lamond, A.I., and Bickmore, W.A. (2004). 3D3/lyric: a novel transmembrane protein of the endoplasmic reticulum and nuclear envelope, which is also present in the nucleolus. Exp Cell Res *294*, 94-105.

Tan, C., Etcubanas, E., Wollner, N., Rosen, G., Gilladoga, A., Showel, J., Murphy, M.L., and Krakoff, I.H. (1973). Adriamycin--an antitumor antibiotic in the treatment of neoplastic diseases. Cancer *32*, 9-17.

Theobald, D.L., Mitton-Fry, R.M., and Wuttke, D.S. (2003). Nucleic acid recognition by OB-fold proteins. Annu Rev Bioph Biom *32*, 115-133.

Theodoropoulos, P.A., Polioudaki, H., Agelaki, S., Kallergi, G., Saridaki, Z., Mavroudis, D., and Georgoulias, V. (2010). Circulating tumor cells with a putative stem cell phenotype in peripheral blood of patients with breast cancer. Cancer Lett *288*, 99-106.

Thirkettle, H.J., Girling, J., Warren, A.Y., Mills, I.G., Sahadevan, K., Leung, H., Hamdy, F., Whitaker, H.C., and Neal, D.E. (2009). LYRIC/AEG-1 Is Targeted to Different Subcellular Compartments by Ubiquitinylation and Intrinsic Nuclear Localization Signals. Clin Cancer Res *15*, 3003-3013.

Tong, L., Wang, C., Hu, X., Pang, B., Yang, Z., He, Z., He, M., Wei, L., and Chu, M. (2016). Correlated overexpression of metadherin and SND1 in glioma cells. Biol Chem *397*, 57-65.

Tong, X., Drapkin, R., Yalamanchili, R., Mosialos, G., and Kieff, E. (1995). The Epstein-Barr-Virus Nuclear-Protein-2 Acidic Domain Forms a Complex with a Novel Cellular Coactivator That Can Interact with Tfiie. Mol Cell Biol *15*, 4735-4744.

Tremont, A., Lu, J., and Cole, J.T. (2017). Endocrine Therapy for Early Breast Cancer: Updated Review. Ochsner J *17*, 405-411.

Tsuchiya, N., Ochiai, M., Nakashima, K., Ubagai, T., Sugimura, T., and Nakagama, H. (2007). SND1, a component of RNA-induced silencing complex, is up-regulated in human colon cancers and implicated in early stage colon carcinogenesis. Cancer Res *67*, 9568-9576.

Tuunnemann, G., Ter-Avetisyan, G., Martin, R.M., Stoockl, M., Herrmann, A., and Cardoso, C. (2008). Live-cell analysis of cell penetration ability and toxicity of oligo-arginines. J Pept Sci *14*, 469-476.

Valineva, T., Yang, J., Palovuori, R., and Silvennoinen, O. (2005). The transcriptional co-activator protein p100 recruits histone acetyltransferase activity to STAT6 and mediates interaction between the CREB-binding protein and STAT6. Journal of Biological Chemistry *280*, 14989-14996.

Vives, E., Brodin, P., and Lebleu, B. (1997). A truncated HIV-1 Tat protein basic domain rapidly translocates through the plasma membrane and accumulates in the cell nucleus. J Biol Chem *272*, 16010-16017.

Vladimir, S. (2018). RNA interference.

Wan, L.L., Lu, X., Yuan, S., Wei, Y., Guo, F., Shen, M.H., Yuan, M., Chakrabarti, R., Hua, Y.L., Smith, H.A., Blanco, M.A., Chekmareva, M., Wu, H., Bronson, R.T., Haffty, B.G., Xing, Y.N., and Kang, Y.B. (2014). MTDH-SND1 Interaction Is Crucial for Expansion and Activity of Tumor-Initiating Cells in Diverse Oncogene- and Carcinogen-Induced Mammary Tumors. Cancer Cell *26*, 92-105.

Wang, Y.Q., Cui, H.J., Schroering, A., Ding, J.L., Lane, W.S., McGill, G., Fisher, D.E., and Ding, H.F. (2002). NF-kappa B2 p100 is a pro-apoptotic protein with anti-oncogenic function. Nature cell biology *4*, 888-893.

Weiss, L. (1990). Metastatic inefficiency. Adv Cancer Res *54*, 159-211.

Wender, P.A., Mitchell, D.J., Pattabiraman, K., Pelkey, E.T., Steinman, L., and Rothbard, J.B. (2000). The design, synthesis, and evaluation of molecules that enable or enhance cellular uptake: Peptoid molecular transporters. P Natl Acad Sci USA *97*, 13003-13008.

WHO (2018). Fact Sheets by Cancer. Globocan 2018.

Wicha, M.S., Liu, S.L., and Dontu, G. (2006). Cancer stem cells: An old idea - A paradigm shift. Cancer Res *66*, 1883-1890.

Widmann, C., Gibson, S., and Johnson, G.L. (1998). Caspase-dependent cleavage of signaling proteins during apoptosis - A turn-off mechanism for anti-apoptotic signals. Journal of Biological Chemistry *273*, 7141-7147.

Will, C.L., and Luhrmann, R. (2001). Spliceosomal UsnRNP biogenesis, structure and function. Curr Opin Cell Biol *13*, 290-301.

Wren, B.G. (2007). The origin of breast cancer. Menopause *14*, 1060-1068.

Wymann, M.P., Zvelebil, M., and Laffargue, M. (2003). Phosphoinositide 3-kinase signalling - which way to target? Trends Pharmacol Sci *24*, 366-376.

Xia, Y.F., Shen, S., and Verma, I.M. (2014). NF-kappa B, an Active Player in Human Cancers. Cancer Immunol Res *2*, 823-830.

Xiang, T., Ohashi, A., Huang, Y.P., Pandita, T.K., Ludwig, T., Powell, S.N., and Yang, Q. (2008). Negative Regulation of AKT Activation by

BRCA1. Cancer Res *68*, 10040-10044.

Xiao, G.T., Harhaj, E.W., and Sun, S.C. (2001). NF-kappa B-inducing kinase regulates the processing of NF-kappa B2 p100. Mol Cell *7*, 401-409.

Xing, A.M., Pan, L., and Gao, J.Z. (2018). p100 functions as a metastasis activator and is targeted by tumor suppressing microRNA-320a in lung cancer. Thorac Cancer *9*, 152-158.

Xu, J., Liu, D., and Zhou, S.Y. (2002). The role of Asp-462 in regulating Akt activity. Journal of Biological Chemistry *277*, 35561-35566.

Yang, J., Aittomaki, S., Pesu, M., Carter, K., Saarinen, J., Kalkkinen, N., Kieff, E., and Silvennoinen, O. (2002). Identification of p100 as a coactivator for STAT6 that bridges STAT6 with RNA polymerase II. Embo J *21*, 4950-4958.

Yang, J., Valineva, T., Hong, J., Bu, T., Yao, Z., Jensen, O.N., Frilander, M.J., and Silvennoinen, O. (2007). Transcriptional co-activator protein p100 interacts with snRNP proteins and facilitates the assembly of the spliceosome. Nucleic Acids Res *35*, 4485-4494.

Yang, W.D., Chendrimada, T.P., Wang, Q.D., Higuchi, M., Seeburg, P.H., Shiekhattar, R., and Nishikura, K. (2006). Modulation of microRNA processing and expression through RNA editing by ADAR deaminases. Nature Structural & Molecular Biology *13*, 13-21.

Yin, J., Ding, J.M., Huang, L., Tian, X., Shi, X.B., Zhi, L., Song, J., Zhang, Y., Gao, X.J., Yao, Z., Jing, X., and Yang, J. (2013). SND1 Affects Proliferation of Hepatocellular Carcinoma Cell Line SMMC-7721 by Regulating IGFBP3 Expression. Anat Rec *296*, 1568-1575.

Yoo, B.K., Emdad, L., Lee, S.G., Su, Z.Z., Santhekadur, P., Chen, D., Gredler, R., Fisher, P.B., and Sarkar, D. (2011a). Astrocyte elevated gene-1 (AEG-1): A multifunctional regulator of normal and abnormal physiology. Pharmacol Ther *130*, 1-8.

Yoo, B.K., Emdad, L., Lee, S.G., Su, Z.Z., Santhekadur, P., Chen, D., Gredler, R., Fisher, P.B., and Sarkar, D. (2011b). Astrocyte elevated gene-1 (AEG-1): A multifunctional regulator of normal and abnormal physiology. Pharmacol Therapeut *130*, 1-8.

Yoo, B.K., Santhekadur, P.K., Gredler, R., Chen, D., Emdad, L., Bhutia, S., Pannell, L., Fisher, P.B., and Sarkar, D. (2011c). Increased RNA-Induced Silencing Complex (RISC) Activity Contributes to Hepatocellular Carcinoma. Hepatology *53*, 1538-1548.

Yu, F., Yao, H., Zhu, P., Zhang, X., Pan, Q., Gong, C., Huang, Y., Hu, X., Su, F., Lieberman, J., and Song, E. (2007). let-7 regulates self renewal and tumorigenicity of breast cancer cells. Cell *131*, 1109-1123.

Yu, L., Di, Y., Xin, L., Ren, Y., Liu, X., Sun, X., Zhang, W., Yao, Z., and Yang, J. (2017). SND1 acts as a novel gene transcription activator recognizing the conserved Motif domains of Smad promoters, inducing TGF beta 1 response and breast cancer metastasis. Oncogene *36*, 3903-3914.

Yu, L., Liu, X., Cui, K., Di, Y., Xin, L., Sun, X., Zhang, W., Yang, X., Wei, M., Yao, Z., and Yang, J. (2015a). SND1 Acts Downstream of TGFbeta1 and Upstream of Smurf1 to Promote Breast Cancer Metastasis. Cancer Res *75*, 1275-1286.

Yu, L., Liu, X., Cui, K., Di, Y.B., Xin, L.B., Sun, X.M., Zhang, W., Yang, X., Wei, M.X., Yao, Z., and Yang, J. (2015b). SND1 Acts Downstream of TGF beta 1 and Upstream of Smurf1 to Promote Breast Cancer Metastasis. Cancer Res *75*, 1275-1286.

Zagryazhskaya, A., Surova, O., Akbar, N.S., Allavena, G., Gyuraszova, K., Zborovskaya, I.B., Tchevkina, E.M., and Zhivotovsky, B. (2015). Tudor staphylococcal nuclease drives chemoresistance of non-small cell lung carcinoma cells by regulating S100A11. Oncotarget *6*, 12156-12173.

Zhang, P., Wei, Y., Wang, L., Debeb, B.G., Yuan, Y., Zhang, J.S., Yuan, J.S., Wang, M., Chen, D.H., Sun, Y.T., Woodward, W.A., Liu, Y.Q., Dean, D.C., Liang, H., Hu, Y., Ang, K.K., Hung, M.C., Chen, J.J., and Ma, L. (2014). ATM-mediated stabilization of ZEB1 promotes DNA damage response and radioresistance through CH K1. Nat Cell Biol *16*, 864-875.